MODELING SLOPE FAILURE IN THE JONES CREEK WATERSHED, ACME, WASHINGTON

By

Brandon M. Brayfield

Accepted in Partial Completion
Of the Requirements for the Degree
Master of Science

Kathleen Kitto, Dean of the Graduate School

ADVISORY COMMITTEE

Chair, Dr. Robert J. Mitchell

Dr. Douglas H. Clark

Dr. Scott R. Linneman

MASTER'S THESIS

In presenting this thesis in partial fulfillment of the requirements for a master's degree at Western Washington University, I grant to Western Washington University the non-exclusive royalty-free right to archive, reproduce, distribute, and display the thesis in any and all forms, including electronic format, via any digital library mechanisms maintained by WWU.

I represent and warrant this is my original work, and does not infringe or violate any rights of others. I warrant that I have obtained written permissions from the owner of any third party copyrighted material included in these files.

I acknowledge that I retain ownership rights to the copyright of this work, including but not limited to the right to use all or part of this work in future works, such as articles or books.

Library users are granted permission for individual, research and non-commercial reproduction of this work for educational purposes only.

Any further digital posting of this document requires specific permission from the author.

Any copying or publication of this thesis for commercial purposes, or for financial gain, is not allowed without my written permission.

Signature: Brandon Brayfield

Date: 11-15-2013

MODELING SLOPE FAILURE IN THE JONES CREEK WATERSHED, ACME, WASHINGTON

A Thesis
Presented to
The Faculty of
Western Washington University

In Partial Fulfillment
Of the Requirements for the Degree
Master of Science

By
Brandon M. Brayfield
May 2013

Abstract

Mountain watersheds in the Pacific Northwest are particularly susceptible to shallow landslides and debris flows during periods of intense precipitation. The Jones Creek watershed near Acme, WA, is a 6.7 km^2 basin that hosts several active landslides. Shallow mass wasting on the unvegetated landslide toes, and deep-seated rotational slide movement can lead to landslide dam outburst floods and debris flows. There are approximately 100 buildings constructed on a 0.75 km^2 alluvial fan deposited by debris flows sourced in the watershed. Predicting the occurrence of mass wasting and deep-seated movement events as they relate to the duration and intensity of antecedent precipitation conditions is important for land-use planning and emergency preparedness in the surrounding Acme community.

The Distributed-Hydrology-Soil-Vegetation Model (DSHVM) simulates a water and energy balance at the pixel scale of a digital elevation model (DEM). I use DHSVM hydrology simulations, coupled with an infinite-slope failure model, to determine the probability of shallow mass-wasting events for a variety of historical precipitation scenarios. The infinite slope model uses a stochastic approach to predict the probability of slope failure on a cell-by-cell basis. Following the methods of Godt (2004), I use the simulated failure probabilities, paired with antecedent precipitation and intensity, to define a series of predictive antecedent precipitation thresholds for slope failure probability in the Jones Creek watershed. Although basin hydrology is not well-constrained in this study, the failure probability thresholds compare favorably with similar, more rigorous studies performed in the Pacific Northwest.

Timber harvest can increase the rate of slope failure in steep basins due to reduced evapotranspiration and root strength loss. In order to supplement current logging prescriptions in the Jones Creek basin, I use DHSVM to model slope failure probability for a design storm event under a number of hypothetical harvest scenarios. DHSVM simulations suggest that root strength is the most important factor for the stabilization of slopes in the

Jones Creek basin, and that a total basin harvest would significantly increase the susceptibility to slope failure. Based on the results of this study, I recommend expansion of the current logging prescriptions to include more harvest-restricted area.

I also use RocScience SLIDE© version 6.0 software to model the influence of groundwater and soil mechanical properties on deep-seated slope stability for four deep-seated landslides in the Jones Creek watershed. Slide uses a comprehensive suite of tools for probabilistic modeling of complex failures, and incorporates a standalone finite element model for groundwater flow. SLIDE results indicate that the transition from unconsolidated material to weak bedrock on the toes of the deep seated landslides is likely to occur at a depth of less than two meters, which agrees with observed conditions in the basin.

.

Acknowledgements

Numerous individuals and organizations contributed to the completion of this research. I gratefully acknowledge their contributions of intellectual guidance, discussion, and resources. Funding for the project was provided by the Western Washington University Geology Department, the Steven and Edit Grega Memorial Fellowship, and the Digges Endowment. Paula Cooper at the Whatcom County River and Flood Division, and Paul Pittman provided insight and discussion of geologic processes at Jones Creek. William Wright, at the USGS Sedro-Woolley office, helped compile meteorological and stream flow data for Jones Creek. Curtis Clement, Brian Huggett, and Eric Tangedahl helped me develop my understanding of DHSVM and via many lengthy discussions. Craig and Robin Bruntil allowed me to install a temporary stream monitoring station on their property.

Many individuals assisted me with field work. Foremost, Brit Litwin assisted during almost every field day, and provided valuable input on the design and construction of stream monitoring equipment. Brit's assistance, advice, and input were incredibly helpful to me over the entirety of the project. Lynni Bennet assisted with stream flow measurements for several storms. Several of my graduate student colleagues also provided assistance and feedback.

My thesis committee members, Dr. Doug Clark and Dr. Scott Linneman, provided excellent guidance, discussion, and editorial assistance for this project, and I am grateful for the flexibility and understanding they demonstrated as this project evolved. My thesis advisor, Dr. Mitchel, guided me through every phase of this project, and demonstrated extraordinary patience and humor when needed. Dr. Mitchell's expert mentorship and instruction has allowed me to develop my problem solving, critical thinking, and writing skills immeasurably during the course of this project, and I am glad to have had the opportunity to study with him.

Finally, I appreciate the support and encouragement from friends and family, especially Erin, who spent many mornings recording stream flow measurements in the rain, and supported me so completely through this entire process. Thank you.

Contents

List of Figures

List of Tables

1.0 Introduction

Understanding the potential impacts of landslides on human life and property is becoming increasingly important as the global population expands to reside in new areas. However, funding for in-depth evaluation of hazards is often limited or nonexistent (McCann and Forster, 1990). In the United States, landslides cause approximately two billion dollars in damages and 25 to 50 deaths annually (Clague and Roberts, 2012; Highland and Bobrowsky, 2008; Spiker and Gori, 2003). Mountain watersheds in the Pacific Northwest are particularly susceptible to landslides due to steep slopes and high winter precipitation. Quantifying the annual state-level impact of landslides is challenging because of year-to-year variability in occurrence; as an indication, however, the Washington State Department of Transportation generally budgets 15 million dollars per year for landslide cleanup on highways (Washington State DNR, 2013). The Jones Creek watershed, a 6.8 km^2 tributary basin to the South Fork Nooksack River in Whatcom Country, WA, is exemplary of the type of basin that is particularly susceptible to landslides and debris flows. Numerous groups, including residents of the South Fork Nooksack River valley, Whatcom County land managers, and logging corporations are all interested in hazard investigations for the watershed. This study aims to contribute to the evaluation of hazards in the basins using numerical modeling tools and high resolution digital spatial data.

Slope stability is primarily governed by slope angle, soil, rock and vegetation mechanical properties, and water table-induced pore fluid pressure. Landslides are commonly triggered hydrologically by water table elevation during storm events (Dhakal and Sidle, 2004). Failures can also be triggered by seismic events, by loss of vegetative root strength following forest fires, or by a number of human activities such as logging or mining (Bowling and Lettenmaier, 2001; Brardinoni et al., 2002; Jibson and Harp, 2011). Shallow failures, generally less than three meters in depth, may occur quickly in response to triggering mechanisms, whereas deep-seated landslides may be tens of meters in depth and can be complex in geometry, subsurface hydrology, weathering of surface materials, and

movement (Baum et al., 2007; Fell et al., 2000; Leroueil, 2001). Deep-seated landslides can be rooted in soil, bedrock, or both. The phrases 'soil' and 'bedrock' are broad and have different meanings in different disciplines. For example, a soil scientist defines a soil as 'the unconsolidated mineral or organic material on the immediate surface of the Earth that has been subjected to and shows the effects of climate and macro- and microorganisms' (Natural Resource Conservation Service, 2013). An engineer, however, defines any unconsolidated material as soil, regardless of the ability to support organisms. For this study, the term 'soil' is used in the engineering sense, and refers to unconsolidated regolith. The term 'bedrock' refers to consolidated, or semi-consolidated rock-based material that may or may not include failure planes for deep-seated landslides.

Timber harvest in steep, hydrologically sensitive basins frequently leads to increased rates of landsliding, surface erosion, and total annual sediment flux (Jakob, 2000; Montgomery et al., 2000; Roering, 2003; Schmidt et al., 2001). Tree removal affects hydrological processes and the mechanical stabilization of tree roots on steep slopes (Sidle et al., 1985). Immature timber stands and shrubs replacing mature forests are less effective at intercepting precipitation and removing soil pore water through transpiration, resulting in increased water table elevation and soil pore pressure (Dhakal and Sidle, 2004). Roots for shrubs and immature forest are also typically shallower, less dense, and weaker than for mature forests, resulting in reduced effective soil strength (Montgomery et al., 2000).

The interactions of factors that control stability are complex and may vary temporally and spatially. As such, implementing a method for predicting the occurrence of slope failures that is simultaneously quantitative and practical for public use is challenging. One approach is to approximate the likelihood of slope failure by using easily measured variables as proxies. For example, some researchers have used statistical methods to relate the historical occurrence of landslides with storm intensity and magnitude (e.g., Berti et al., 2012; Chleborad, 2000; Godt, 2004). Others have investigated the spatial distribution of root density and strength with documented landslides (e.g., Roering et al., 2003; Schmidt et al., 2001). Many studies have taken advantage of recent advances in computational power

and high-resolution digital spatial data to use numerical modeling methods for characterizing slope failure susceptibility (e.g., Doten et al., 2006; Godt, 2004; Huang et al., 2006).

Numerical modeling is a useful and inexpensive tool for evaluating the various factors that contribute to slope stability. The Distributed Hydrology Soil Vegetation Model (DHSVM), developed at the University of Washington and Pacific Northwest National Laboratory (Doten et al., 2006; Wigmosta et al., 1994), and the RocScience SLIDE© 6.0 software program (www.rocscience.com) are two numerically-based tools for investigating the relationship between hydrology, soil and vegetation properties, surface morphology, and slope stability. In the Jones Creek basin, steep slopes combined with high annual precipitation and weak bedrock cause pervasive shallow and deep-seated slope instability. A variety of complex geomorphic and hydrologic processes contribute to frequent slope failures and debris flows of various magnitudes that pose a significant risk to the surrounding community (Jakob et al., 2004). The goal of my research is to use numerical modeling to evaluate the effects of precipitation on failure probability, and the potential implications of timber harvest, in the Jones Creek basin.

2.0 Background

2.1 Basin Characteristics

2.1.1 Location

The Jones Creek watershed is located approximately 30 kilometers east of Bellingham, Washington in western Whatcom County, directly west of the community of Acme on Washington State Route 9 (Figure 1). The creek drains a 6.8 km^2 basin on the east side of Stewart Mountain into the South Fork Nooksack River. The land on the north side of the creek channel is currently owned by Sierra Pacific, a timber company (Figure 2). The land on the south side of the creek is managed by the Washington State Department of Natural Resources (DNR). Approximately 250 people live and work in 100 buildings built on a composite fan deposited by the creek on the South Fork flood plain. In 2004, the buildings had an assessed value of 6.8 million dollars, and the total assessed land value exceeded 10 million dollars (Jakob et al., 2004).

Access to the watershed is limited to logging roads in the upper basin, and to Galbraith, Turkington, and Hudson Roads in the lower basin (Figure 3). Turkington Road provides the only direct public access to the creek. Bridges on the roads span the creek at the fan apex, 500 meters downstream from the fan apex and at the confluence of the creek with the South Fork, respectively. The Burlington Northern-Santa Fe Railroad crosses the creek six meters downstream from the Hudson Road bridge, where the creek is directed through a concrete culvert.

2.1.2 Topography

Elevation in the basin ranges from approximately 85 meters at the South Fork confluence to 950 meters at the top of Stewart Mountain. Slope varies from gentle at the mouth of the basin to steep gradients exceeding 50 degrees on the gorges flanking the stream channel (Figure 4). The creek channel can broadly be classified into three main reaches (Jakob et al., 2004; Figure 4). Reach one has a mean channel gradient of 12 degrees

and includes the stream above the fan apex. Reach two has a mean channel gradient of three degrees and includes the stream channel below the fan apex and above the Turkington Road bridge. Reach three includes the stream channel below the Turkington Road bridge and above the confluence of Jones Creek with the South Fork Nooksack River. The channel in this reach has been significantly modified has a mean gradient of one degree.

2.1.3 Geologic Setting

Two bedrock units underlie the Jones Creek watershed, separated by a northeast-trending fault (Jakob et al., 2004; Lapen, 2000; Figure 5). The upper two-thirds of the watershed are underlain by the Bellingham Bay member of the Chuckanut Formation. The Chuckanut Formation is comprised of Eocene-aged nonmarine sedimentary rocks deposited by a large meandering river system. The Bellingham Bay member is defined by fining-upwards cycles of sandstone, conglomerate, and mudstone (Johnson, 1984; Lapen, 2000). The lower third of the watershed is underlain by the Cretaceous-aged Darrington Phyllite. The Darrington Phyllite was likely derived from blueschist-grade subduction-related metamorphism of marine sediments ~120-130 million years ago (Brown, 1987; Lapen, 2000).

The phyllite is a mechanically weak unit that is prone to landslides due to extensive folding and faulting, pervasive sheared and foliated zones, a clay rich-mineralogy, and steep slopes (Thorsen, 1989). Numerous small rotational and infinite slope-style failures have been identified in phyllite-derived soils within the basin (Jakob et al., 2004). Additionally, there are four large deep-seated landslides hosted in the phyllite, situated directly adjacent to the stream channel. Various names have been used to identify the deep-seated landslides, but they are most commonly known as the Cutblock, Darrington, South and Straight slides (Currie and Morgan, 2010; Figure 5).

Estimating the extents of the active portions of the deep-seated landslides is challenging because of numerous ancient head scarps and uneven hummocky topography

that exist across the lower watershed. From mapping by Jakob et al. (2004), the surface areas of the Cutblock, Darrington, South and Straight slides are approximately 12,500 m^2, 162,600 m^2, 25,200 m^2, and 65,500 m^2, respectively. Depths and subsurface geometries of the slides are not well understood. Movement of the slides has not been quantified, but they are thought to be slow-moving and perhaps only episodically active (P. Pittman, personal communication, 2012).

All four of the slides, except the Cutblock, have at least partially unvegetated toes adjacent to the stream channel (Figure 6). The Darrington slide has the largest unvegetated area of approximately 1600 m^2 (Jakob et al., 2004). The South and Straight slides have unvegetated or partially unvegetated areas of 6,800 m2 and 2,500 m^2, respectively. Episodic shallow mass wasting on the unvegetated landslide toes, as well as unstable soils and channel cuts throughout the basin, provide a significant source of sediment to the stream. Over time, debris flows and fluvial processes have redistributed these sediments on a fan on the South Fork floodplain. Fans deposited exclusively by fluvial processes are called alluvial fans, and fans deposited exclusively by debris flows are called debris flow or colluvial fans (Jakob et al., 2004). Jones Creek is defined to be a composite fan because of combined fluvial and debris flow depositional processes.

The composite fan covers an area of 0.75 km^2 at the base of Stewart Mountain. The fan apex is located approximately 1.2 kilometers upstream of the confluence of Jones Creek with the South Fork. The fan comprises poorly sorted sands and gravels and displays a general lack of bedding. Stratigraphy suggests that both fluvial and debris flow processes have contributed to growth of the fan, with debris flows dominating (Jakob et al., 2004). Fan sediments are almost exclusively derived from the phyllite, suggesting that the lower watershed is the dominate source of debris flows in the basin (Jakob et al., 2004).

2.1.4 Vegetation

Vegetation cover in the upper watershed is defined by mixed shrub and grasses in logged areas, and coniferous forest (NOAA, 2006; Figure 2). The lower watershed is

primarily coniferous forest, with interspersed areas of mixed deciduous and coniferous forest. The composite fan has undergone significant urbanization and removal of tree cover, except for a 0.2 km^2 section of mixed forest that spans from the apex of the fan to the Turkington Road bridge (Jakob et al., 2004).

The watershed has been logged several times over the last century. Land on the south side of the creek was last logged in the 1980s. The most recent major logging cycle started in the late 1990s on the north side of Jones Creek and included activity in second growth forest in the groundwater recharge zones for both the Cutblock and Darrington slides (Jakob et al., 2004). Although the potential consequences of logging on the groundwater recharge zones of deep-seated landslides is unclear, some researchers have suggested that logging in the Jones Creek basin is likely to decrease slope stability for a period of five to ten years after harvest due to reduced evapotranspiration and root strength (Jakob et al., 2004).

2.1.5 Regional Climate

Weather patterns in western Washington are typical of a maritime climate (Elsner et al., 2010). Winters are usually mild, with an extended rainy season characterized by long periods of light to moderate intensity precipitation, and summers are generally cool and dry. High intensity storms that trigger slope failures generally occur from October through March, and may occur multiple times in a single winter season, or may not occur for a period of years. Although the duration and magnitude of high intensity storms is variable, they are generally characterized by a significant amount of precipitation falling in a period of one to three days. For example, in November, 2006, western Washington was inundated with approximately 18 inches of rain in 36 hours. In December, 2007, fifteen inches of rain fell over southwestern Washington in 24 hours. In January, 2009, approximately eight inches of rain fell in 48 hours over western Washington, with pronounced precipitation over Whatcom and Skagit Counties. Thousands of shallow slope failures in Washington State have been attributed to these storms alone (Washington Forest Protection Association,

2012). There are few precipitation gauges in the South Fork valley, but annual totals have been estimated at 40 to 50 inches (Raines et al., 1996).

The 'transient snow zone' is defined as the elevation range in which precipitation can fall as either snow or rain, and occurs in Washington between approximately 365 and 1220 meters (Washington Forest Practices Board, 1997). A large portion of the Jones Creek watershed falls in this range, although snowpack in the basin is usually minimal and intermittent. Winter temperatures in western Washington frequently fluctuate around freezing, and incoming warm fronts may quickly melt shallow snow packs. The influence of rain-on-snow events on slope failure is complex and depends on a number of factors, including the antecedent soil moisture conditions, the amount of water released from the snowpack, and the proportion of melt water that infiltrates the soil versus migrating to stream channels via overland flow (Powell et al., 2010). Rain-on-snow events are recognized as significant to both floods and slope failures throughout the Pacific Northwest (Harr and Coffin, 1992).

2.1.6 Slope Failure and Debris flow history

Slope failures in the Jones Creek watershed mostly go unobserved because of a lack of monitoring equipment and no residential population above the apex of the fan. Small debris flows and debris floods that are contained in the channel and cause aggradation on the fan are not uncommon, but are generally unreported because the impact to local residents is minor. Channel aggradation on the fan is an ongoing land management issue, particularly at the Turkington Road bridge where the county frequently dredges (P. Cooper, personal communication, 2011).

Major debris flows occurred in the watershed in 1953, 1983, 1990 and 2009 (Currie and Morgan, 2012; Jakob et al., 2004; Raines et al., 1996). All four events were associated with significant winter storms during which high precipitation totals fell over a short amount of time. Damage from the debris flows was significant and included flattened stands of mature trees at the fan apex, damage to both the Turkington and Galbraith

bridges, and overtopping of the Jones Creek channel on the fan. A likely trigger mechanism for large debris flows is a landslide dam outburst flood sourced at the toe of one of the large deep-seated slides (Jakob et al., 2004). Because of steep, narrow channels in the Jones Creek watershed, a landslide dam could impound a significant amount of water before outburst. A landslide dam could develop either by deep-seated rotational movement at the toe of one of the large landslides, or by shallow mass wasting.

2.2 Previous Research

The first slope stability investigation specific to Jones Creek was commissioned to aid in a land transaction between the state and the Trillium logging corporation (Thorsen et al., 1992). The report assigned slope stability classes to areas in the watershed based on air photo analysis and supplementary field investigations. In 1994, the Trillium Corporation funded a hydrologic and slope stability analysis of the Acme Watershed Administrative Unit (AWAU), which covers an area of 90 km^2 in the lower South Fork valley and includes the Jones Creek watershed (Figure 1; Figure 7). The watershed analysis was motivated by the need to identify the different types of hillslope hazards in the AWAU and assign specific logging prescriptions for the areas hosting the hazards. Ten unique Mass Wasting Unit (MWU) designations were used to classify hazardous areas in the AWAU, four of which are identified in the Jones Creek watershed (Crown Pacific Limited Partnership, 1999; Figure 8; Table 1). The MWU designations are based on analyzing aerial photographs from 1970 through 1995, and field reconnaissance in 1994 and 1998 (Crown Pacific Limited Partnership, 1999). Hillslope characteristics, including slope, topography classifications (convergent, divergent, planar), and stream order were recorded for each documented landslide. The MWU designations are based on the interpreted hillslope characteristics that are most often associated with landslides in the AWAU. MWU designations rely heavily on slope, and are based in part on field clinometer measurements of average hillslope gradients (Crown Pacific Limited Partnership, 1999). Prescriptions for the Jones Creek basin recommend against logging in MWUs, and particularly on the active portion of the deep-

seated landslides, and advocate maintaining an uncut buffer in the groundwater recharge zone of deep-seated landslides with an area equivalent to 50 percent of the active area of the slide (Crown Pacific Limited Partnership, 1999).

Impacts from the 1983 and 1990 debris flows provided motivation for a reconnaissance study and review of debris flow mechanics in the South Fork Valley by Raines et al. (1996), who assigned a return period of approximately 65 years to the 1983 debris flow based on trenching and dating of debris flow materials for nearby drainages. Concerned about the effects that longer return period events could have on the community surrounding Jones Creek, Whatcom County commissioned Kerr Wood Leidal Associates (KWL) in the early 2000s to continue the work started by Raines et al. (1996) and provide a detailed hazard assessment and mitigation recommendations (Jakob et al., 2004). The Kerr Wood Leidal investigation included a detailed trenching survey on the Jones Creek fan and continued reconnaissance study of the landslides above the fan apex. KWL identified six catastrophic-level debris flow sequences on the fan deposited over the past 7000 years, and concluded that a 500 year return-period debris flow having a total sediment volume in excess of 90,000 m^3 should be used as a design event for mitigation. The report also concluded that lax enforcement of logging recommendations in the groundwater recharge zones of the deep-seated landslides on the north side of Jones Creek alters basin hydrology and thus, significantly decreases slope stability in the basin for at least 10 years after harvest (Jakob et al., 2004). The 2009 debris flow provided motivation for a follow up report by KWL in 2010 (Currie and Morgan, 2010). The follow up report concluded that risk for landslide dam outburst floods at Jones Creek is slightly higher than suggested in the 2004 report due to increased activity on the deep seated landslides, but that 2004 design recommendations remain appropriate.

2.3 Slope Stability

2.3.1 Conceptual Overview

Slope stability is influenced by a variety of controlling factors, including slope geometry, material strength, and hillslope hydrology (e.g., Burton and Bathurst, 1998; Hammond et al., 1992; Wu and Sidle, 1995). Slope failure can occur when external stress exceeds soil strength. Hence, slope stability is fundamentally a function of the balance of forces acting on a soil or rock mass. One method that has been widely used for quantifying the force balance is limit equilibrium analysis, which defines the state at which shear stress and shear strength are in equilibrium (e.g., Duncan and Wright, 2005; Lu and Godt, 2013; Nash, 1987; Stead and Coggan, 2012). A brief explanation of slope stability in the context of simple two-dimensional limit equilibrium follows.

The weight of a mass resting on a slope can be divided in to two components. The first component, known as the driving force, acts parallel to the slope in a down slope direction and pulls the material mass down the slope. By trigonometry, the magnitude of the driving force is defined as

$$F_D = W sin\alpha \quad (1)$$

where F_D is the driving force, W is the soil weight, and α is the slope angle. The second component, known as the normal force, acts perpendicular to the slope and holds the soil mass in place. The magnitude of the normal force is quantified as

$$F_N = W cos\alpha \quad (2)$$

where F_N is the normal force , W is the soil weight, and α is the slope angle. Normal force acts to hold the soil mass in place by generating a friction force at the slip surface (Lu and Godt, 2013). Friction acts in all directions, including opposite to the driving force. Some

soils also have a cohesive force due to molecular attraction between grains, pore water surface tension, or intergranular cementation (e.g., Lu and Likos, 2006). Normal force, friction force, and cohesion are collectively known as resisting forces and determine the total magnitude of soil shear strength. Shear strength is defined by the Mohr-Coulomb failure criterion in units of stress as

$$\tau = \sigma tan\phi + c \tag{3}$$

where τ is the soil shear strength, σ is normal stress acting on the slope, ϕ is the friction angle of the soil and c is the molecular cohesion of the soil (Coulomb, 1776; Labuz and Zang, 2012; Mohr 1900). Equation 3 can be expressed in units of force as

$$F_R = Wcos\alpha tan\phi + cA \tag{4}$$

where F_R is the total resisting force and A is the area of the potential failure surface. The ratio of resisting force to driving force is known as the factor of safety

$$FS = \frac{F_R}{F_D} \tag{5}$$

where FS is the factor of safety, F_R is the resisting force, and F_D is the driving force. If the magnitude of the resisting force is less than the magnitude of the driving force, the factor of safety is less than one and the slope is unstable. Substituting equations 1 and 4 in to Equation 5 gives the generalized factor of safety equation for sliding on a planar slip surface:

$$FS = \frac{Wcos\alpha tan\phi + cA}{Wsin\alpha} \tag{6}$$

2.3.2 Pore Fluid Pressure

Pore water in a soil affects the force balance in two ways. The added weight of pore water increases the weight of the soil mass, and thus the magnitude of both the driving and resisting forces. However, pore fluid pressure imparts a buoyancy force on the soil grains that acts upwards and perpendicular to the water table. If the water table is parallel to the slope, the buoyancy force counteracts the normal force and results in a reduced effective normal stress (Terzaghi, 1936, 1943). Terzaghi's effective stress is quantified as

$$\sigma' = \sigma - u_w \qquad (7)$$

where σ' is the effective stress, σ is the total stress due to the weight of the overlying soil and water, and u_w is the pore fluid pressure. The effective stress concept is important in slope stability analysis, because the magnitude of the effective normal stress dictates the frictional resistance to failure (Equation 3). The greater the saturated thickness of the soil, the greater the pore fluid pressure at the slip surface, and the less the soil shear strength and hence, factor of safety.

2.3.3 Soil Cohesion

The term 'cohesion,' as it relates to soil mechanics, has a number of meanings and usages in quantitative slope stability analysis (Lu and Godt, 2013). In general, cohesion refers to some additional strength in the soil beyond what is offered by the friction angle (ϕ). Hence, cohesive soils may be stable even when surface slope exceeds the friction angle. An important distinction between cohesion and the friction angle (ϕ) is that resisting forces due to cohesion are independent of soil weight (Equation 6). Sources of soil cohesion include electrostatic attraction between soil particles, intergranular cementation, and negative pore pressure due to matric suction in the unsaturated zone (Lu and Godt, 2013; Sidle et al., 1985).

Electrostatic attraction and van der Waals forces between soil particles is a common source of cohesion in soils rich in clays and silts (de Blasio, 2011; Sidle et al., 1985; Six et al., 2000). Silt and clay minerals typically have complex molecular structures. Isomorphous substitution of cations of differing charges in the mineral framework, and imperfections in molecular structure, can result in changes in the surface charge of the soil particles (Mitchell, 1976). The resulting intermolecular forces between the particles act to bind the soil mass and hold it in place. Sandy soils dominated by silica typically lack this kind of cohesive strength, and are sometimes referred to as 'cohesionless' even if they have cohesive strength offered by other mechanisms. The magnitude of cohesion lent by intermolecular forces is influenced by particle size, crystalline properties, type of adsorbed cations, pore water chemistry, and degree of saturation, and can be on the order of tens of kilopascals (Lu and Godt, 2013; Mitchell, 1976).

Intergranular cementation is the strength lent by precipitation of dissolved minerals at particle contacts. The additional binding in cemented soils can significantly increase the shear strength of soil (Fernandez and Santamarina, 2001). Cementation usually occurs in the unsaturated zone of the soil (Lu and Godt, 2013). On the west coast of the United States, cementation in unconsolidated deposits is most likely to occur in emergent coastal bluffs (Collins and Sitar, 2011).

In the unsaturated zone of a soil, pore pressure may be negative due to capillary forces resulting from the interaction of soil, water, and air (surface tension) in the soil pore space. This suction stress can increase effective stress in the same way that positive pore pressures can decrease effective stress in the saturated zone (Lu and Likos, 2006; Lu et al., 2010). Hence, partially saturated soils may have an apparent cohesion due to binding effects of water tension (e.g., Cho and Lee, 2001; Kayadelen et al., 2007; Kim et al., 2004). The magnitude of suction stress depends on the degree of soil saturation. Transient changes in apparent cohesion in the unsaturated zone are complex and may represent an important control on slope stability, particularly for fine-grained soils (Lu and Godt, 2013).

In the Pacific Northwest, where the Jones Creek basin is located, soils commonly have high water contents during the winter months. The effects of pore pressures in the unsaturated zone are not likely to have a significant effect on slope failures in the basin. Cemented soils, which are most common in soils where evaporation is active, or where there is a high concentration of dissolved salts in the groundwater, are also unlikely given the geographic setting of the basin (Lu and Godt, 2013). For this study, 'cohesion' means the portion of soil shear strength lent by intermolecular forces in silts and clays. Suction stress and cementation are not considered.

2.3.4 Root Cohesion

Vegetation can increase slope stability through the binding effects of roots in soil. Although this binding effect is actually a mechanical reinforcement, it is generally treated as additional source of cohesion in the Mohr-Coulomb failure criterion for computational simplicity (e.g., Burton and Bathurst, 1998; Doten et al., 2006; Hammond et al., 1992; O'Loughlin, 1974). Root cohesion varies with species, growth maturity, health, and growth density, and generally ranges from two to 40 kPa (Coppin and Richards 1990; Lu and Godt, 2013; Montgomery et al., 2000).

Root strength is tensile, and is a function of root size, density, and depth (Nilaweera and Nutalaya, 1999). Understanding the conversion of tensile root strength to soil shear strength is important and represents a significant challenge to quantitative slope stability analysis (Bischetti et al., 2005; Lu and Godt, 2013). In general, small roots have a higher tensile strength than coarse roots, but a lower resistance to bending (Bischetti et al., 2005). Small roots bolster soil strength by providing tensional resistance to sliding, and frictional resistance at the soil-root interface (Gray and Leiser, 1982; Schmidt et al., 2001; Zhou et al., 1998). Large, stiff roots can act as anchors that directly bolster shear strength across potential failure planes (Schmidt et al. 2001). Small roots typically far outnumber large roots. As much as 96 percent of tree roots are less than a centimeter in diameter for most species (Abernethy and Rutherfurd, 2001).

Root density is one of the most important factors governing the contribution of roots to soil strength. Root density is significantly more important than tensile strength for stabilizing slopes (DeBaets et al., 2008). Because small roots typically have a higher root density than large roots, small roots are probably most important in stabilizing shallow soils (Abernethy and Rutherfurd, 2001). Root density decreases with soil depth, particularly for small roots, and so the stabilizing effects of small roots may be negligible in thick soils (Abernethy and Rutherfurd, 2001). Peak root density is typically found between 20 to 30 centimeters of depth in the soil for most tree species (Bischetti et al., 2005). Large anchoring roots are often the only significant source of root cohesion in deep soils, and if root density is low, failures may simply propagate around them (Cammeraat et al., 2005)

Although many slope stability analyses treat root cohesion as being uniformly distributed throughout the soil mass, root cohesion is often heterogeneous, even over small areas, in both the vertical and horizontal directions (Montgomery et al., 2000; Schmidt et al., 2001). This is primarily due to substantial spatial variability in both intraspecies and interspecies root density (Abernethy and Rutherfurd, 2001; Bischetti et al., 2005). In fact, back analysis techniques using values for root cohesion, soil cohesion, friction angle, and water table depth typical of Pacific Northwest slopes often predict stability for areas where landslides have occurred. Therefore, spatial and temporal heterogeneity in root cohesion may be a governing factor for slope stability (Roering et al., 2003).

2.3.5 Friction Angle

The friction angle is the maximum slope angle that a soil mass can achieve before failing, when additional shear strength lent by cohesion is ignored. Friction angle describes the degree of roughness that exists between grains, independent of overlying soil weight. However, friction force does depend on the overlying soil weight, and is defined as the portion of soil weight acting normal to the slope multiplied by the tangent of the friction angle (Equation 3). Hence, friction force increases with increasing depth in a soil profile.

Friction angle is a function of particle shape and roughness, which are determined by mineralogy, physical and chemical weathering history, and packing arrangement (Albert et al., 1997; Nougier-Lehon et al., 2003). Coarse, sand-sized particles are dominantly shaped by mechanical processes, and finer silt and clay-size particles are dominantly shaped by chemical processes (Margolis and Krinsley, 1974). Sand particles are more likely than silts and clays to have surface blemishes due to brittle chipping and breaking during transport (Cho et al., 2006). Silt and clay size particles tend to break along molecular planes of weakness and form platy, elongated grains of relatively low surface roughness. Hence, friction at grain-to-grain contact points is usually greater for sands than for silts and clays (Lambe and Whitman, 1979). Because sand grains are typically more equidimensional than silt and clay grains, they can occupy a more interlocked packing arrangement that provides additional frictional resistance to sliding, which is sometimes called an apparent cohesion (Lu and Godt, 2013). Friction angles in soils, which usually contain a mix of particle sizes and shapes, range from less than eight degrees in soils dominated by clays and silts to greater than 40 degrees in soils dominated by sands (Lambe and Whitman, 1979).

2.3.6 The Infinite Slope Equation

Limit equilibrium analysis defines the state at which shear stress and shear strength are in equilibrium. Infinite slope analysis is one limit equilibrium technique that is commonly used when soil thickness is thin compared to slope length (Burton and Bathurst, 1998; Figure 9). Infinite slope analysis applies when a soil mantle overlies an impermeable layer of bedrock or higher-density soil (Sidle et al., 1985). Water table fluctuations elevate pore pressure at the interface between the layers and may trigger slope failures. Infinite slope analysis is frequently used in modeling applications because it is computationally simple, the governing variables are easily measured and widely reported in the literature; and it describes a failure mechanism that is common in forested watersheds (e.g., Muntohar and Liao, 2009; Montgomery and Dietrich, 1994; Wu and Sidle, 1995). The infinite slope equation follows the Mohr-Coulomb failure criterion, with additional

geometric manipulations and terms that quantify the effects of root cohesion, loading stress due to overlying vegetation weight, and water-table induced changes in effective stress and soil weight. A detailed derivation is found in Abramson et al. (2002). The infinite slope equation for a cohesive, partially saturated soil is defined as

$$FS = \frac{C_r + C_S + cos^2\alpha[q_o + \gamma(D - D_w) + (\gamma_{sat} - \gamma_w)D_w]tan\varphi}{sin\alpha cos\alpha[q_o + \gamma(D - D_w) + \gamma_{sat}D_w]} \quad (8)$$

where *FS* is the factor of safety, C_r is root cohesion (kPa), C_s is soil cohesion (kPa), α is the slope angle (degrees), q_o is vegetation surcharge (the loading stress due to the weight of overlying vegetation; kPa), γ is unsaturated soil unit weight (kg/m^3), γ_{sat} is saturated soil unit weight (kg/m^3), γ_w is water unit weight (kg/m^3), D is total soil thickness (m), D_w is saturated soil thickness (m), and ϕ is friction angle (degrees).

The infinite slope equation depends on several assumptions. Soil thickness is assumed to be uniform, and soil cohesion, root cohesion, and friction angle are assumed to be uniformly distributed at the potential slip plane (Sidle et al., 1985). The water table is assumed to be planar and parallel to the ground surface, which is generally valid for colluvial slopes (Hammond et al., 1992). Because the infinite slope equation is calculated in two dimensions, it is assumed that resistance along the sides of the failure is small compared to resistance along the base. The infinite slope equation may underestimate the factor of safety for long, narrow failures where a large proportion of the failure surface is on the sides of the block (Abramson et al., 2002; Hammond et al., 1992; Tarolli and Tarboton, 2006). For this study, failures are calculated over 10 meter grid cells that are significantly wider than they are deep, and resistance along the cell sides is not likely to be significant compared to resistance along the base.

The infinite slope factor of safety increases with increasing friction angle and soil and root cohesion, and decreases with increasing slope, soil depth, soil unit weight, saturated thickness, and vegetation surcharge. The degree to which the infinite slope equation is

sensitive to each parameter depends in part on the range of values over which it is evaluated. In general, the equation is most sensitive to changes in slope, root and soil cohesion, and soil thickness, moderately sensitive to friction angle and saturated soil thickness, and least sensitive to soil unit weight and vegetation surcharge (Gray and Megahan, 1981).

The relative sensitivity to some infinite slope equation parameters depends on the magnitude of the other parameters. This is particularly true for soil thickness and slope angle. For example, thin soils are more sensitive to soil and root cohesion than thick soils, and less sensitive to friction angle (e.g., Wu and Sidle, 1995). Sensitivity to cohesion increases with increasing slope angle, because normal force, and hence the contribution of friction to shear strength, decreases with increasing slope angle (Sidle, 1984). Similarly, water table fluctuations have a greater effect on the factor of safety for cohesionless soils than cohesive soils, because all else being equal, shear strength is less in cohesionless soils (Sidle, 1984). In the Jones Creek watershed, phyllite-derived soils are clay-rich and likely to be at least moderately cohesive, slopes are steep, and soil profiles are likely to be thin (Jakob et al., 2004). Hence, infinite slope analysis is likely to be most sensitive to soil and root cohesion, followed by friction angle and water table fluctuation.

2.3.7 Method of Slices

For rotational landslides, the slope angle varies along the base of the failure, and the depth to the slip plane and saturated soil thickness are not constant. A slope stability equation assuming a planar failure surface is not appropriate. One approach for approximating the factor of safety of a rotational slip plane is to divide the potential failure mass in to a number of slices of equal width, and calculate the factor of safety as either a summation of forces at the base of each slice, or a summation of moments (e.g., Al-Karni and Al-Shamrani, 1999; Zhang, 2012; Figure 10). The limitation of this method is that some of the forces acting on each slice are simplified or ignored, in order to make the analysis determinate (Fredlund et al., 1981).

Different limit equilibrium techniques deal with the force equilibrium problem in different ways. The forces that must be considered include interslice vertical, (shear), interslice horizontal, slice base normal, and slice base shear (Fredlund and Krahn, 1977; Figure 10). Interslice vertical force is the shear force acting at the interface between slices. Interslice horizontal force is the normal force acting perpendicular to the interface between slices. Slice base normal force is the portion of the slice weight acting normal to the slip surface. Slice base shear force is the portion of slice weight acting parallel to the slip surface. The fundamental difference between the various limit equilibrium methods lies in how interslice forces are treated, because the normal force at the base of each slice is dependent on the forces acting on the sides (Krahn, 2003).

Three common methods of slices techniques are Spencer's Method, Janbu's Simplified Method, and Bishop's Simplified Method. Spencer's method assumes a constant relationship between interslice shear and normal forces (Spencer, 1967). The normal force at the slice base is calculated by summing forces perpendicular to the interslice forces. Spencer's Method gives two factor of safety equations, one based on a summation of moments, and one based on a summation of forces parallel to the interslice forces. Janbu's Simplified Method uses a correction factor, based on cohesion, friction angle, and the geometry of the slip surface, to account for interslice shear forces (Janbu et al., 1956). The correction factor is used in a summation of vertical forces to derive the normal force at the slice base, and the factor of safety is calculated based on horizontal force equilibrium. Bishop's Simplified Method, used in this study, ignores interslice shear forces and assumes that normal or horizontal forces adequately characterize the stress distribution on each slice (Bishop, 1955). The factor of safety is derived by summing the moments around a common axis of rotation. Hence, Bishop's Simplified Method satisfies moment equilibrium, but not force equilibrium. One form of the factor of safety equation for Bishop's Simplified Method is

$$FS = \frac{\sum \frac{c + \left(\left(\frac{W}{b}\right) - u\right) tan\phi}{cos\alpha + \frac{sin\alpha tan\phi}{FS}}}{\sum \left(\frac{W}{b}\right) sin\alpha} \quad (9)$$

where *FS* is the factor safety, *c* is soil cohesion (kPa), *W* is the slice weight (kg/m^3), *u* is pore fluid pressure at the base of the slice (kPa), ϕ is friction angle (degrees), α is the angle from horizontal that a tangential line makes with the base of the slice (degrees), and *b* is the slice width (m). The *FS* term appears on both sides of the equation, meaning the equation is transcendental and must be solved iteratively.

The accuracy of limit equilibrium methods for slope stability analysis depends on the complexity of the slope geometry and materials being analyzed. The Bishop's Simplified Method is most accurate in situations where the slide is approximately moving as a single coherent mass (Krahn, 2003). In this situation, interslice shear force is not likely to have a great impact on the factor of safety (Spencer, 1967). In geologically complex landslides that are comprised as series of rotating blocks, interslice shear forces play an important role in the overall factor of safety for the slope, and Bishop's Simplified Method may give a conservative factor of safety compared to more rigorous, time consuming methods of analysis (Sharma and Lovell, 1983).

2.3.8 Effects of Timber Harvest on Slope Stability

Timber harvest can influence slope stability in two broad ways: alteration of watershed hydrology and root strength loss. Soils in post-harvest landscapes are generally characterized by increased water table elevation, and hence, a loss of shear strength (Brown and Sheu, 1975; Sidle et al., 1985). Vegetation reduces recharge and storage by drawing water from the soil and by intercepting a portion of direct precipitation in the canopy (Dhakal and Sidle, 2004). Some of the water stored in the canopy evaporates, and some is gradually delivered to the soil by leaf and stem drip (Spittlehouse, 1998).

Therefore, the vegetation canopy acts as a buffer that dampens the effective precipitation intensity and slows the rate of water delivery to the soil. The magnitude of canopy interception is species and growth stage-dependent (Sakals et al., 2006). For example, conifer forest canopies are typically denser than deciduous forest canopies, and intercept a greater percentage of precipitation (Link et al., 2004). In basins defined by coniferous forest, such as the Jones Creek watershed, canopy interception and loss is usually about 10 to 30 percent of total rainfall (Link et al., 2004). When forest canopy coverage is reduced after harvest, the water table may elevate more rapidly, and to a greater degree, in response to storm events (Dhakal and Sidle, 2004; Keim and Skaugset, 2003; Swanston, 1974).

Whereas the hydrologic effects of canopy loss are immediate following harvest, the reduction in soil shear strength due to the loss of root cohesion is more gradual. After harvest, a residual root mass is retained in the soil and slowly decays. Depending on species, the onset of root decay starts within three weeks to 12 months (Watson et al., 1999). The rate of decay is variable, but in general, root strength is reduced by half within two to three years after harvest, and is usually completely reduced within five years (O'Loughlin, 1974; Wu et al., 1979). Root strength can regenerate over time, as replacement vegetation matures. However, root strength in mature forests can be considerable, and a return to pre-harvest stability conditions through the maturation of replacement-stand vegetation may take many years, or never be achieved at all (Schmidt et al., 2001). If shrubs replace harvested trees, the new root morphology may have a shallow rooting depth and reduced tensile strength. Hence, slopes may be permanently destabilized after the residual root strength has fully decayed, particularly in thick soils where the anchoring effects of deep tap roots are important.

The combined effects of reduced evapotranspiration and root strength have significant implications for slope stability in mountain watersheds. Researchers have found that landslide density in clear-cut forests is at least two to three times greater than in natural forests (e.g., Montgomery et al., 2000, Snyder, 2000). The greatest change in

landsliding rates are often most accentuated on moderate slopes. For example, Brardinoni et al. (2002) found that post-harvest failure volumes on moderate slopes is comparable to those found at gradients as much as 10 degrees steeper in naturally forested basins. Also, the geomorphic and hydrologic effects of harvest can be long-lasting. Significantly increased mass wasting and erosion rates may pervade for more than 15 years after harvest (Brardinoni et al., 2002; Jakob, 2000).

2.4 Models

2.4.1 DHSVM Hydrology Model

The DHSVM is a physically based, spatially distributed hydrologic model developed at Pacific Northwest National Laboratory and the University of Washington (Wigmosta et al., 1994). The foundation for the DHSVM is a digital elevation model (DEM). Every grid cell in the DEM is assigned a characteristic vegetation class, soil class, and soil depth. Vegetation classes include parameters that define rooting depths and total evapotranspiration potential. Soil classes include parameters that characterize vertical and lateral hydraulic conductivity, infiltration rate, surface albedo, porosity, and bulk density. Precipitation, air temperature, wind speed, relative humidity, short wave radiation and long wave radiation are applied as inputs to the model over a user defined time step that ranges from one hour to one day.

The DHSVM simultaneously simulates a water and energy balance for every grid cell at each time step. Hydrologic processes considered in the model calculations include evapotranspiration, snowpack accumulation and melt, canopy snow interception and release, unsaturated and saturated subsurface flow, overland flow, and channel flow. Water migrates between cells by saturated subsurface flow, or by overland flow. Overland flow occurs when precipitation intensity exceeds the infiltration capacity of the soil, or when the entire thickness of the soil column becomes saturated. Water is eventually routed to the stream network and transported out of the basin.

The DHSVM hydrology model was first validated for the 2900 km^2 Middle Fork Flathead River basin in northwestern Montana (Wigmosta et al., 1994). DHSVM has also been used as a tool for investigation in to the effects of land use change on watershed hydrology. Various studies have examined the effects of logging roads, timber removal, watershed urbanization, and climate change on stream flow and the timing and magnitude of flood events (e.g., Bowling et al., 2000; Bowling and Lettenmaier, 2001; Cuo et al., 2008; Dickerson, 2010; Leung and Wigmosta, 1999; Storck et al., 1995; Storck et al., 1998; Wigmosta and Perkins, 2001).

2.4.3 DHSVM Sediment Module

The DHSVM sediment module was developed as secondary application of the DHSVM hydrology model (Doten et al., 2006). Output from the hydrology model is redistributed across a high-resolution DEM, and is combined with mechanical soil properties to simulate sediment flux by four processes: mass wasting, hill slope erosion, road erosion, and channel routing (Figure 11). Mass wasting is the only component of the sediment module used in this study.

The DHSVM mass wasting algorithm is computationally intensive and only runs during the time step with the greatest basin saturation during a storm event. In order to maximize computational efficiency, the DHSVM uses a screening process for each grid cell prior to performing failure calculations. First, each cell is checked for the presence of sediment. Cells without sediment are discarded from the screening process. Second, cells that do not meet a minimum user-defined surface slope are not considered likely candidates for slope failure and are discarded. Doten et al. (2006) noted that shallow failures rarely occur in soils with surface slopes below ten degrees, and used that as the minimum value for cells considered in the mass wasting algorithm.

All cells that are not discarded during the screening process are subject to a slope failure calculation based on an infinite slope model (e.g., Burton and Bathurst, 1998; Hammond et al., 1992). The DHSVM uses a Monte-Carlo style stochastic approach for

simulating slope failure. Values for soil cohesion, friction angle, root cohesion and vegetation overburden are chosen randomly from user-defined probability distributions, and are then used to solve the infinite slope failure equation. The process is repeated for a user-defined number of iterations. Typically, 1000 iterations is a sufficient for reproducible results (Hammond et al., 1992). Final output is a cell-by-cell probability of failure, given by the following equation:

$$P = \frac{x}{n} \qquad (9)$$

Where P is the probability from 0 to 1, x is the number of iterations for which failure is predicted, and n is the total number of iterations. The two primary advantages of a stochastic model over a deterministic model are that some of the heterogeneity of natural systems can be quantified, and uncertainty in the true field conditions of the soil and vegetation can be accounted for (Hammond et al., 1992).

The DHSVM sediment module was first validated for the 44 km^2 Rainy Creek basin in north central Washington State (Doten et al., 2006). Slope failures predicted by the model matched reasonably well with failures observed in a historical air photo survey. The annual simulated sediment yield matched well with literature values based on basin size. Other applications of the sediment module include investigation in to the effects of forest fires, logging, and watershed urbanization on watershed sediment yield (e.g., Barik, 2010; Ottenbreit, 2011; Surfleet et al., 2012; Tangedahl, 2006).

2.4.4 RocScience SLIDE Software

The RocScience SLIDE© 6.0 software program is a comprehensive tool for modeling slope failures (RocScience SLIDE version 6.0 released June, 2010; www.rocscience.com). SLIDE includes a full suite of tools for defining slope geometries, soil mechanical properties, groundwater conditions, as well as probabilistic and sensitivity analysis capabilities. Because the program is primarily designed to evaluate large failures with slip planes below

the rooting zone, it does not consider the effects of vegetation root strength or evapotranspiration. SLIDE is an industry-standard software tool and has been used in numerous academic and professional applications (e.g., Brandon et al., 2008; Brideau et al., 2009; Duncan et al., 2008; Gao et al., 2010; Neuffer and Shultz, 2006).

All of the standard method of slices analysis techniques can be used in SLIDE, including Spencer's, Janbu's and Bishop's methods. Although the calculations for these techniques are not overly difficult, it is time consuming to manually perform them over a wide range of failure geometries. SLIDE can quickly calculate the factor of safety for thousands of surfaces at a variety of depths and orientations. Thus, given a slope profile, SLIDE can isolate the most likely failure geometry by finding the failure surface with the lowest factor of safety.

2.5 Precipitation Thresholds

Precipitation thresholds curves are tools used for predicting the occurrence of landslides. The fundamental concept behind precipitation thresholds is that the likelihood that a storm results in slope failure depends on both the total magnitude of precipitation, and the rate at which it falls (Chleborad, 2000). Rate, or intensity, is the average precipitation magnitude that falls per some unit of time. Total storm magnitude is determined by the intensity and the duration of the storm. Precipitation intensity and duration influence the behavior of the water table response to storms. For example, a low-intensity, long-duration storm could deliver the same total magnitude of precipitation to a hillslope as a high-intensity, short-duration storm. However, high-intensity precipitation may overwhelm the soil's ability to transmit water downslope, causing a rapid rise in the water table (Crosta, 1998). Hence, slope failure is more likely for the high-intensity storm. In this hypothetical case, the difference in failure likelihood is solely driven by a difference in storm intensity. In reality, total precipitation magnitude is likely to vary between storms, and so magnitude and intensity are both important.

Precipitation thresholds are constructed by compiling precipitation data for historical storm events that resulted in slope failure, and then plotting the events according to various parameters that describe the antecedent precipitation conditions that led to failure. Parameters that are commonly used for precipitation thresholds include intensity, duration, and total magnitude. A minimum threshold that describes the range of precipitation characteristics that are likely to trigger landslides can then be interpreted and characterized with an equation. The first global intensity –duration threshold was proposed by Caine (1980). Several researchers have since proposed precipitation thresholds at a variety of geographic scales. For example, Chleborad's (2000) cumulative precipitation threshold for landslides in the Seattle area compares total rainfall for the three days prior to a landslide to total rainfall in the previous 15 days (Figure 12). Godt's (2004) intensity-duration threshold for the Seattle area compares storm duration in hours to storm intensity (Figure 13). In the case of the Godt threshold, storms considered likely to trigger slope failure have an intensity that is at least equivalent to

$$I = 3.257D^{-1.13} \qquad (11)$$

where *I* is intensity (inches per hour), and *D* is duration (hours).

Deterministic precipitation thresholds never achieve the ideal of always correctly predicting slope failure, primarily because precipitation is only one of many factors that influence the occurrence of landslides (Aleotti and Chowdhury, 1999). One way to handle this problem is to statistically derive failure probabilities associated with threshold exceedance (e.g., Frattini et al., 2009; Jaiswal and van Westen, 2009). Exceedance probabilities can be estimated by statistically analyzing the number of times that historical storms exceeding the interpreted threshold have actually resulted in slope failures. For example, exceedance of the Chleborad (2000) threshold corresponds to an eight percent probability of slope failure, and exceedance of the Godt (2004) threshold corresponds to a 42 percent probability of slope failure.

3.0 Research Objectives

The relationship between precipitation, groundwater, and soil and vegetation has important implications for slope stability and appropriate land management practices in the Jones Creek watershed and surrounding community. Numerical modeling is a useful, inexpensive tool for slope stability analysis. The primary objectives for this study are to establish probability thresholds for shallow failures on the unvegetated landslide toes, supplement current logging prescriptions by using high-resolution digital data sets to investigate the potential effects of timber harvest on shallow slope stability, and construct some simple models to evaluate the likelihood of deep rotational failures in the unconsolidated landslide material. The secondary objective for this study is to evaluate the use of the DHSVM as a tool for predicting slope failure susceptibility in geomorphically complex watersheds.

4.0 Methods

4.1 Scope of Work

To satisfy my research objectives, this project required seven main tasks:

1. Develop the grid-based DHSVM inputs for the Jones Creek watershed.
2. Collect and format a meteorological time series for the model (approximately 35 years).
3. Collect stream discharge data at the basin outlet and calibrate the model to the measurements.
4. Run the mass wasting component of DHSVM for the largest storm event of each year in the meteorological time series, and create composite failure susceptibility maps.
5. Run the mass wasting component of DHSVM for a range of historical storm events and create precipitation threshold curves that relate antecedent precipitation duration and intensity to failure probability.
6. Modify the vegetation inputs to reflect hypothetical logging scenarios and compare the failure maps for pre and post logging scenarios.
7. Use the RocScience SLIDE software to evaluate deep-seated rotational slope instability at the unvegetated landslide toes.

4.2 Field Methods

Field investigations for this project included stream flow monitoring and field reconnaissance to verify the position of the previously mapped landslide toe locations (e.g., Jakob et al., 2004; Thorsen et al., 1992). I used a Marsh McBirney Flo-Mate and a wading rod to take 15 stream flow measurements over five storms from October, 2011 to March, 2012, following the USGS midpoint method, approximately 25 meters downstream from the Turkington Road bridge (Rantz, 1982). I timed flow measurements to coincide with storms in order to capture a range of stream flow magnitudes with which to calibrate DHSVM simulated stream flow. I attempted to capture the stream flow response to precipitation by

taking multiple measurements for each storm**.** Additionally, I compiled supplementary stream stage data from a USGS-operated stream gauge located at the bridge. The stream gauge measures the height of water at a single point in the channel over time, and does not directly measure volumetric discharge. If channel morphology is relatively constant, stage can be related to volumetric discharge by fitting a regression model to measured stage and discharge data pairs. Thus, stage records and manual flow measurements are generally used together to characterize transient stream flow behavior. However, The USGS stream flow data from the Turkington Road bridge gauge are not usable for this study. The stream channel near the bridge is geomorphically unstable and is frequently aggrading and changing position during the winter months (P. Cooper, Personal Communication, 2011). Consequently, the gauge frequently malfunctions or becomes buried and does not record an accurate stream flow record. The channel migrated several times during the course of this study.

Field reconnaissance revealed numerous small slope failures and unvegetated channel cuts in the basin, in addition to the four major landslides. One study limitation is that land cover and soil type grids are input to DHSVM at 30 meter resolution. Smaller features cannot always be correctly resolved with the DHSVM spatial inputs. Hence, small, localized failures may be under-predicted by DHSVM.

4.3 DHSVM Modeling

4.3.1 Model Setup

Physical data inputs required by DHSVM that are publicly available in digital format include land cover, DEMs, and soil type. I used ESRI's ArcGIS 10.0 software to process and format the data to make it suitable for use in DHSVM. All of the data had to be converted to grid format, and matched to a basin boundary I determined with ArcGIS watershed delineation tools. An explanation of the model setup process is detailed in the work of previous researchers (e.g., Dickerson, 2010).

I obtained DEMs for the basin from the Puget Sound LiDAR Consortium. LiDAR (Light Distance And Ranging) employs an airborne scanning laser rangefinder to produce detailed topographic surveys (Puget Sound LiDAR Consortium, 2006). For this study, I resampled the LiDAR DEMs to 30 meter resolution for the hydrology model, and 10 meter resolution for the sediment model (Figure 14). Although 30 meter and 10 meter DEMs are available from sources other than LiDAR surveys, resampled LiDAR data may more accurately depict some landforms because of high-resolution bare earth characterization. The DHSVM mass wasting model is optimized to distribute soil moisture data from the 30 meter hydrology grids to a 10 meter DEM for failure simulation. I chose to run the model at the optimized resolution, because some researchers have reported problems with the model output when deviating to other resolutions, even for small basins (B. Huggett, personal communication, 2013).

Soil data are available from the United States Department of Agriculture (USDA) State Soil Geographic (STATSGO) database. STATSGO is a broad inventory of soil types and their geographic extents (Natural Resource Conservation Service). While the raw USDA soils data defined separate soils overlying the two bedrock units in the watershed, the landslides are likely to have different hydrologic and mechanical properties than the surrounding soils and are not characterized in the STATSGO data. I used ArcGIS to add a unique soil class to represent the landslides (Figure 15).

Land cover data are available from the National Oceanic and Atmospheric Association (NOAA). The most recent NOAA land cover data for Washington State was collected in 2006 using 30 meter resolution Landsat Thematic Mapper and Landsat Enhanced Thematic Mapper satellite imagery (National Oceanic and Atmospheric Association, 2006). The NOAA data define most of the bare landslide toes as coniferous forest. I used Esri's ArcGIS 10.0 to redefine bare zones on a cell-by-cell basis, following my own field observations and the mapping of previous researchers (Currie and Morgan, 2010; Jakob et al., 2004; Figure 16).

DHSVM requires a stream network and a soil depth grid. Both of these parameters are derived from a DEM, using slope, with an Arc Macro Language (AML) script developed for the DHSVM (Figure 17; Figure 18). Verifying the AML-generated stream network location is easily accomplished by visual comparison with the observed stream channel. The generated soil depth, however, is nearly impossible to verify at the basin scale and has a significant effect on simulated hydrology and mass wasting. Thus, soil depth is an important parameter that is adjusted during model calibration.

4.3.2 Meteorological Data

I used meteorological data from the Abbotsford A weather station in Abbotsford, BC. The station is located approximately 40 kilometers north of the study area (Figure 1). I chose Abbotsford A because it has an hourly weather record dating to the mid-1970s. Many other stations in closer proximity to the study area have either shorter records, lower temporal resolution, or both. For example, A USGS-operated tipping bucket rain gauge was installed at the Turkington Road Bridge in 2009, but the tipping bucket frequently malfunctions because of leaves and other debris interfering with the system (W. Wright, personal communication, 2012). An hourly record is required for this study in order to sufficiently characterize the hydrologic processes occurring in the basin, because the basin is steep and has a quick stream flow response to precipitation. A long record is required because mass wasting simulations are performed for numerous historical storm events. One of the goals for this study is to produce a tool for predicting slope failure, so it is important that the weather station that the DHSVM is calibrated to is reliable. Abbotsford A is a well-established weather station that is likely to remain in operation for the foreseeable future.

The lack of detailed precipitation gauges in the South Fork valley makes it difficult to verify the applicability of the Abbotsford A data to the Jones Creek basin. Localized areas of high relief in western Washington influence weather patterns, and precipitation can vary, even over small distances (Daly et al., 1994). One weather station that can be compared to

Abbotsford A is at Brannian Creek on the south end of Lake Whatcom, located approximately seven kilometers southwest of the study area (Figure 1). A ten-year weekly precipitation comparison between the two stations from January, 1990 to December, 1999 indicates that they while they record a similar record, there are some differences in timing and magnitude (Figure 19). A simple linear regression model suggests that Brannian Creek generally experiences slightly less weekly precipitation than Abbotsford A. Mean monthly precipitation is consistently higher for Abbotsford A than Brannian Creek (Figure 20). From November through March, when the most rain falls, the mean monthly precipitation at Abbotsford A varies from 0.36 to 3.3 centimeters more than Brannian Creek, with the greatest difference in November. Because of the general agreement between the weather stations, I assume that the Abbotsford A record is sufficient for exploratory modeling. Although differences in precipitation timing between records may cause difference in simulated stream flow timing, differences in precipitation magnitude can be adjusted with an elevation-dependent lapse rate during the calibration process.

The Abbotsford record includes precipitation, temperature, wind speed and direction, and relative humidity. DHSVM also requires longwave and shortwave radiation in order to simulate evapotranspiration. I used a model developed by Dr. Mitchell to estimate radiation based on the other weather parameters and a cloudiness factor. In the Pacific Northwest, radiation is not likely to have a significant effect on hydrology in the winter months when evapotranspiration is low.

4.3.3 Model Calibration

Calibrating the DHSVM requires adjustment of hydrologic model parameters until simulated stream flow matches the observed record over some period of time. In low snow basins, the parameters that most effect simulated stream flow are lateral hydraulic conductivity, soil thickness, and an elevation-dependent precipitation lapse rate (Dickerson, 2010; Wigmosta et al., 1994). Thick soils and low conductivity values result in a long, muted stream flow response to precipitation because there is a large soil water storage capacity

and water moves slowly through the soil profile to the stream. Thin soils and high conductivity values result in a quick, flashy stream flow response to precipitation because the soil water storage capacity is small and water moves quickly through the soil profile.

The calibration process is somewhat subjective, and depends in part on the quantity of observed data there is for comparison to simulations. Peak flows can be difficult to calibrate for small, steep basins where minor changes in soil infiltration rates can have a significant effect on partitioning of high-intensity precipitation between runoff and soil recharge (Thomas and Megahan, 1998). Accurately reproducing the post-storm recession in streamflow, which is quite sensitive to the hydrologic characteristics of soil and vegetation, generally results in a better characterization of basin hydrology than calibrating to peak flows (Hogue et al., 2000).

Calibrating the DHSVM mass wasting module is not possible for this study for two reasons. Although slope failures occur throughout the Jones Creek watershed, there is no record of the precise timing of the failures, and therefore no way to characterize the events that triggered them. Debris flows large enough to have been recorded have not occurred often enough to be useful as a proxy for slope failure. Additionally, the stochastic nature of the mass wasting module results in a probability of failure to a given storm event, not an actual failure prediction. Thus, the mass wasting output is more closely related to failure susceptibility than discrete failures, and is most effectively used to examine the sensitivity of failure susceptibility to a range of hydrologic conditions.

4.3.4 Defining Soil and Vegetation Mechanical Properties

The DHSVM automatically assigns a range and probability distribution to each soil and vegetation class for soil cohesion, friction angle, root cohesion, and vegetation overburden. The degree to which the assigned properties reflect true conditions depends on the quality of the spatial input data. Assigned mechanical properties for vegetation type can usually be accepted with more confidence than those for soil type, because vegetation is measured with remote sensing techniques at a relatively high resolution, and the mapped locations of

soil units may include interpretation and interpolation without field verification. All of the mechanical properties can be adjusted to reflect observed conditions.

The DHSVM uses normal, triangular, and uniform probability distributions to define mechanical properties (Doten et al., 2006; Figure 21). A normal distribution is defined by a mean and a standard deviation. The mean value is the most likely, with probability decreasing symmetrically with positive and negative variation from the mean. The standard deviation describes variability from the mean. Sixty-eight percent of the area under a normal distribution curve falls within plus or minus one standard deviation from the mean. Ninety-five percent falls within plus or minus two standard deviations. In probabilistic slope stability analysis, normal distributions are used for parameters that are reasonably well-understood and are likely to be normally distributed (Hammond et al., 1992). Triangular and uniform distributions are used for parameters that are not as well-understood.

Triangular distributions are defined by a minimum, maximum, and a mode. The mode is the most likely value. The probability is nearly zero at the minimum and maximum values. Triangular distributions can be symmetrical, or skewed towards the maximum or minimum. They are used in slope stability analysis when the field conditions are not completely understood or are not normally distributed, but when there is at least enough information to define a likely range and mode (Hammond et al., 1992). Uniform distributions are only defined by a minimum and maximum value. Every value within the range is equally likely. Uniform distributions are used for heterogeneous materials, or when there is too little information known to define a mean or mode (Hammond et al., 1992).

I modified parameters summarized by Doten and Lettenmaier (2004) for the loam soil, the fine sandy loam soil, and land cover, which were derived from numerous studies investigating slope stability in the Pacific Northwest (e.g., Montgomery et al., 2000; Roering et al., 2003; Table 2**).** I slightly reduced the literature parameter values for soil cohesion and friction angle for two reasons. First, soil shear strength parameters are variable, and I wanted to be sure to present conservative (i.e., poorly-constrained) estimates of slope stability in the absence of well-constrained material property data. Second, initial modeling

using literature values resulted in unrealistically high slope stability estimates, even for large historical storms that are known to have caused slope failures in the AWAU.

The deep-seated landslides are not uniquely identified on the USDA soil map, and the complexity of landslides makes them difficult to characterize with mechanical values from the literature. Thus, I had to manually define landslide boundaries and soil cohesion and friction angle parameters. Brief reconnaissance examination indicates that the soils comprising the landslides are generally comprised of a mix of clay and gravel-sized phyllite chips. Also, landslide material seems to be more loosely packed than soils in the surrounding area, particularly on the active toes. I chose slightly reduced values of cohesion and friction angle for the landslides, relative to the other soils, to reflect the influence of the phyllite-derived clays and the loose material packing on the unconsolidated landslide material (Jakob et al., 2004; Table 2).

4.3.5 Precipitation Threshold Analysis

In order to evaluate the relationship between antecedent precipitation and failure probability for each of the deep-seated landslides, I performed mass wasting simulations for 87 storms of a wide range of magnitudes from the 1980 to 2011 water years. For each storm simulation, I recorded the total magnitude and duration of rainfall from the onset of the storm to the time of maximum soil saturation, and the maximum DHSVM-predicted failure probability at the toe of each deep seated landslide. Adapting the methods used by Godt (2004) for probabilistic analysis, I constructed failure probability thresholds by plotting the storms according to duration (hours) and intensity (cm/hour). I coded each storm by failure probability, and interpreted minimum probability thresholds at 10 percent intervals (Figure 22). It is important to note that thresholds represent the interpreted minimum storm duration and intensity conditions required for a given failure probability, and do not represent failure probability isolines. For example, a modeled storm with a maximum failure probability of 35 percent could hypothetically plot above the 40 percent probability threshold, but not below the 30 percent threshold.

One DHSVM output is basin saturation, which is the percentage of grid cells that are saturated at a given time step, regardless of where they are in the basin. The basin saturation is a useful parameter for slope stability analysis because it is a good basic measure of water table conditions at the basin scale, it can be retrieved from the model output files with minimum processing, and it is easily correlated with storm magnitude. For each landslide, I plotted the failure probability for each storm as a function of basin saturation to determine if there are threshold saturation levels above which failure probability rapidly increases.

4.3.6 Timber Harvest Scenarios

I used the January 9, 2009 storm as a design event to evaluate failure susceptibility for current land cover conditions compared to a hypothetical clear cut logging scenario in which all coniferous, deciduous, and mixed forest stands are replaced by shrubs (Figure 23). Shrubs are a likely replacement species following timber harvest, and typically have reduced root strength and evapotranspiration potential (Zeimer, 1981). For this study, shrubs are also used to represent replanted trees, which initially have immature root morphology. An underlying assumption is that residual root strength is completely decayed, and shrub rooting provides the only source of root cohesion to the soil. Shrub rooting depth is typically shallower than for mature trees, and it is possible that the replacement roots would not fully penetrate the soil thickness, leaving zones of little or no root cohesion at depth (Canadell et al., 1996). Also, while the probabilistic approach used in this study is designed to deal with uncertainty in the mechanical properties that govern slope stability, intermolecular soil cohesion is highly dependent on saturation, and the defined statistical distributions might overestimate the true soil cohesion (Lu and Godt, 2013).

To evaluate the effects of reduced soil and root cohesion, I modeled slope failure for hypothetical basin-wide timber harvests over a range of root cohesion and soil cohesion distributions. Scenario A assumes the standard soil cohesion values defined in Table 2, and DHSVM-default values for shrub root cohesion. Scenario B assumes an approximate 25

percent reduction in soil cohesion. Scenario C assumes an approximate 50 percent reduction in soil cohesion. Scenario D assumes a 50 percent reduction in the default shrub root cohesion. Scenario E assumes a 50 percent reduction in root cohesion, and a 25 percent reduction in soil cohesion. Scenario F assumes a 50 percent reduction is soil cohesion, and a 50 percent reduction in root cohesion. The parameters used in the timber harvest scenarios are summarized in Tables 3 and 4.

In order to evaluate the current MWU designations, I compared the spatial distribution of failures predicted for each scenario with the mapped MWUs. For each MWU zone, I recorded the number of unstable cells, and the range of simulated failure probabilities. I also recorded unstable cells and probabilities predicted outside of MWU zones to see if MWU designations should be expanded to any areas not currently under logging prescriptions.

DHSVM slope failure output is dependent on modeled water table fluctuations that may or may not be representative of real conditions. Thus, it is possible that failure mechanics are accurately represented, but not the spatial distribution. One advantage of using high resolution, spatially distributed GIS data in slope failure modeling is that failure susceptibility can be extrapolated from cells where failure is predicted to other cells that share similar traits. Because soil cohesion, root cohesion, and friction angle do not vary appreciably across the basin in individual timber harvest scenarios, slope appears to be the primary factor that governs stability. I used ArcGIS to establish a mathematical relationship between failure probability magnitude and the associated minimum slope angle for each harvest scenario, and then applied that relationship to a 0.5 meter-resolution LiDAR-derived slope grid to interpret a series of failure susceptibility maps that include the entire basin. The advantage of this approach is twofold. First, the progressive reduction in the slope angle-failure probability relationship with decreasing shear strength is quantified. Second, a more complete characterization of the distribution of failure susceptibility with respect to the MWU zones is possible than for the model output alone.

4.4 Rotational SLIDE Modeling

The unconsolidated material thickness above bedrock on the deep-seated landslide toes has important implications for the type and probability of slope failure. A thin soil mantle of approximately two meters or less is most likely to fail by infinite slope, while a thicker soil profile is most likely to fail by deep rotational movement (Hammond et al., 1992). I used the RocScience SLIDE program to evaluate failure probability in the event that the unconsolidated material is thick. I used ArcGIS to generate surface profiles from LiDAR data for the landslide toes, and then imported the profiles in to SLIDE (Figure 24). I chose profiles that followed the steepest slope path, which, geometrically, represent the most likely location for rotational slope failures. I used the same ranges and statistical distributions for mechanical parameters I defined in DSHVM for the rotational analysis, except root cohesion and vegetation surcharge, which have a negligible effect on deep seated slope stability and are not considered in SLIDE.

I assumed a fully saturated soil profile. This is appropriate because the water table is likely to be relatively close to the ground surface during the winter months. If the failure surface is deep, fluctuation in the water table has little effect on soil shear strength, because the constant pore pressure induced by the total saturated thickness of the soil is significantly greater than the changes induced by changes in the water table (Equation 7). Therefore, the transient water table changes provided by DHSVM are not needed to evaluate deep rotational slope failures.

SLIDE evaluates the risk of rotational failure by performing a stochastic Bishop's Simplified method of slices analysis for thousands of possible circular surfaces throughout the soil profile. Failure probability is calculated in the same way as for the stochastic DHSVM infinite slope simulations (Equation 9). Model output can be viewed in a number of ways, but in general, SLIDE highlights the surface with the highest failure probability on the cross-sectional soil profile, and the other surfaces are color coded by factor of safety.

5.0 Results

5.1 Model Calibration Results

The DHSVM simulated stream flow for the 2011-2012 winter season compares favorably with 15 stream flow measurements taken over the same period of time (Figure 25). Although there are some differences in the magnitude and timing of flow, the values for observed and simulated stream flow seem to match well enough on the hydrograph recessions to provide a reasonable approximation of basin hydrology. The measured and simulated stream flows suggest that stream flow recedes sharply after storm events, and base flow is minimal in between periods of precipitation (Figure 25). The accuracy of simulated peak flows is a source of uncertainty for this study. For most of the storms, I was not able to reach the site in time to take a measurement during peak stream flow, because the stream responds rapidly to precipitation. The few times I was able to observe a peak flow, conditions were too dangerous to risk wading.

I calibrated the DHVM by testing a range of soil depths and hydraulic conductivities in the model parameters to determine the conditions that reflect the observed stream flow record (Figure 25). Soil depth is an important parameter in the infinite slope equation, and so is important to accurately characterize in the hydrology calibration. My modeling indicates stream flow response to be quite sensitive to changes in soil depth, and that even moderately thick soil profiles result in excess soil water storage and extended stream flow recessions that substantially over-predict the observed record. Likewise, the initial hydraulic conductivity values I used were too low and resulted in a delayed flow response. I used a thin soil layer and high hydraulic conductivities to develop a hydrograph shape more consistent with the measured data, and an elevation-dependent precipitation lapse rate to adjust the magnitude of simulated flows. Increasing the precipitation lapse rate increases total precipitation defined in the meteorological input record, and decreasing the lapse rate reduces precipitation (Table 5).

The DHSVM is calibrated to stream flow at the outlet of the basin. Given multiple soil types, several different combinations of calibrated parameters can result in similar stream flow simulations. A successfully calibrated stream flow record does not imply that hydrology is being accurately represented at the pixel scale of the model. This is acceptable when simulating stream flow is the primary objective for using the model. For this study, pixel-scale hydrology is important because slope failure is dependent on pore pressure induced by the water table. Sparse stream flow data, paired with uncertainty in pixel-scale hydrologic processes, make the hydrologic model calibration for this study approximate, and so it should be amended with ongoing understanding of the hydrology of the Jones Creek watershed.

5.2 Infinite Slope Failure Probability Thresholds

The DHSVM-predicted failure probabilities on the South and Straight landslides are sensitive to water table fluctuations and vegetation cover, and encompass a wide range of values for the 87 modeled storms, ranging from less than 10 percent to greater than 70 percent. The abundance and range of failure probability data for those two landslides make the implementation of probability thresholds straightforward. However, the model predicts slope instability on the Darrington landslide only for seven of the largest storms, with probability ranging from 20 to 37 percent. The minimum total storm precipitation that resulted in predicted failures on the Darrington Landslide was nine centimeters over 48 hours. Predicted failures on the Cutblock slide are also few, and none exceed a five percent failure probability.

The few predicted failures on the Darrington and Cutblock landslides is likely due to the influence of gentle surface slopes on the Darrington landslide and vegetation on the Cutblock landslide toe. The Darrington slide has a significant unvegetated portion, but has a relatively shallow surface slope compared to the other landslides (Figure 4). Slope on the Darrington slide ranges from 27 to 35 degrees on the unvegetated toe, while slopes on the other slides are as high as 45 degrees (Puget Sound LiDAR Consortium, 2006). The shallow

surface slope on the Darrington slide results in a lower proportion of soil weight acting downslope, and thus the factor of safety for the slope is increased. The Cutblock slide, which is steep but completely vegetated, has root cohesion that is not present on the unvegetated portions of the other landslides. Soil shear strength is bolstered by mechanical binding of the roots, increasing the factor of safety on the Cutblock slide relative to the unvegetated landslides. Because of these factors, the model predicts too few failures, and too narrow a range of failure probabilities, to assign failure probability thresholds to the Darrington and Cutblock slides. For this study, I present probability thresholds for the South and Straight landslides.

Thresholds for 10, 20, 30, 40, and 70 percent failure probability are interpreted for the Straight slide (Figure 26; Table 6). Storms that produced failure probabilities of 40 to 70 percent plot erratically above the forty percent probability threshold and cannot be separated in to meaningful groups, so they are represented by a single probability threshold. For storm durations less than 25 hours, higher probability thresholds are more sensitive to changes in storm duration than lower probability thresholds, and have a steeper slope on the intensity-duration plot. All probability thresholds flatten and become insensitive to changes in storm duration beyond 35 hours. The exact location of the inflection point for each threshold is subjective and depends in part on the distribution of plotted storm data. Spacing between thresholds decreases as storm duration increases. The change in spacing is due to a change in total precipitation. A change in precipitation intensity for a long duration storm results in more total water falling on the basin compared to the same intensity change for a short duration storm. Consequently, there is more soil water recharge and a greater increase in failure probability.

The South slide probability thresholds are similar to the Straight slide thresholds (Figure 27; Table 6). None of the modeled storms predicted failures with a 50 to 60 percent failure probability for the South slide, so that threshold interval is missing. Instead, there is a direct transition from the 40 percent probability zone to the 60 percent probability zone. Thresholds for the South slide plot at lower positions on the duration-intensity curve than

equivalent thresholds for the Straight slide, meaning failure probability is generally higher for the South slide, and a smaller amount of precipitation is required to initiate failure. The probability thresholds for the South slide are also less sensitive to storm duration, as indicated by relatively shallow slopes on the intensity-duration plot, and become insensitive to storm durations longer than 30 hours. The 70 percent probability threshold is an exception. It plots higher on the intensity duration curve than the equivalent Straight slide threshold and is more sensitive to changes in storm duration. Because storms of such a high intensity and short duration are not common, there are few data to constrain the 70 percent probability threshold curve and the position is approximate at best.

The Godt (2004) intensity-duration threshold curve for the Seattle region compares favorably to the Jones Creek probability thresholds (Figure 26; Figure 27). The Jones Creek probability thresholds are insensitive to changes in duration for longer storms. The Godt threshold decreases in sensitivity with increasing storm duration, but does not become insensitive to storm duration. The probability of failure for storms exceeding the Godt threshold is 42 percent. For Storms exceeding 30 hours, the curve coincides with the 10 and 20 percent probability zones for the Straight and South landslides. For shorter storms, the curve coincides with the 30 percent probability zone for the Straight slide and the 40 percent probability zone for the South slide.

As described in section *4.3.5*, one general measure of the DHSVM-simulated water table conditions is basin saturation, which is the percentage of grid cells in the basin that are saturated at a given time step, regardless of where they are located. I plotted the maximum failure probability predicted at the toes of Straight and South Slides for each of the 87 historical storms, as a function of DHSVM-predicted basin saturation. Simulated failure probability for the Straight and South slides generally increases as a function of basin saturation (Figure 28; Figure 29). The relationship is not perfect because fluctuation in total basin saturation is only an approximation for water table fluctuations at the landslide scale, but a number of basic observations can be made from the plots. From five to eight percent basin saturation, failure probability on the Straight slide steadily increases and ranges from

one to 35 percent. From eight to 14 percent saturation, failure probability varies erratically from one to 65 percent. Above 14 percent saturation, failure probability varies from 65 to 80 percent but does not vary systematically with saturation.

Failure probability on the South slide changes more linearly with basin saturation. This can be attributed to the fact that there are fewer unstable cells on the South slide toe, and thus less scatter in the data due to differences in surface slope between grid cells. From five to 15 percent saturation, failure probability varies from 20 to 45 percent. At 16 percent saturation, failure probability increases rapidly to 60 percent. Above 16 percent saturation, failure probability increases linearly from 60 to 83 percent, but with more variance than it does at lower saturation levels.

5.3 Timber Harvest Scenarios

5.3.1 Failure simulations

Simulated timber harvest conditions result in increased failure susceptibility relative to current land cover throughout the Jones Creek basin. Timber harvest effects are broadly characterized by a significant number of cells that are stable in pre-harvest conditions transitioning to unstable in post-harvest conditions, with failure probabilities less than five percent (Table 7). All harvest scenarios predict an increased number of unstable cells. One way to compare the unstable cell counts between MWU zones, while ignoring differences in MWU zone size, is to examine the number of unstable cells per unit area (Figure 30). The relative number of unstable cells per area fluctuates between MWUs depending on the harvest scenario, but it always lower outside MWU zones than inside. All harvest scenarios except scenario A predict increased mean failure probability for unstable cells (Figure 31). As described in section 4.3.6, intermolecular soil cohesion is highly dependent on saturation, and the statistical distributions for soil cohesion defined for the precipitation threshold analysis might overestimate the true soil cohesion. Thus, some timber harvest scenarios incorporate reductions in effective cohesion in order to evaluate the sensitivity of the basin to soil cohesion under harvest conditions. Mean failure probability is highest for

scenarios that simulate a 50 percent reduction in effective soil cohesion. The effects of reduced soil cohesion are accentuated when combined with post-harvest reduced root cohesion.

Simulated failures under current land cover conditions are closely associated with steep inner gorges adjacent to the creek channel (Figure 32). The highest concentration of unstable cells occur upstream of the Darrington landslide, on the north side of the creek channel. Failures are almost entirely less than five percent probability (Figure 31). A few very localized high probability failures exceeding 70 percent probability are concentrated on the deep seated landslide toes. There are three areas outside of the MWUs where instability is consistently predicted for every harvest scenario. At the east end of the basin, on the north side of the creek channel, failures are concentrated on the steep front slopes above the fan (Figure 32). There are several small tributary channels that drain this area. On the west side of the Darrington slide, several failures are concentrated on a steep slope near the head scarp (Figure 32). In the upper watershed north of the creek channel, there is a wedge of failures that that appear to be associated with a logged area (Figure 2; Figure 32). Failure per area, while generally low, is highest in MWUs 2 and 10 due to their close spatial proximity to the main creek channel.

Harvest scenario A, which simulates a change to shrub vegetation for all cells with trees, results in widespread increase in unstable cells relative to the current land cover simulation (Figure 33). Failure per unit area approximately doubles for every zone compared to the current land cover simulation, due to reduced root cohesion for shrubs. Mean failure probability is lower than for the current land cover simulation for every zone, because the additional unstable cells are heavily biased towards low probability failures (Figure 31). Failure density is significantly increased directly west of the Darrington landslide on both the north and south side of the creek channel, as well as on the steep front slopes at the east end of the basin.

Harvest scenario B, which simulates a change to shrub vegetation with a 25 percent reduction in effective soil cohesion, is characterized by increased mean failure probability

throughout the basin, and increased failure density west of the Darrington slide and on the front slopes on the northeast end of the basin (Figure 34) . Relative to scenario A, the change in mean failure probability is more significant than the change in failures per unit area for all zones (Figure 30; Figure 31). Unlike scenario A, scenario B predicts a higher mean failure than the current land cover scenario of about one to two percent for all zones.

Harvest scenario C, which simulates a change to shrub vegetation and a 50 percent reduction in effective soil cohesion, is characterized by increased failure probability for cells south and west of the Darrington landslide, highly unstable cells on the deep seated landslide toes, and increased unstable area on the northeast front slopes (Figure 35). Relative to scenario B, mean failure probability is increased by approximately 50 percent for all MWU zones, and is almost doubled for MWU 2 (Figure 31). While failure per unit area is increased compared to scenario B, the change is not as accentuated as for mean failure probability (Figure 30).

Harvest scenario D, which simulates a change to shrub vegetation and an approximate 50 percent reduction in root cohesion relative to the DHSVM-default shrub parameters, is defined by a failure distribution similar to harvest scenarios A, B, and C (Figure 36). Some differences in the respective roles of root and soil cohesion are apparent by examining the failures per area and mean failure probability statistics for scenario D. First, the change in failures per unit area for harvest scenarios A, B, C is relatively consistent between all MWU zones, meaning no single zone shows any unique sensitivity in failure density to changes in mechanical properties (Figure 30). In scenario D, MWU 1 has a disproportionately increased number of failures per unit area relative to the other zones. In fact, MWU 1 has an increased number of failures per area in scenario D relative to scenario C, where the other zones decrease or show no change. Second, while harvest scenario C results in increased failures per unit area relative to Harvest scenario A (default shrub root cohesion and default soil cohesion), the mean failure probability does not increase significantly. There is a similar relationship between scenario C and the current land cover condition, where full tree rooting strength is in effect through much of the basin (Figure 31).

This seems to be the opposite effect that a 50 percent reduction in soil cohesion has on mean failure probability in scenario C, which is significantly increased relative to scenario A and the current land cover scenario (Figure 31).

Scenario E, which simulates a 25 percent reduction in soil cohesion with a 50 percent reduction in root cohesion, is characterized by a slight increase in failure per unit area and a significant increase in mean failure probability relative to scenario D (Figure 37; Figure 31). Most of the change in failure per unit area is concentrated outside of the MWUs (Figure 31). The combined effects of reduced soil and root cohesion are apparent. Although the reduction in root cohesion in scenario C does not result in an appreciable change in mean failure probability, it does seem to influence mean failure probability in scenario E. Mean failure probability is greater for all MWU zones in scenario E than in scenario B, which simulates an equivalent soil cohesion reduction to scenario E.

Scenario F simulates a 50 percent reduction in soil cohesion and a 50 percent reduction in root cohesion. The drastic reduction in soil shear strength in scenario F predicts failures exceeding thirty percent probability throughout the lower basin and the tributary channels in the upper basin (Figure 38). Mean failure probability and failure per area are increased relative to all other scenarios (Figure 30; Figure 31). Simulated failure density and probability for this scenario is likely indicative that the realistic lower bound for soil cohesion has been surpassed.

5.3.2 Harvest Scenario Susceptibility Maps

There is a distinct relationship between failure probability and associated minimum slope angle for each timber harvest scenario (Figure 39). Correlation coefficients are reasonably high for exponential regression models fit to the data. Residuals reflect other variables that influence failure probability. Although some of the other variables are probabilistic, every failure calculation is based on 1000 stochastic iterations, which is sufficient for reproducible results (Hammond et al., 1992). As expected, the effects of the differences in soil and root cohesion between harvest scenarios are evident in the

exponential expressions. For example, the regression model for scenario C predicts higher failure probability than scenario A for equivalent slopes, due to reduced soil cohesion (Figure 39). The regression models are conservative because they are based on the highest modeled failure probability associated with each slope angle, and so often predict higher failure probability than the DHSVM model output from which they are derived. This is primarily because a small number of high probability failures on the deep-seated landslide toes are weighted heavily in the regression models and interpreted across the entire basin. For example, high failure probabilities associated with the landslides are extended to all other cells in the basin with equivalent or steeper slopes.

The regression models, combined with the LiDAR slope grid, give total-basin susceptibility maps for each timber harvest scenario (Figures 40- 45). The maps represent the worst-case scenario for each grid cell. They are not intended to predict specific failures, but to help identify specific areas that might be prone to slope failure in a post-harvest landscape. All of the maps are based on a common slope grid, altered by similar exponential functions. As such, the basic spatial distribution of probabilities is similar between them. In general, probability is low at the edges of the basin where slopes are gentle, and increase with increasing slope towards the center of the basin. High probabilities are primarily concentrated along the main channel and tributaries, and are particularly pronounced on the north side of the main channel at the intersection with the first major tributary upstream of the Cutblock slide. The differences between the susceptibility maps are driven by the differences in DHSVM model output detailed in the previous section. The frequency distribution of failure probabilities is skewed towards low probability for harvest scenario A, and gradually skews toward higher probability as soil and root cohesion are reduced for scenarios B, C, D, E, and F (Figures 46-51).

There are two common themes repeated for all of the susceptibility maps. The first is that some high failure probability zones centered in the main and tributary channels extend outward for as much as 200 meters with no intermediate breaks in failure probability (Figure 40). The outer portions of these zones are not always contained within

MWU boundaries (Figure 40). This is particularly evident in the upper watershed. The second is that there are two prominent zones of instability exceeding 60 percent probability that are situated completely outside the MWUs (Figure 40). These two zones are also defined by groups of closely-spaced unstable cells directly predicted by DHSVM (i.e., Figure 38).

A challenge to using probabilistic methods to aid land management decisions in the Jones Creek basin is that results are not determinate. For example, it is challenging to determine the magnitude of failure probability that represents an acceptable risk for logging, and how management prescriptions should be accordingly adjusted. In this case, multiple criteria and assumptions must be used to aid decision making. Precipitation threshold analysis for the South and Straight landslides revealed that failure probability increases rapidly above the 40 percent probability with continuing precipitation. Hence, failures may be more widespread with minimal additional precipitation beyond what is required to reach above 40 percent. I combine this assumption with the probabilistic modeling approach to form the basis for a recommendation for additional logging prescriptions in the Jones Creek basin. In this case, harvest buffers (areas restricted to logging) near MWUs should be expanded to include continuous or semi-continuous zones of unstable cells of that DHSVM predicts to have at least 40 percent failure probability for the January, 2009 design storm, that are in close proximity to the main stream channel or tributaries where debris flows or landslide dams may be initiated. Although all of the susceptibility maps are informative of the basin sensitivity to changes in soil and root cohesion, harvest scenario A is the best representation of literature values for mechanical parameters. Hence, the scenario A susceptibility map serves as the basis for identifying regions that should be afforded the same logging restriction as the MWUs (Figure 52).

Many of the unstable cells predicted by harvest scenario A lie inside MWU boundaries. However, there are several areas where there are groups of unstable cells in close proximity to stream channels that are situated outside of MWU boundaries. The additional areas I recommend for logging-restricted harvest buffer zones are summarized as

follows. In the upper basin, the three main tributary channels on the north side of Jones Creek all require lateral expansion of a harvest buffer to account for groups of unstable cells extending outside of MWU boundaries (Figure 52). Small tributaries on the south side of the main channel in the upper basin also require some additional harvest buffers. It is not immediately clear if the MWU units are correctly digitized in the DNR GIS data base for this area of the watershed. Many of the MWU units seem to be misaligned with the tributary stream channels (Figure 52). In the middle reaches of the basin, the group of unstable cells on the north side of the main channel requires a small additional harvest buffer. Directly east, there is a separate zone of unstable cells that are not associated with an MWU. I choose to add a large harvest buffer to that zone, even though there is a slope break separating this zone of cells from the main channel (Figure 52). Recharge zones for both the Darrington and Cutblock slides are present there, and logging in the recharge zones of deep-seated landslides is likely to contribute significantly to localized slope instability in the Jones Creek basin (Jakob et al., 2004). On the south side of the channel in the same area, three tributary channels require additional buffers, as well as a small area adjacent to the main channel (Figure 52). Lastly, a large harvest buffer should be added to the steep front slopes at the east end of the basin (Figure 52). Although the front slopes do not lie directly adjacent to the main channel, there are several small high-water channels that could likely provide transport pathways for debris flows to buildings located on the fan and Nooksack floodplain.

5.4 SLIDE Modeling

SLIDE predicts rotational instability at the toes of all of the deep seated landslides under saturated conditions (Figures 53-56). Almost every stochastic failure surface has a factor of safety below one and a probability of failure of 100 percent. Even when soil shear strength is artificially bolstered by allowing friction angle and cohesion to be unreasonably high at 40 degrees and 20 kPa, the results are similar (Figure 57). The lowest factor of safety is predicted for the Straight slide, which has the most severely over-steepened toe.

The highest factor of safety, which is still less than one, is predicted for the Darrington slide, which has the gentlest slopes.

Although the soil profiles are perhaps unrealistically deep, all rotational surfaces deeper than about one and a half meters predict failure. Based on the rotational model, if the unconsolidated landslide material is thicker than predicted by DHSVM, rotational failures should be occurring frequently, even considering the possibility of a transition to a stronger, partially weathered material at depth. Although the Bishop's Simplified Method gives a conservative factor of safety, the uncertainty in the characterization of interslice forces that is probably not significant considering the low estimated factor of safety values.

6.0 Discussion

6.1 Probability Thresholds

The relationship between failure probability, basin saturation, and antecedent precipitation is erratic between 40 and 70 percent probability for both the South and Straight landslides. This could represent a transitional zone where small changes in soil saturation cause minor fluctuations around a factor of safety of one, and therefore significant variability in failure probability. For example, it is important to consider that if the model stochastically predicts the factor of safety to be 0.99 for every iteration, the probability of failure is considered to be 100 percent. Conversely, if the factor of safety is predicted to be one for every iteration, the failure probability is considered to be zero percent. In reality, there is considerable uncertainty in the stability of slopes with a factor of safety close to one, and slopes with a factor of safety just above one can be unstable (Krahn, 2003). Thus, assuming the parameters that control failure have been adequately characterized, the 40 percent failure probability thresholds can be thought of as a major break point above which failures may be quite likely. An abrupt change in stochastic failure probability beyond a certain soil saturation level can be indicative of a real failure probability threshold, even if the actual exceedance probability differs from the modeled probability (Berti et al., 2012).

Although the DHSVM predicted failure probability thresholds cannot be statistically validated without a detailed chronological record of slope failures, the similarity to the Godt (2004) intensity-duration threshold provides some measure of validation. Exceedance failure probability compares well between the Godt curve and the Jones Creek probabilities for short duration storms, but differs considerably for longer duration storms. The difference could be due to a difference in land cover between the Seattle area and the Jones Creek basin. Urbanization can have a significant effect on watershed hydrology (White and Greer, 2006). The Seattle area is significantly urbanized and many areas have a high proportion of impervious surfaces. Precipitation falling on impervious surfaces cannot

infiltrate the soil at the point it falls on. Instead, it travels downhill by overland flow, and infiltrates in to soils in concentrated areas (Paul and Meyer, 2001). Thus, localized areas may experience a disproportionate rise in water table elevation, and an increase in failure susceptibility, during low intensity storm events. Also, urbanization results in a reduced vegetation canopy. A significant portion of low intensity precipitation can be intercepted in the canopy and returned to the atmosphere or delivered to the ground surface at a reduced rate (Spittlehouse, 1998). Due to reduced canopy, urban areas can have a greater proportion of low intensity precipitation delivered to the soil than forested watersheds, increased water table recharge, and consequently increased failure susceptibility.

The likely flashy nature of the Jones Creek basin provides another possible explanation for the relatively low failure probability predicted by long duration, low intensity storm events. The hydraulic conductivity values defined during the calibration process are relatively high. High hydraulic conductivity, paired with steep slopes, allows water to migrate quickly through the soil in steep basins (Lu and Godt, 2013). Due to the rapid flux of groundwater toward the creek channel, low intensity precipitation may elevate the water table to a lesser height in highly transmissive soils compared to less transmissive soils (Crosta, 1998). The Godt curve is constructed from data from a large area and a wide range of soils, some of which are likely to be less transmissive than the soils at Jones Creek.

Using the probability thresholds to predict the actual occurrence of slope failures is challenging due to the sparse observed record of failure events and the stochastic modeling approach used in this study. Some of the recorded debris flows can be correlated with high DHSVM failure probabilities. For example, debris flows that were triggered by the January, 2009 storm originated at the toes of the Darrington and Straight landslides, where DHSVM predicted high failure probability relative to the rest of the watershed (Powell, 2010). However, the 1983 event likely originated in the upper watershed, where DHSVM predicted a low failure probability relative to the unvegetated landslide toes (Jakob et al., 2004). Realistically, no precipitation threshold can provide a deterministic prediction of slope failure that is consistently accurate, but they can provide useful insight on the relationship

between precipitation and slope failure (e.g., Berti et al., 2005; Chleborad, 2000; Godt, 2004).

6.2 Timber Harvest Effects

6.2.1 Influence of Root Cohesion

Timber harvest simulations generally predict an increase in failures with less than five percent probability. Reducing soil and root cohesion to account for interspersed areas of low root density and saturation-dependent cohesive soils results in higher simulated failure density and probability. Differences between the DHSVM simulated failures between harvest scenarios seems to indicate that the basin is sensitive to changes in soil cohesion, meaning accurate soil information is important. The change from current land cover conditions to a shrub-covered basin increases the number of simulated failures, but does not significantly increase mean failure probability. However, the unvegetated deep-seated landslide toes, which are modeled with a uniform absence of root cohesion, frequently simulate failure probabilities exceeding fifty percent in response to heavy storms. Hence, root cohesion seems to act to stabilize slopes, even at low magnitudes. In that case, shallow failures in the Jones Creek basin may dominantly be controlled by interspersed zones of zero root cohesion, which is consistent with the findings of other researchers employing the infinite slope model for Pacific Northwest slopes (e.g., Roering et al., 2003).

The possibility that complete lack of root cohesion is the dominant factor governing slope stability in the Jones Creek basin makes it challenging to use probabilistic modeling methods to predict the occurrence of shallow landslides. There does not seem to be a practical way to use a statistical distribution to characterize root cohesion if the low root cohesion and zero root cohesion give significantly different failure probabilities. Characterizing the spatial distribution of root cohesion is challenging over large areas, and is probably most effectively done after slope failure has occurred and exposed roots in head

scarps (e.g., Roering et al., 2003). Even in that case, predicting the spatial distribution of zero root cohesion in areas that have not failed represents a significant challenge.

Even with the uncertainty in the spatial distribution of root cohesion in the basin, the failure simulations make it clear that the timber harvest is likely to increase the occurrence of shallow slope failures in the Jones Creek basin. Although DHSVM assumes a uniform distribution and depth for root cohesion, shrubs typically have shallow root systems, and it is possible that root cohesion will completely decay at the soil-bedrock interface if harvested trees are replaced by shrubs. Although it is challenging to quantitatively predict the spatial distribution of failures that would result from harvest, the importance of root cohesion in stabilizing slopes is quantifiable, and the DHSVM mass wasting model provides a good tool for doing that.

6.2.2 Hydrological effects

The difference in modeled instantaneous and net stream flow between harvest scenarios is negligible. Therefore, the changes in modeled failure susceptibility between the harvest scenarios almost entirely reflect a reduction in root strength, and not a change in evapotranspiration and water table recharge. Although it seems counterintuitive, there are a number of possible explanations why such a significant reduction in forest cover would have a minimal impact on water table fluctuation during storms. Evapotranspiration is generally minimal in the cool winter months in the Pacific Northwest, and is most pronounced in the summer, when there is increased temperature and solar radiation, lower air humidity, and longer daylight hours (Jassal et al., 2009). Also, the proportion of precipitation that can be intercepted in the vegetation canopy depends on part on storm intensity. During high-intensity storms like the January, 2009 event, the canopy quickly becomes saturated and a relatively small percentage of the total precipitation is intercepted and returned to the atmosphere via evapotranspiration compared to the same magnitude of rain falling in a low intensity storm (Dhakal and Sidle, 2004). Thus, vegetation cover may

have a more significant effect on seasonal groundwater fluctuations than for individual, high-intensity storms.

Even considering that evapotranspiration is low during the winter and canopy interception is less during high-intensity storms, this study does not definitively demonstrate that a change to a harvested landscape would have a negligible impact on basin hydrology on a storm-by-storm basis. The DHVM, as with all hydrologic models, cannot fully characterize the complexities of soil water storage and flux. For example, deep percolation and infiltration of soil water in to bedrock, which may be significant in the phyllite, is not considered by DHSVM. Preferential subsurface water flow and routing during storms, which is influenced in part by the rate at which precipitation is attenuated through the vegetation canopy, are also likely to be oversimplified in some cases. Hence, timber harvest may result in changes in basin hydrology that are not simulated by DHSVM.

In some cases, even a small increase in soil water infiltration during storms can have a significant effect on water table elevation and pore fluid pressure. In the Pacific Northwest, where soils are typically wet during the winter months, pore space in the unsaturated zone may be dominated by water, with only small amounts of air. In this case, pore pressure is atmospheric, and pore water is held by surface tension and does not contribute to the water table or changes in effective stress. However, a small amount of precipitation that infiltrates the soil may be sufficient to replace the air in the pore spaces, releasing the rest of the pore water from tension, and thus rapidly elevating the water table in a phenomenon known as the reverse Wieringermeer effect (Dingman, 2002; Jaber et al., 2006; Weeks, 2002). This has important implications for slope stability, but validating it with the DHSVM is difficult. .

6.2.3 Land Management Recommendations

Advancement in the availability of high-resolution digital spatial data has greatly increased in the decade since the original logging prescriptions were defined for the Jones Creek basin. High-resolution slope data, combined with probabilistic infinite slope

modeling, suggests that the MWU zones should be supplemented with additional harvest buffers in some regions in the basin. This study did not find any particular difference between the MWUs in shallow failure probability, or the number or unstable cells per area, other than that MWU one might be more sensitive to changes in root cohesion than the other MWUs. As such, the recommendations here are based on broadly treating MWU units as no harvest zones, and increasing their extent with additional buffers in some areas. Land management recommendations based on this study are as follows:

1) Expand the current areas restricted to timber harvest to include the areas interpreted in this study to be highly susceptible to the reduced soil shear strength that could result from a hypothetical timber harvest (Figure 52).
2) Increase the harvest buffer zone on the north side of the creek beyond what would normally be required for shallow slope instability to account for the groundwater recharge areas for the Cutblock and Darrington landslides.
3) Revise the digitized locations for MWUs on the south side of the main creek channel in the upper basin. MWU locations do not seem to correctly reflect topography in this part of the basin.

The harvest buffer zones suggested in this study are based on only one of a series of timber harvest susceptibility maps. The literature values for soil and root cohesion used in harvest scenario A are the best available estimate for field conditions in the Jones Creek basin. However, the other susceptibility maps should be retained in the event that future research validates a different range of mechanical parameter values. Because the susceptibility maps predict progressively higher failure probability by slope angle, the harvest buffers should be amended if soil and root cohesion is found to be more aligned with the parameters used in one of the other susceptibility maps.

Susceptibility maps are based on exponential regression models relating the highest failure probability associated with each slope angle. As such, they may bias towards the

failures predicted at the deep seated landslide toes where root cohesion is zero. Also, they may overestimate effects of preferential groundwater flow by interpreting anomalous conditions for a few cells over the entire extent of the basin. However, this may be beneficial for management strategies, because the worst case scenario is considered. The susceptibility maps are intended to be conservative approximations of the spatial distribution of failure probability

6.3 Deep rotational failure

The depth of the unconsolidated, clay rich material on the unvegetated landslide toes has important implications for failure susceptibility at Jones Creek. Small, shallow infinite slope-style failures could hypothetically go unnoticed or unrecorded due to relatively small failure volumes and a lack of damage on the alluvial fan. Larger, deep-seated rotational failures on the landslide toes would deliver significant quantities of material to the creek channel and would almost certainly result in damage on the fan (Jakob et al., 2004). It is reasonable to assume that events of this magnitude would be recorded. Large debris flows and landslides have been recorded at Jones Creek about six times in the last 70 years (Jakob et al., 2004).

Rotational failure modeling with the RocScience SLIDE software suggests that if the unconsolidated, clay-rich material on the unvegetated toes of the landslide is more than a few meters thick, large rotational failures should be more frequently occurring due to severely over steepened slopes and high pore fluid pressure at depth, even if the soil shear strength is estimated to be unreasonably high. Given the relative infrequency of catastrophic landslides, it seems reasonable that the unconsolidated landslide material represents relatively thin, severely weathered phyllite that is overlying foliated, sheared bedrock through which the deep-seated failures planes extend. This is supported by visual evidence of near-surface bedrock on the toes of all the landslides, and particularly the South slide. A thin mantle of soil overlying impermeable bedrock is more stable on over

steepened slopes than a thick, saturated soil profile, due to reduced pore pressure at the soil-bedrock interface and a lesser contribution of soil water weight acting downslope.

A thin soil mantle is more sensitive to storm-induced water table fluctuations than a thick saturated soil, because water table fluctuations on the scale of a storm represent a relatively small percentage change in total saturated thickness above deep failure planes. Deep seated failures, and the rate of movement along preexisting deep-seated slip planes, are often more closely correlated with seasonal changes in regional groundwater fluctuation than individual high-intensity storm events, or show a delayed response to high intensity precipitation (Fell et al., 2000; Leroueil, 2001). Although the sample population is small, observed landslides and debris flows at Jones Creek seem to coincide temporally with individual high-intensity storm events that have a greater immediate impact on shallow slope stability than deep-seated stability, lending further support to the idea that most slope failures that occur adjacent to the creek channel are relatively shallow in depth (Jakob et al., 2004). Slow-moving masses that may be deeply rooted in partially weathered-bedrock occur throughout the Jones Creek basin, but evaluating the seasonal influences of groundwater and fluid pressure in bedrock at depth is complex and beyond the scope of this study.

6.4 Study Limitations and Uncertainty

6.4.1 Hydrology Calibration

The hydrologic calibration for this study is not rigorous due to challenging field conditions. In particular, constant cycles of aggradation and reworking of the channel in the vicinity of the USGS gauge prevented a reliable record of stream flow to be recorded between site visits. In the fall of 2012, the in-channel gauge was replaced with a radar gauge that is mounted on the Turkington Road bridge. Although the continuing evolution of the stream channel will likely prevent a meaningful discharge-stage relationship from ever being established at Jones Creek, data from the radar gauge should be instrumental in

establishing an improved understanding of stream flow at Jones Creek through the collection of important qualitative data such as time to peak.

The DHSVM is calibrated for this study based on data from a meteorological station that is located a significant distance away from the study area. Use of the probability thresholds should be limited to precipitation recorded at the Abbotsford A station, because the water table response to precipitation is calibrated to that record. Although the variability in precipitation between the two sites is probably not significant compared to the uncertainty in the assumed values for other parameters in this study, the results of this study would benefit from a reliable hourly precipitation recorded at a location closer to the Jones Creek basin.

The influence of rain-on-snow storms in this study is difficult to evaluate. Without a historical streamflow record, it is practically impossible to evaluate if the model is correctly simulating snowpack dynamics. Previous researchers have found that DHSVM reliably reproduces observed temporal changes in snowpack (e.g., Bewley et al., 2010). The DSHVM does predict the presence of a shallow snow pack prior to the onset of several of the modeled storms, but it is generally only present in the upper portions of the watershed, not overlying the deep-seated landslides where the effects of rain-on-snow events would have the greatest effect on the failure probability. The contribution of snow melt to modeled failure probability is not always clear. On steep slopes, a high proportion of water from rapidly-melted snowpack may migrate to the stream channel by overland flow rather than infiltrating in to soils (Jakob et al., 2004). However, in the case of a rain-on-snow event and previously saturated soils, even a small contribution of infiltrated melt water may be enough to trigger slope failures. In any case, a warm winter storm, paired with the presence of a snowpack in the lower watershed, could result in a higher failure probability than is predicted by the probability thresholds suggested in this study.

6.4.2 Influence of Landslide Heterogeneity

Landslides are notorious for heterogeneity in the mechanical properties that define shear strength, hence the necessity of a stochastic approach. The challenge in selecting statistical distributions and ranges for landslide properties lies in choosing a range that is wide enough to account for heterogeneity, but not so wide as to make model output meaningless. The range of mechanical strength in the landslide is likely to vary over a wider range than I have chosen for this study, due to differential weathering of the phyllite and variability in vegetation growth stage. It is even possible that a single statistical distribution for each parameter is not appropriate to apply over the scale of an entire landslide.

Soil thickness is probably the single most important, and most poorly constrained, variable in this study. Soil thickness has important implications for both hydrology and slope failure. While the DHSVM assumes a uniformly developed soil mantle, all of the landslides at Jones Creek show intermingling surface exposures of bedrock and soil, variable stages of phyllite breakdown, and presumably, significant variation in the depth to bedrock below soils. Thus, it is difficult to accept the model's failure probability predictions with certainty, even if there is some data for measured soil depth available. Comprehensive soil depth measurements over the entirety of a complex variable landform would require an impractical time commitment and extraordinary cost. One modeling strategy designed to accommodate this problem prescribes the treatment of soil thickness as a stochastic variable (e.g., Hammond et al., 1992). This approach would be feasible if the other stochastically defined variables were better constrained than they are in this study. In the case of this study, adding another stochastic variable would only introduce more uncertainty in the model output.

One advantage of linking the stochastic slope failure model to the DHSVM hydrology model is that the regional soil depth can be partially constrained during the calibration process. For example, soils in the Jones Creek basin are likely to be about one to one and a half meters thick, given the observed stream flow response to precipitation. However, this provides little constraint on the variation in soil depth at the pixel scale. Indeed, one of the

most significant limitations to this study is that there is no practical way to calibrate the DHSVM to reflect complex variation in geomorphology and hydrology at the pixel scale.

6.4.3 Evaluation of DHSVM as a Tool for Slope Stability Analysis

Natural variability in geologic settings, and particularly in landslides, makes an accurate pixel-scale slope stability analysis impractical without a well-constrained record of the timing of slope failures. The DHSVM is probably most prudently applied as a tool for broadly assessing slope stability at the basin scale. In particular, DHSVM is useful for investigating the effects of land cover change on slope stability. For example, post-forest fire landscapes, timber harvest, and urbanized watersheds all have implications for changes in slope stability that could by approached using numerical modeling. In general, numerical modeling should be viewed as one tool of many that can be used for slope stability analysis, and should not be exclusively used as the basis for making decisions regarding hillslope hazards (e.g., Hammond et al., 1992).

Although heterogeneity in mechanical properties makes predicting the spatial distribution of failures challenging, modeling does provide a good way to evaluate the relative sensitivity of input parameters. For example, one outcome for this study is that even small amounts of root cohesion can greatly stabilize hill slopes, and hence, the vertical and lateral distribution of root morphology may be a controlling factor for the occurrence of slope failures in the basin. Thus, numerical modeling techniques provide an excellent tool for the evaluating the relative importance of the various factors that control slope stability, and in that sense, can help aid management decisions.

One element that can make the application of the DHSVM mass wasting algorithm more robust is a well-constrained landslide inventory (Doten et al., 2006). If the timing and spatial distribution of slope failures are well understood in a region, various statistical methods can be used to correlate predicted failure probability to the occurrence of actual landslides. For example Huang et al. (2006) used a stacking technique to combine 200 probability maps that best characterized the landslide inventory for mountainous

watersheds in Taiwan, and then created a susceptibility map for the region by using a GIS to identify characteristics common to the failed areas. In a heavily forested watershed like the Jones Creek basin, it is extremely challenging to identify failures, even with a robust air photo record. Therefore, it might be more practical to apply the DHSVM mass wasting algorithm to a more densely populated region, where the occurrence of landslides is more likely to be documented.

6.5 Future Work

There are a number of field-based studies that could supplement the refinement of the DHSVM as a tool for predicting slope failures in the Jones Creek watershed. Automated camera systems situated directly across the creek channel from each unvegetated landslide toe would be one of the most useful. A detailed photographic record of the evolution of the landslide toes would provide a much-needed understanding of the frequency of small slope failures that are not otherwise observed or recorded. Such a study would have to be implemented over the course of several years to be useful for assessing DHSVM predictions. Installation of shallow piezometers on the landslides would be useful for a more rigorous DHSVM hydrology calibration at the pixel scale. A shallow groundwater study could be implemented over a shorter period of time than a remote camera study. Water table fluctuation data spanning one or two winter seasons would likely provide a sufficient characterization of shallow hydrology. Last, any number of geophysical techniques for shallow subsurface characterization could be applied to improve the understanding of the nature of the boundary between the unconsolidated landslide material and bedrock at depth. A baseline geophysical survey of the landslide toes, while expensive, could likely be conducted over the course of a few days.

7.0 Conclusion

This study provides an initial evaluation of the relationship between precipitation and failure probability, and possible consequences of timber harvest, in the Jones Creek watershed. The estimated probability of shallow slope failures due to high intensity, low duration storms at Jones Creek compare favorably to other studies that have been conducted for the Pacific Northwest. The basin seems to be relatively insensitive to low intensity, long duration storms, likely because of the steep slopes and flashy hydrologic conditions that allow water to quickly move through soils.

Root cohesion may be the most important controlling factor governing slope stability in the basin. Although it is difficult to predict the spatial distribution of the reduction in root strength due to a hypothetical timber harvest scenario, failure probability in areas with a complete loss in root cohesion would likely be dramatically increased. While the effects of timber harvest on shallow water table fluctuation during high-intensity storms seems to be minimal, the implications for increased deep percolation of water in to a bedrock-rooted slip plane on a seasonal scale are beyond the scope of this study and should not be dismissed.

There is significant variability in almost every parameter that controls slope stability at Jones Creek. The geomorphic and hydrologic complexity of a variable landform such as a deep-seated landslide makes the applicability of numerical modeling techniques for predicting the probability of slope failure suspect without a significant amount of supplementary field study. However, from a practical point of view, field studies can require significant financial resources, while numerical modeling is relatively inexpensive. In cases when financial resources are limited, such as at Jones Creek, a standalone modeling analysis is a reasonable option. . This study provides an initial modeling approach for slope stability analysis in the Jones Creek basin that will contribute to, and benefit from, ongoing research.

8.0 References

Abernethy, B., and Rutherfurd, I. D., 2001, The distribution and strength of riparian tree roots in relation to riverbank reinforcement: *Hydrological Processes,* Vol. 15, pp. 63-79.

Abramson, L. W., Lee, T. S., Sharma, S., and Boyce, G. M., 2002, *Slope Stability and Stabilization Methods:* John Wiley and Sons*,* New York, NY, 736 p.

Albert, R., Albert, I., Hornbaker, D., Schiffer, P., and Barabasi, A. L., 1997, Maximum angle of stability in wet and dry spherical granular media: *Physical Review E,* Vol. 56, No. 6, pp. 3708-3711.

Aleotti, P., and Chowdhurry, R., 1999, Landslide hazard assessment: Summary review and new perspectives: *Bulletin Engineering Geology Environment*, Vol. 58, pp. 21-44.

Al-Karni, A., and Al-Shamrani, M., 1999*,* Study of the effect of soil anisotropy on slope stability using method of slices*: Computers Geotechnics*, Vol. 26, pp. 83-103.

Barik, M. G., 2010, *Landslide Susceptibility Mapping to Inform Land Use Management Decisions in an Altered Climate*: Unpublished M.S. Thesis, Department of Civil and Environmental Engineering, Washington State University, Pullman, WA, 55 p.

Baum, R., Harp, E., and Highland, L., 2007, *Landslide Hazards in the Seattle, Washington area*: U.S. Geological Survey Fact Sheet 2007-3005, 4 p.

Berti, M., Martina, M. L. V., Franceschini, S., Pignone, S., Simoni, A., and Pizziolo, M., 2012, Probabilistic rainfall thresholds for landslide occurrence using a Bayesian approach: *Journal Geophysical Research,* Vol. 117, 20 p.

Bewley, D., Alila, Y., and Varhola, A., 2010, Variability of snow water equivalent and snow energetics across a large catchment subject to Mountain Pine Beetle infestation and rapid salvage logging: *Journal Hydrology*, Vol. 388, pp. 464-479.

Bischetti, B. G., Chiaradia, E. A., Simonato, T., Speziali, B., Vitali, B., Vullo, P., and Zocco, A., 2005, Root strength and root area ratio of forest species in Lombardy, Northern Italy: *Plant Soil*, Vol. 278, pp. 11-22.

Bishop, A. W., 1955, The use of the slip circle in the stability analysis of slopes: *Geotechnique*, Vol. 16, No. 2, pp. 89-130.

Bowling, L. C., Storck, P., and Lettenmaier, D. P., 2000, Hydrologic effects of logging in western Washington, United States: *Water Resources Research,* Vol. 36, No. 11, pp. 3223-3240.

Bowling, L. C. and Lettenmaier, D. P., 2001, The effect of forest roads and harvest on catchment hydrology in a mountainous maritime environment. In Burges, S., and Wigmosta, W. (Eds), *Land Use Watersheds: Human Influence Hydrology Geomorphology Urban Forest Areas.* Water Science and Application, The American Geophysical Union, pp. 145-164.

Brandon, T. L., Wright, S.G., and Duncan, J. M., 2008, Analysis of the stability of I-Walls with gaps Between the I-Wall and the levee fill: *Journal Geotechnical Geoenvironmental Engineering ASCE*, May, 2008, pp. 692-700.

Brardinoni, F., Hassan, M. A., and Slaymaker, H. O., 2002, Complex mass wasting response of drainage basins to forest management in coastal British Columbia: *Geomorphology,* Vol. 49, pp. 109-124.

Brideau, M., Yan, M., and Stead, D., 2009, The role of tectonic damage and brittle rock fracture in the development of large rock slope fractures: *Geomorphology*, Vol. 103, pp. 30-49.

Brown, C. B., and Sheu, M. S., 1975, Effects of deforestation on slopes: *Journal Geotechnical Engineering Division (ASCE),* Vol. 101, No. 2, pp. 142-165.

Brown, E. H., 1987, Structural and accretionary history of the Northwest Cascades system, Washington and British Columbia: *Geological Society America Bulletin,* Vol. 99, pp. 201-214.

Burton, A., and Bathurst, J. C., 1998, Physically based modeling of shallow landslide sediment yield at a catchment scale: *Environmental Geology,* Vol. 35, pp. 89–99.

Caine, N., 1980, The rainfall intensity-duration control of shallow landslides and debris flows: *Geografiska Annaler, Series A-Physical Geography,* Vol. 62, No. 2, pp. 23-27.

Cammeraat, E., Van Beek, R., and Kooijman, A., 2005, Vegetation succession and its consequences for slope stability in SE Spain: *Plant Soil,* Vol. 278, pp. 135-147.

Canadell, J., Jackson, R. B., Ehlleringer, J. B., Mooney, H. A., Sala, O. E., and Schulze, E.D., 1996, Maximum rooting depth of vegetation types at the global scale: *Oecologia,* Vol. 108, No. 4, pp. 583-595.

Chleborad, A. F., 2000, *A method for anticipating the occurrence of precipitation-induced landslides in Seattle, Washington*: U.S. Geological Survey Open-File Report 00-469, 29 p.

Cho, G. C., Dodds, J., and Santamarina, J. C., 2006, Particle shape effects on packing density, stiffness, and strength: natural and crushed Sands: *Journal Geotechnical Geoenvironmental Engineering,* Vol. 132, No. 5, pp. 591-602.

Cho, S. E., and Lee, S. R., 2001, Instability of unsaturated soil slopes due to infiltration: *Computers and Geotechnics,* Vol. 28, No. 3, pp. 185-208.

Clague, J.C., and Roberts, N.J., 2012, Landslide Hazard and Risk. In Clague, J.J., and Stead, D. (Eds.), *Landslides: Types, Mechanisms and Modeling*: Cambridge University Press, New York, NY, 420 p.

Collins, B. D., and Sitar, N., 2011, Stability of steep slopes in cemented sands: *Journal of Geotechnical Geoenvironmental Engineering,* Vol. 137, No. 1, pp. 43-51.

Cooper, P., 2011, personal communication, Whatcom County River and Flood Division, 2930 Newmarket Street Suite 111, Bellingham, WA, 98226.

Coppin, N. J., and Richards, I. G., 1990, *Use of vegetation in civil engineering:* Construction Industry Research and Information Association, London, U.K, 292 p.

Coulomb, C. A., 1776, Essai sur une application des regles des maximis et minimis a quelques problemes de statique relatifs a l'architecture: *Memoires de l'Academie Royale pres Divers Savants,* Vol. 7**,** pp. 343-382.

Crosta, G., 1998, Regionalization of rainfall thresholds: an aid to landslide hazard evaluation: *Environmental Geology,* Vol. 35, No. 2, pp. 131-145.

Crown Pacific Limited Partnership, 1999*, Acme Watershed Analysis, Mass Wasting Assessment*: A Report prepared for Washington State Department of Natural Resources, Forest Practices Division, 69 p.

Cuo, L., Lettenmaier, D. P., Mattheussen, B. V., Storck, P., and Wiley, M., 2008, Hydrologic prediction for urban watersheds with the Distributed Hydrology-Soil-Vegetation Model: *Hydrological Processes,* Vol. 22, pp. 4205-4213.

Currie, M.V., and Morgan, L., 2010, Review of Debris Flow Mitigation for Jones Creek: A report prepared for the Whatcom County Flood Control Zone District, 93 p.

Dakhal, A. S., and Sidle, R. C., 2004, Pore water pressure assessment in a forest watershed: simulations and distributed field measurements related to forest practices: *Water Resources Research*, Vol. 40, No. 2, pp. 757-776.

Daly, C., Neilson, R., and Phillips, D. L., 1994, A statistical topographic model for mapping climatological precipitation over mountainous terrain: *Journal Applied Meteorology,* Vol. 33, pp. 140-158.

DeBaets, S. J., Poesen, B., Reubens, L., Wymans, J., DeBaerdemaeker, J., and Muys, B., 2008, Root tensile strength and root distribution of typical Mediterranean plant species and their contribution to soil shear strength: *Plant Soil,* Vol. 305, pp. 207-226.

De Blasio, F. V., 2011, *Introduction to the Physics of Landslides: Lecture notes on the dynamics of mass wasting*: Springer-Verlag, New York, NY, 408 p.

Dickerson, S., 2010, *Modeling the effects of climate change forecasts on streamflow in the Nooksack River basin*: Unpublished M.S. Thesis, Department of Geological Sciences, Western Washington University, Bellingham, WA, 132 p.

Dingman, S.L., 2002, *Physical Hydrology*: Prentice Hall, Upper Saddle River, NJ, 646 p.

Doten, C. O. and Lettenmaier, D. P., 2004, *Prediction of sediment erosion and transport with the distributed hydrology-soil-vegetation model*: Water Resources Research Series Technical Report 178, 70 p.

Doten, C. O., Bowling, L. C., Lanini, L. S., Maurer, E. P., and Lettenmaier, D. P., 2006, A spatially distributed model for the dynamic prediction of sediment erosion and transport in mountainous forested watersheds: *Water Resources Research*, Vol. 42, No. 4, 15 p.

Duncan, J. M., and Wright, S. G., 2005, *Soil Strength and Slope Stability*: John Wiley and Sons, Hoboken, NJ, 297 p.

Duncan, J. M., Brandon, T. L., Wright, S. G., and Vroman, N., 2008, Stability of I-Walls in New Orleans during Hurricane Katrina: *Journal Geotechnical Geoenvironmental Engineering ASCE*, May, 2008, pp. 681-691.

Elsner, M. M., Cuo, L., Coisin, N., Deems, J. S., Hamlet, A. F., Vano, J. A., Mickelson, K., Lee, S. Y., and Lettenmaier, D. P., 2010, Implications of 21st century climate change for the hydrology of Washington State: *Climactic Change,* Vol. 102, pp. 225-260.

Fell, R., Hungr, O., Leroueil, S., and Riemer, W., 2000, Geotechnical engineering of the stability of natural slopes, and cuts and fills in soil: Paper presented at GeoEng2000: International conference on geotechnical and geological engineering, Melbourne, Australia, 100 p.

Fernandez, A. L., and Santamarina, J. C., 2001, Effect of cementation on the small-strain parameters of sands: *Canadian Geotechnical Journal,* Vol. 38, pp. 191-199.

Frattini, P., Crosta, G., and Sosio, R., 2009, Approaches for defining thresholds and return periods for rainfall-triggered shallow landslides: *Hydrological Processes,* Vol. 23, pp. 1444-1460.

Fredlund, D. G., and Krahn, J., 1977, Comparison of slope stability methods of analysis: *Canadian Geotechnical Journal,* Vol. 14, No. 3, pp. 429-439.

Fredlund, D. G., Krahn, J., and Pufahl, D. E., 1981, The relationship between limit equilibrium slope stability methods: Proceedings of the 10th International Conference on Soil Mechanics and Foundation Engineering, Stockholm, Sweden, pp. 409-416.

Gao, C., Song, Z., and Shan, R., 2010, The slope stability of dump analysis based on SLIDE and Plaxis: *Microcomputer Information,* Vol. 33, pp. 261-262.

Godt, J. W., 2004, *Observed and modeled rainfall for shallow landsliding in the Seattle, Washington area*: Unpublished Ph.D. Thesis, University of Colorado Boulder, Boulder, CO, 151 p.

Gray, D. H., and Megahan, W. F., 1981, *Forest vegetation removal and slope stability in the Idaho Batholith*: USDA Forest Service Research Paper INT-271, 23 p.

Hammond, C., Hall, D., Miller, S., and Swetik, P., 1992, *Level l Stability Analysis (LISA) Documentation for Version 2.0*: USDA Forest Service General Technical Report INT-285, 190 p.

Harr, R. D., and Coffin, B. A., 1992, Influence of timber harvest on rain-on-snow runoff: a mechanism for cumulative watershed effects. In Jones, M. E., and Laenen, A. (Eds.), *Interdisciplinary approaches in hydrology and hydrogeology*. American Institute of Hydrology, pp. 456-469.

Highland, L.M., and Bobrowsky, P., 2008, *The landslide handbook-a guide to understanding landslides*: U.S. Geological Survey Circular 1325, 129 p.

Hogue, T. S., Sorooshian, S., and Gupta, H., 2000, A multistep automatic calibration scheme for river forecasting models: *Journal Hydrometeorology,* Vol. 1, No. 6, pp. 524-542.

Huang, J. R., Kao, S. J., Hsu, M. L., and Lin, J. C., 2006, Stochastic procedure to extract and to integrate landslide susceptibility maps: an example of mountainous watersheds in Taiwan: *Natural Hazards Earth System Sciences,* Vol. 6, pp. 803-815.

Hugget, B., 2013, personal communication, Humboldt State University, Department of Environmental Science and Management, 1 Harpst ST., Arcata, CA 95521.

Jabar, F.H., Shukla, S., and Srivastava, S., 2006, Recharge, upflux and water table response for shallow water table conditions in southwest Florida: *Hydrological Processes*, Vol. 20, pp. 1895-1907.

Jaiswal, P., and van Westen, C. J., 2009, Estimating temporal probability for landslide initiation along transportation routes based on rainfall thresholds: *Geomorphology,* Vol. 112, pp. 96-105.

Jakob, M., 2000, The impacts of logging on landslide activity at Clayoquot Sound, British Columbia: *Catena,* Vol. 38, pp. 279-300.

Jakob, M., Currie, M., and Weatherly, H., 2004, *Jones Creek debris flow study*: A report prepared for the Whatcom County Flood Control Zone District, 128 p.

Jassal, R. S., Black, T. A., Spittlehouse, D. L., Brummer, C., and Nesic, Z., 2009, Evapotranspiration and water use efficiency in different aged Pacific Northwest douglas-fir stands: *Agricultural Forest Meteorology,* Vol. 149, No. 6, pp. 1168-1178.

Janbu, N., Bjerrum, L., and Kjaernsli, B., 1956, *Sabilitetsberegning for fyllinger skaeringer og naturlige skraninger:* Norwegian Geotechnical Publication Number 16, 93 p.

Jibson, R.W., and Harp, E.L., 2011, *Field reconnaissance report of landslides triggered by the January 12, 2010, Haiti earthquake*: U.S. Geological Survey Open-File Report, 2011-10223, 24 p.

Johnson, S. Y., 1984, Stratigraphy, age, and paleogeography of the Eocene Chuckanut Formation, northwest Washington: *Canadian Journal Earth Sciences,* Vol. 21, pp. 92-106.

Kayadelen, C., Tekinsoy, M. A., and Taskiran, T, 2007, Influence of matric suction on shear strength behavior of a residual clayey soil: *Environmental Geology,* Vol. 53, pp. 891-901.

Keim, R. F., and Skaugset, A. E., 2003, Modeling effects of forest canopies on slope stability, *Hydrological Processes,* Vol. 317, pp. 1457-1467.

Kim, J., Jeong, S., Park, S., and Sharma, J., 2004, Influence of rainfall-induced wetting on the stability of slopes in weathered soils: *Engineering Geology,* Vol. 75, pp. 251-262.

Krahn, J., 2003, The 2001 R.M. Hardy Lecture: The limits of limit equilibrium analysis: *Canadian Geotechnical Journal,* Vol. 40, pp. 643-660.

Labuz, J., and Zang A., 2012, Mohr-Coulomb failure criterion: *Rock Mechanics Rock Engineering,* Vol. 45, No. 6, pp. 975-979.

Lambe, T. W., and Whitman, R. V., 1979, *Soil Mechanics, SI Version*: John Wiley and Sons, New York, NY, 553 p.

Lapen, T. J., 2000, *Geologic Map of the Bellingham 1:100,000 Quadrangle, Washington*: WADNR Open File Report 2000-5.

Leroueil, S., 2001, Natural slopes and cuts: Movement and failure mechanics: *Geotechnique,* Vol. 51, No. 3, pp. 197-243.

Leung, L. R., and Wigmosta, M. S., 1999, Potential climate change impacts on mountain watersheds in the Pacific Northwest: *Journal American Water Resources Association*, Vol. 35, No. 6, pp. 1463-1471.

Link, T. E., Unsworth, M., and Marks, D., 2004, The dynamics of rainfall interception by a seasonal temperate rainforest: *Agricultural Forest Meteorology,* Vol. 124, pp. 171-191.

Lu, N., and Likos, W. J., 2006, Suction stress characteristic curve for unsaturated soils: *Journal Geotechnical Geoenvironmental Engineering,* Vol. 132, No. 2, pp. 131-142.

Lu, N., Godt, J. W., and Wu, D. T., 2010, A closed-form equation for effective stress in unsaturated soil: *Water Resources Research,* Vol. 46, No. 5, 14 p.

Lu, N., and Godt, J. W., 2013, *Hillslope Hydrology and Stability*: Cambridge University Press, New York, NY, 437 p.

Margolis, S. V., and Krinsley, D. H., 1974, Processes of formation and environmental occurrence of microfeatures on detrital quartz grains: *American Journal Science,* Vol. 274, pp. 449-464.

McCann, D. M., and Forster, A., 1990, Reconnaissance geophysical methods in landslide investigations: *Engineering Geology,* Vol. 29, No. 1, pp. 59-78.

Mitchell, J. K., 1976, *Fundamentals of Soil Behavior*: John Wiley and Sons, New York, NY, 422 p.

Mohr, O., 1900, Welche Umstände bedingen die Elastizitätsgrenze und den Bruch eines Materials: *Zeit des Ver Deut Ing,* Vol. 44, pp. 1524–1530.

Montgomery, D. R., and Dietrich, W. E., 1994, A physically based model for the topographic control on shallow landsliding: *Water Resources Research,* Vol. 30, No. 4, pp. 1153-1171.

Montgomery, D. R., Schmidt, K. M., Dietrich, W. E., and Greenberg, H., 2000, Forest clearing and regional landsliding: *Geology*, Vol. 28, pp. 311–314.

Muntohar, A. S., and Lia, H. J., 2009, Analysis of rainfall-induced infinite slope failure during typhoon using a hydrological-geotechnical model: *Environmental Geology,* Vol. 56, pp. 1145-1159.

Nash, D. F. T., 1987, A comparative review of limit equilibrium methods of stability analysis. In Anderson, M.G., and Richards, K.S. (Eds.), *Slope stability-geotechnical engineering and geomorphology*, John Wiley and Sons, New York, NY, pp 11-76.

National Oceanic and Atmospheric Association, 2006, *Coastal change analysis program regional landcover*, electronic dataset, available at http://www.csc.noaa.gov /crs/lca/pacificcoast.html

Natural Resource Conservation Service, 2006, *Soil survey data for the Whatcom County area, Washington*, electronic dataset, available at http://soildatamart.nrcs.usda.gov/ Survey.aspx?County=WA073

Natural Resources Conservation Service, 2013, *What is a soil?:* Electronic document, available at http://soils.usda.gov/education/facts/soil.html

Neuffer, D. P., and Shultz, R. A., 2006, Mechanisms of slope failure in Velles Marineris, Mars: *Quarterly Journal Engineering Geology Hydrogeology,* Vol. 39, pp. 227-240.

Nilaweeara, N. S., and Nutalaya, P., 1999, Role of tree roots in slope stabilization: *Bulletin Engineering Geology Environment,* Vol. 57, pp. 337-342.

Nouguier-Lehon, C., Cambou, B., and Vincens, E., 2003, Influence of particle shape and angularity on the behaviour of granular materials: a numerical analysis*: International Journal Numerical Analytical Methods Geomechanics,* Vol. 27, pp. 1207-1226.

O'Loughlin, C. L., 1974, The effects of timber removal on the stability of forest soils: *Journal Hydrology (NZ),* Vol. 13, No. 2, pp. 121-134.

Operstein, B., and Frydman, S., 2000, The influence of vegetation on soil strength: *Ground Improvement,* Vol. 4**,** pp. 81-89.

Ottenbreit, E. M., 2011*, Modeling the impacts of climate change and agricultural management practices on surface erosion in a dryland agricultural basin*: Unpublished M.S. Thesis, Department of Civil and Environmental Engineering, Washington State University, Pullman, WA, 117 p.

Paul, M. J., and Meyer, J. L., 2001, Streams in urban landscapes: *Annual Review Ecology Systematics,* Vol. 32, pp. 333-365.

Pittman, P., 2012, personal communication, Element Solutions, 1812 Cornwall Avenue, Bellingham, WA 98225.

Powell, J., Lingley, L., and Anderson, G., 2010*, Reconnaissance study of landslides related to the January, 2009 storm in the Acme watershed*: Report for Washington State Department of Natural Resources Forest Practices Division, 46 p.

Puget Sound LiDAR Consortium, 2006, *Airborne LiDAR data set, Puget Sound Region*: electronic dataset, available at http://pugetsoundlidar.ess.washington.edu/

Raines, M., Hung, O., Welch, K. F., and Willing, P., 1996, *Whatcom County lower Nooksack River comprehensive flood hazard management plan, alluvial fan hazards: recommended assessment methodology and regulatory approach*: Report prepared by KCM Inc., 27 p.

Rantz, S. E., 1982, *Measurement and computation of streamflow, volume 1: Measurement of stage and discharge:* U.S. Geological Survey Water-Supply Paper 2175, 18 p.

Roering, J. J., Schmidt, K. M., Stock, J. D., Dietrich, W. E., and Montgomery, D. R., 2003, Shallow landsliding, root reinforcement, and the spatial distribution of trees in the Oregon Coast Range: *Canadian Geotechnical Journal,* Vol. 40, pp. 237-253.

Sakals, M. E., Innes, J. L., Wilford, D. J., Sidle, R. C., and Grant, G. E., 2006, The role of forests in reducing hydrogeomorphic hazards: *Forest, Snow Landscape Research,* Vol. 80, No. 1, pp. 11-22.

Schmidt, K. M., Roering, J. J., Stock, J. D., Dietrich, W. E., Montgomery, D. R., and Schaub, T., 2001, The variability of root cohesion as an influence on shallow landslide susceptibility in the Oregon Coast Range: *Canadian Geotechnical Journal,* Vol. 38, pp. 995-1024.

Sharma, S. S., and Lovell, C. W., 1983, Strengths and weaknesses of slope stability analysis: Proceedings of the 34th Annual Highway Geology Symposium, Atlanta, Georgia, pp. 215-232.

Sidle, R. C., 1984, Shallow groundwater fluctuations in unstable hillslopes of coastal Alaska: *Zeitschriftfur Gletscherkunde und Glazialgeologie,* Vol. 20, No. 2, pp. 79-95.

Sidle, R. C., Pearce, A. J., and O'Loughlin, C. L., 1985, *Hillslope stability and Land Use*: Water Resources Monograph Series 11, American Geophysical Union, Washington, DC, 140 p.

Six, J., Elliot, E. T., and Paustian, K., 2000, Soil structure and soil organic matter ll: A normalized stability index and the effect of mineralogy: *Soil Science Society America Journal,* Vol. 64, No. 3, pp. 1042-1049.

Snyder, K., 2000, *Debris flows and flood disturbances in small mountain watersheds*: Unpublished M.S. Thesis, Department of Forest Science Oregon State University, Corvallis, OR, 57 p.

Spencer, E., 1967, A method of analysis of the stability of embankments assuming parallel interslice forces: *Geotechnique,* Vol. 17, pp. 11-26.

Spiker, E. C., and Gori, P. L., 2003, *National landslide hazards mitigation strategy: A framework for loss reduction*: U.S. Geological Survey Circular 1244, 56 p.

Spittlehouse, D. L., 1998, Rainfall Interception in young and mature conifer forests in British Columbia: Proceedings of the 23rd Conference on Agricultural and Forest Meteorology, Albuqerque, NM, pp. 171-174.

Stead, D., and Coggan, J., 2012, Numerical modeling of rock slope stability. In Clague, J.J., and Stead, D. (Eds.), *Landslides: Types, Mechanisms and Modeling*: Cambridge University Press, New York, NY, 420 p.

Storck, P., Lettenmaier, D. P., Connelly, B. A., and Cundy, T. W., 1995, *Implications of forest practices on downstream flooding: Phase II Final Report*: Washington Forest Protection Association TFW-SH20-96-001, 100 p.

Storck, P., Bowling, L., Wetherbee, .P, and Lettenmaier, D. P., 1998, Application of a GIS-based distributed hydrology model for prediction of forest harvest effects on peak stream flow in the Pacific Northwest: *Hydrologic Processes,* Vol. 12, pp. 899-904.

Surfleet, C. G., Skaugset, A., and Dietterick, B., 2012, *An approach to study the effect of harvest and wildfire on watershed hydrology and sediment yield in a coast redwood forest*: USDA Forest Service General Technical Report PSW-GTR-238, 8 p.

Swanston, D. N., 1974, *Slope stability problems associated with timber harvesting in mountainous regions of the western United States*: USDA Forest Service General Technical Report PNW-1, 19 pp.

Tangedahl, E. L., 2006, *Utilization of the Distributed-Hydrology-Soil-Vegetation-Model (DHSVM) To Quantify Streamflow Changes and Slope Failure Probability Following the Snow-Talon Fire Near Lincoln Montana, USA*: Unpublished M.S. Thesis, Department of Forestry, University of Montana-Missoula, Missoula, MT, 60 p.

Tarolli, P., and Tarboton, D. G., 2006, A new method for determination of most likely landslide initiation points and the evaluation of digital terrain model scale in terrain stability mapping: *Hydrology Earth System Sciences,* Vol. 10, pp. 663-677.

Terzaghi, K., 1936, The shearing resistance of saturated soils: Proceedings of the First International conference on Soil Mechanics, pp. 54-56.

Terzaghi, K., 1943, *Theoretical Soil Mechanics*: John Wiley and Sons, New York, NY, 510 p.

Thomas, R. B., and Megehan, W. F., 1981, Peak flow responses to clear cutting and road in small and large basins, Western Cascades, Oregon: A second opinion: *Water Resources Research,* Vol. 34, No. 12, pp. 3393-3403.

Thorsen, G. W., 1989, *Splitting and sagging mountain*: Washington Geologic Newsletter, Washington State Department of Natural Resources, Division of Geology and Earth Resources, 10 p.

Thorsen, G. W., Orme, A. J., and Orme, A. R., 1992, *Relative slope stability, Jones Creek Basin, Whatcom County, Washington*: Report for Washington State Department of Natural Resources, 14 p.

Washington Forest Practices Board, 1997, *Standard methodology for conducting watershed analysis under Chapter 222-22 WAC, Version 3.0*: Department of Natural Resources Forest Practices Division, 137 p.

Washington Forest Protection Association, 2012, *When the Earth Moves: Geology, Topography, Storms and Landslides in Washington State:* Electronic document, available at http://www.wfpa.org/page/steep-slope-protection/

Washington State DNR, 2013, *Landslide Hazards in Washington State*: Electronic document, available at http://www.dnr.wa.gov/ RESEARCHSCIENCE/ TOPICS/ GEOLOGICHAZARDSMAPPING/PAGES/LANDSLIDES.ASPX

Watson, A., Phillips, C., and Marden, M., 1999, Root strength, growth, and rates of decay: root reinforcement changes of two tree species and their contribution to slope stability: *Plant Soil,* Vol. 217, pp. 39-47.

Weeks, E.P., 2002, The Lisse Effect revisited: *Ground Water*, Vol. 40, No. 6, pp. 652-656.

White, M. D., and Greer, K. A., 2006, The effects of watershed urbanization on the stream hydrology and riparian vegetation of Los Penasquitos Creek, California: *Landscape Urban Planning,* Vol. 74, No. 2, pp. 125-138.

Wigmosta, M. S., Vail, L. W., and Lettenmaier, D. P., 1994, A distributed hydrology-vegetation model for complex terrain: *Water Resources Research,* Vol. 30, No. 6, pp. 1665-1679.

Wigmosta, M. S., and Perkins, W. A., 2001, Simulating the effect of forest roads on watershed hydrology, in Burges, S. J., and Wigmosta, M. S. (Eds.), *Land Use and Watersheds: Human Influence on Hydrology and Geomorphology in Urban and Forest Areas*. American Geophysical Union, Washington, DC, pp. 127-143.

Wu, W., and Sidle, R. C., 1995, A distributed slope stability model for steep forested basins: *Water Resources Research,* Vol. 31, No. 8, pp. 2097-2110.

Wu, T. H., Mckinnell, W. P., and Swanston, D. N., 1979, Strength of tree roots and landslides on Prince of Wales Island, Alaska: *Canadian Geotechnical Journal,* Vol. 16, pp. 19-33.

Zeimer, R. R., 1981, Roots and the stability of forested slopes: *International Association Scientific Hydrology,* Vol. 132, pp. 343-361.

Zhang, L. W., 2012, Influence of anisotropic internal friction angle on the stability of uniform soil slopes: *Applied Mechanics Materials,* Vol. 170, pp. 270-273.

Zhou, Y., Watts, D., Li, Y., and Xiaoping, C., 1998, A case study of effect of lateral roots of *Pinus yunnanensis* on shallow soil reinforcement: *Forest Ecology and Management,* Vol. 103, pp. 107-120.

9.0 Tables

Table 1. Mass Wasting Units (MWU) in the Jones Creek watershed.	
MWU number	Description
1	Convergent topography greater than or equal to 36 degrees, including bedrock hollows, channel heads, and inner gorges of first order channels. These map units are naturally prone to landsliding and are a primary source of debris flows.
2	Inner gorges, greater or equal to 40 degrees in the Chuckanut formation, or greater than or equal to 36 degrees phyllitic terrain, along second order or higher channels.
9	Deep seated slope instability, showing signs of recent activity. Large volumes of readily available sediment adjacent to creek channels.
10	Generally planar topography, 31 to 35 degree hillslopes with primarily thick soils adjacent to inner gorges. Although the relative stability of this unit is higher than for MWU #1 and MWU #2, debris flows and dam-break floods can be triggered from this unit.

Table 2. Assigned mechanical properties for soils and coniferous forest in the Jones Creek watershed.				
Parameter	Probability distribution	Range	Standard Deviation	Mean/Mode
Loam cohesion (kPa)	Normal	NA	8	17
Loam friction angle (degrees)	Uniform	29-38	-	-
Fine sandy loam cohesion (kPa)	Normal	NA	6.5	13
Fine sandy loam friction angle (degrees)	Uniform	27-35	-	-
Landslide cohesion (kPa)	Uniform	7.5-13	-	-
Landslide friction angle (degrees)	Uniform	25-32	-	-
Coniferous forest root cohesion (kPa)	Triangular	2-17	-	9.5
Coniferous forest overburden (kg/m^2)	Uniform	48.9-195.4	-	-

Table 3. Assigned soil cohesion distributions for harvest scenarios (kPa).						
Scenario	**Soil**	**Statistical Distribution**	**Mean**	**Standard Deviation**	**Min**	**Max**
A,D	Soil 4	Normal	13	6.5	-	-
	Soil 6	Normal	17	8	-	-
	Soil 11	Uniform	-	-	7.5	13
B,E	Soil 4	Normal	9.75	4	-	-
	Soil 6	Normal	12.75	6	-	-
	Soil 11	Uniform	4.5	10	-	-
C,F	Soil 4	Normal	6.5	4	-	-
	Soil 6	Normal	8.5	6	-	-
	Soil 11	Uniform	2.5	10	-	-

Scenario A assumes the standard soil cohesion values defined in Table 2, and DHSVM-default values for shrub root cohesion. Scenario B assumes an approximate 25 percent reduction in soil cohesion. Scenario C assumes an approximate 50 percent reduction in soil cohesion. Scenario D assumes a 50 percent reduction in the default shrub root cohesion. Scenario E assumes a 50 percent reduction in root cohesion, and a 25 percent reduction in soil cohesion. Scenario F assumes a 50 percent reduction is soil cohesion, and a 50 percent reduction in root cohesion.

Table 4. Assigned root cohesion distributions for the timber harvest scenarios (kPa).				
Scenario	**Statistical Distribution**	**Mode**	**Min**	**Max**
A,B,C	Triangular	4	2	6
D,E,F	Uniform	-	0	3

Scenario A assumes the standard soil cohesion values defined in Table 2, and DHSVM-default values for shrub root cohesion. Scenario B assumes an approximate 25 percent reduction in soil cohesion. Scenario C assumes an approximate 50 percent reduction in soil cohesion. Scenario D assumes a 50 percent reduction in the default shrub root cohesion. Scenario E assumes a 50 percent reduction in root cohesion, and a 25 percent reduction in soil cohesion. Scenario F assumes a 50 percent reduction is soil cohesion, and a 50 percent reduction in root cohesion.

Table 5. Calibrated DHSVM hydrology parameters.		
Parameter	Value	Units
Soil Depth	1.2-3.6	m
Loam Hydraulic Conductivity	0.003	m/s
Fine Sandy Loam Hydraulic Conductivity	0.005	m/s
Landslide Hydraulic Conductivity	0.002	m/s
Precipitation Lapse Rate	0.0003	m/m

Table 6. Equations for the portions of the intensity (I)-duration(D) probability thresholds sensitive to precipitation duration, for the Straight and South landslides.		
Probability Threshold	Straight	South
0.1	I = -0.005D + 0.23	I = -0.001D +0.12
0.2	I = -0.006D + 0.29	I = -0.002D +0.175
0.3	I = -0.007D + 0.41	I = -0.003D +0.22
0.4	I = -0.009D + 0.5	I = -0.005D +0.315
0.5		-
0.6		I = -0.009D +0.49
0.7	I = -0.01D + 0.65	I = -0.02D +0.86

Table 7. Failure statistics for timber harvest scenarios.				
Scenario	**MWU Zone**	**Failed Cells**	**Failures/km^2**	**Mean Failure Probability (Percent)**
Initial (current land cover)	MWU 1	177	562	2.9
	MWU 2	557	883	3.7
	MWU 9	124	593	3.9
	MWU 10	358	951	2.6
	Outside MWU zones	1303	247	1.7
	Total	2519	370	2.5
Harvest A	MWU 1	579	1838	2.1
	MWU 2	983	1558	3.0
	MWU 9	338	1615	2.5
	MWU 10	637	1692	2.0
	Outside MWU zones	3884	737	1.6
	Total	6421	944	1.9
Harvest B	MWU 1	613	1946	3.6
	MWU 2	1207	1913	4.7
	MWU 9	439	2098	3.9
	MWU 10	700	1860	4.0
	Outside MWU zones	6217	1180	2.8
	Total	9176	1349	3.2

Table 7 (continued). Failure statistics for timber harvest scenarios				
Scenario	**Area**	**Failed Cells**	**Failures/km^2**	**Mean Failure Probability**
Harvest C	MWU 1	865	2746	5.8
	MWU 2	1588	2517	9.0
	MWU 9	580	2772	7.3
	MWU 10	820	2178	7.7
	Outside MWU zones	9121	1731	4.5
	Total	12974	1908	5.5
Harvest D	MWU 1	1099	3488	3.0
	MWU 2	1438	2280	4.3
	MWU 9	488	2332	3.5
	MWU 10	835	2218	3.4
	Outside MWU zones	8290	1574	1.7
	Total	12150	1787	2.7
Harvest E	MWU 1	1134	3599	5.2
	MWU 2	1620	2568	7.0
	MWU 9	536	2562	6.6
	MWU 10	862	2290	7.0
	Outside MWU zones	10640	2020	4.1
	Total	14792	2175	4.8

Table 7 (continued). Failure statistics for timber harvest scenarios				
Scenario	**Area**	**Failed Cells**	**Failures/km^2**	**Mean Failure Probability**
Harvest F	MWU 1	1414	4488	9.6
	MWU 2	2133	3381	13.1
	MWU 9	793	3790	12.8
	MWU 10	982	2609	13.7
	Outside MWU zones	14301	2714	7.3
	Total	19623	2886	8.6

10.0 Figures

Figure 1. Regional study location, including the Acme Watershed Administrative Unit AWAU; (outlined in black), Jones Creek watershed (outlined in red), the Abbotsford A and Brannian Creek weather stations, the communities of Bellingham and Acme, and the Nooksack River drainage.

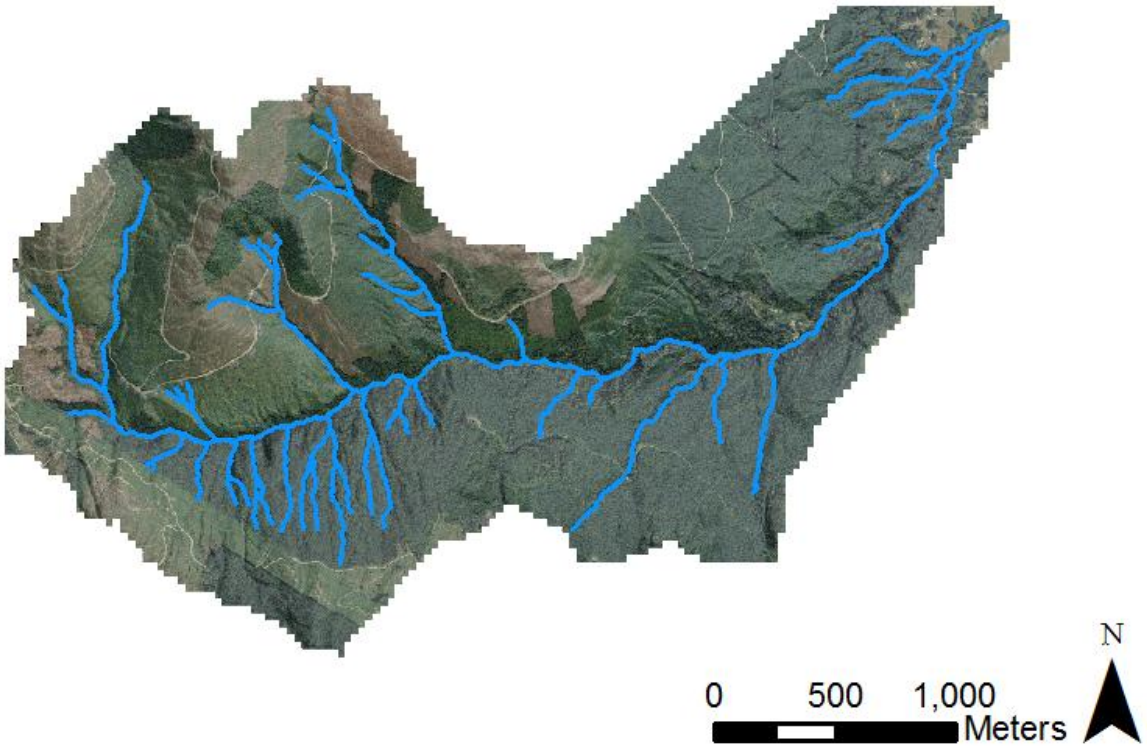

Figure 2. Aerial view of the Jones Creek watershed. Coniferous trees (darker green) have been logged and replaced by shrubs (lighter green) and grassland (tan) in many areas, particularly on the north side of the main channel in the upper watershed.

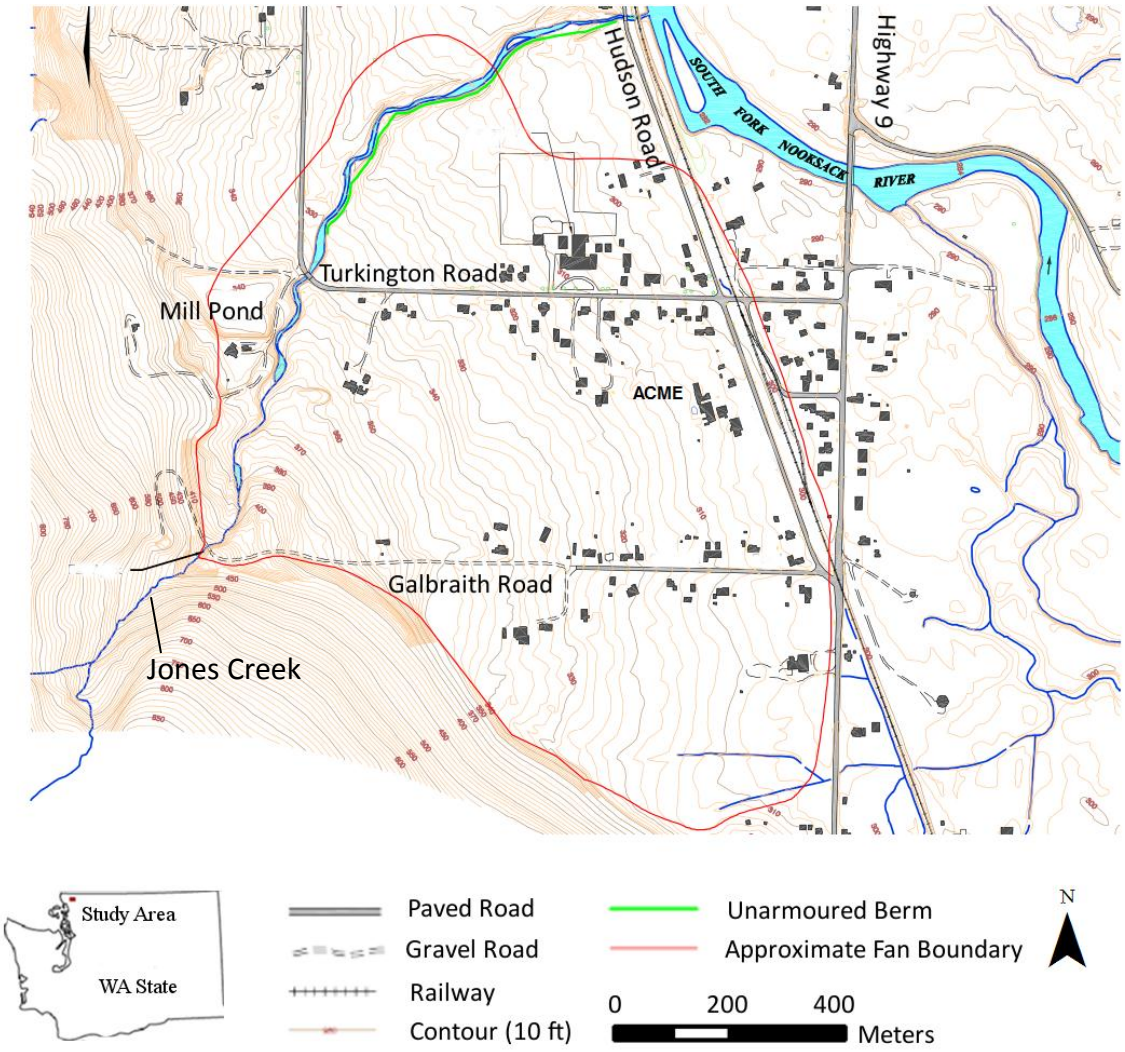

Figure 3. Infrastructure on the Jones Creek fan. Bridges span Jones Creek at Galbraith, Turkington, and Hudson roads. There are approximately 100 buildings constructed on the Jones Creek fan. Modified from Jakob et al. (2004).

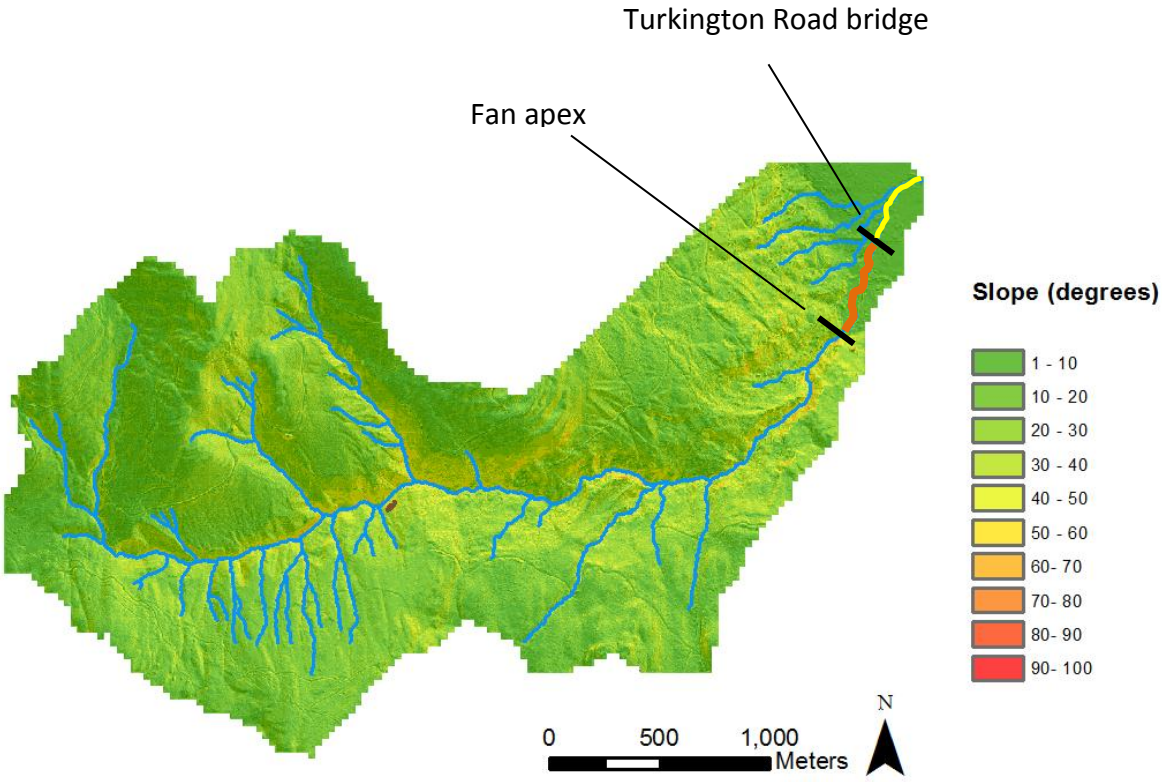

Figure 4. LiDAR-derived slope map of the Jones Creek watershed and stream reaches defined by Jakob et al. (2004). Reach one includes the channel above the fan apex and is shown in blue. Reach two includes the channel between the fan apex and the Turkington Road bridge and is shown in orange. Reach three includes the channel below the Turkington Road bridge and is shown in yellow.

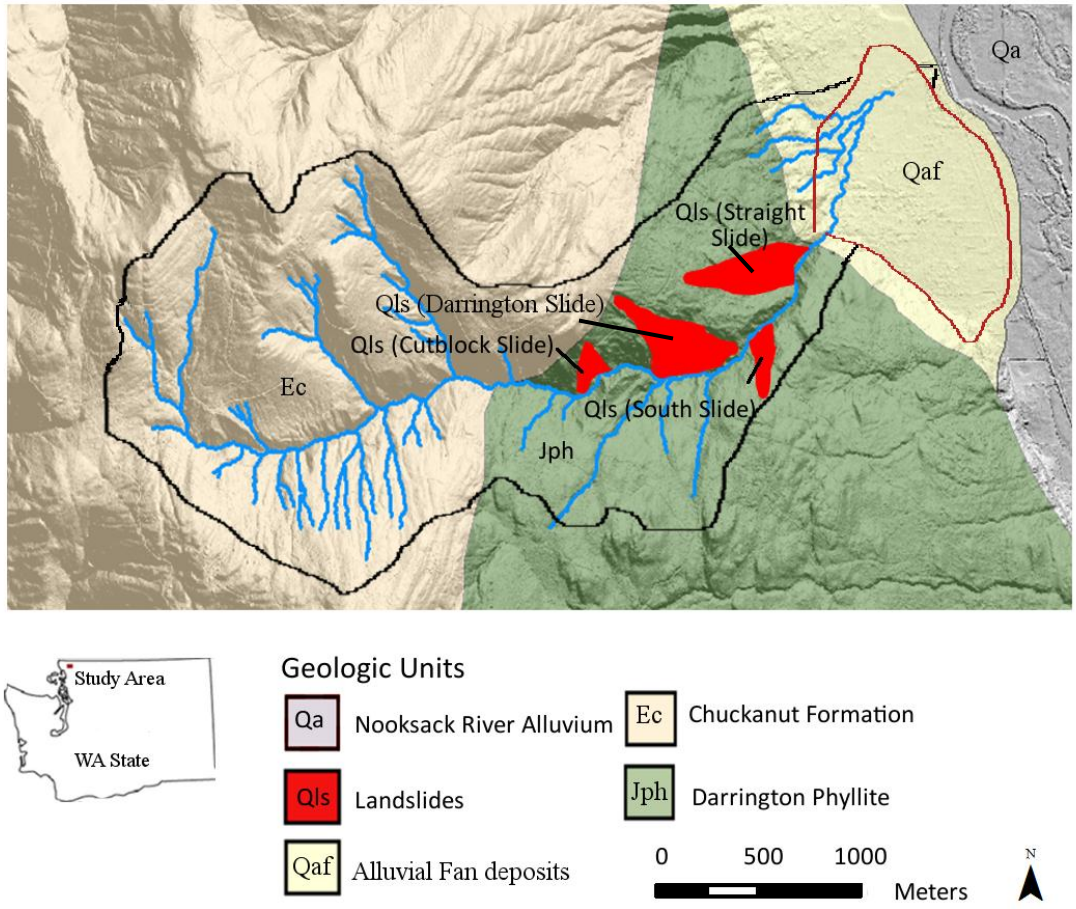

Figure 5. Geologic setting of the Jones Creek watershed. The approximate watershed boundary is outlined in black. Jones Creek is shown in blue. The fan boundary is outlined in red. Modified from Jakob et al. (2004) and Lapen (2000).

Figure 6. View looking northwest of the unvegetated toe of the Darrington landslide. The unvegetated toe is situated directly adjacent to Jones Creek, visible on the left.

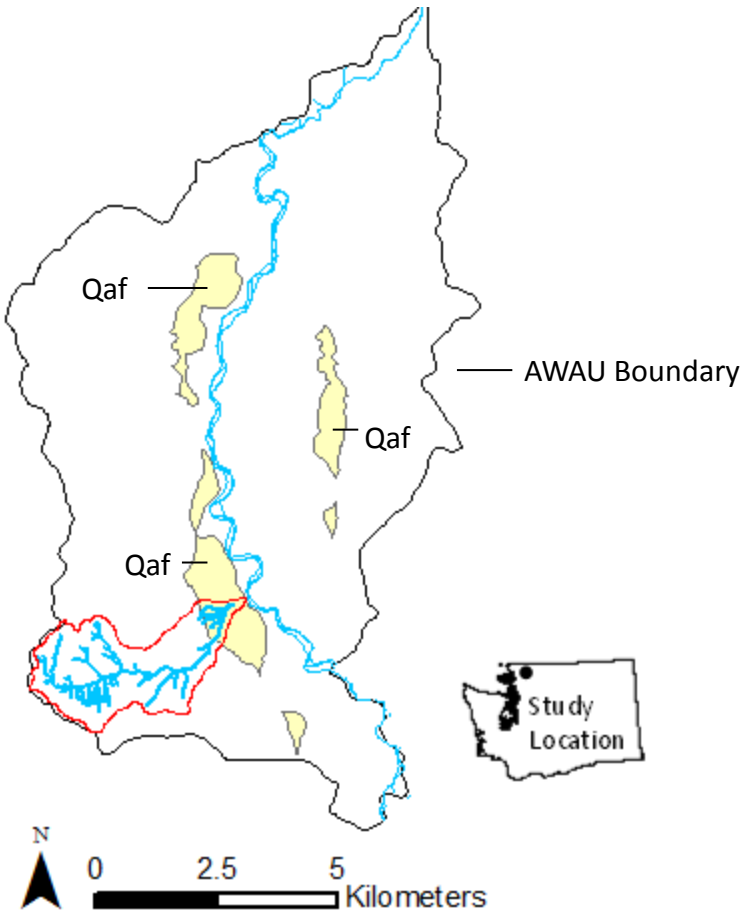

Figure 7. Acme Watershed Administrative Unit (AWAU) boundary in the South Fork Nooksack river valley. Yellow units labeled 'Qaf' are alluvial fans deposits at the bottom of steep drainages on both sides of the valley, including the Jones Creek watershed, which is outlined in red (Crown Pacific, 1999; Lapen, 2000).

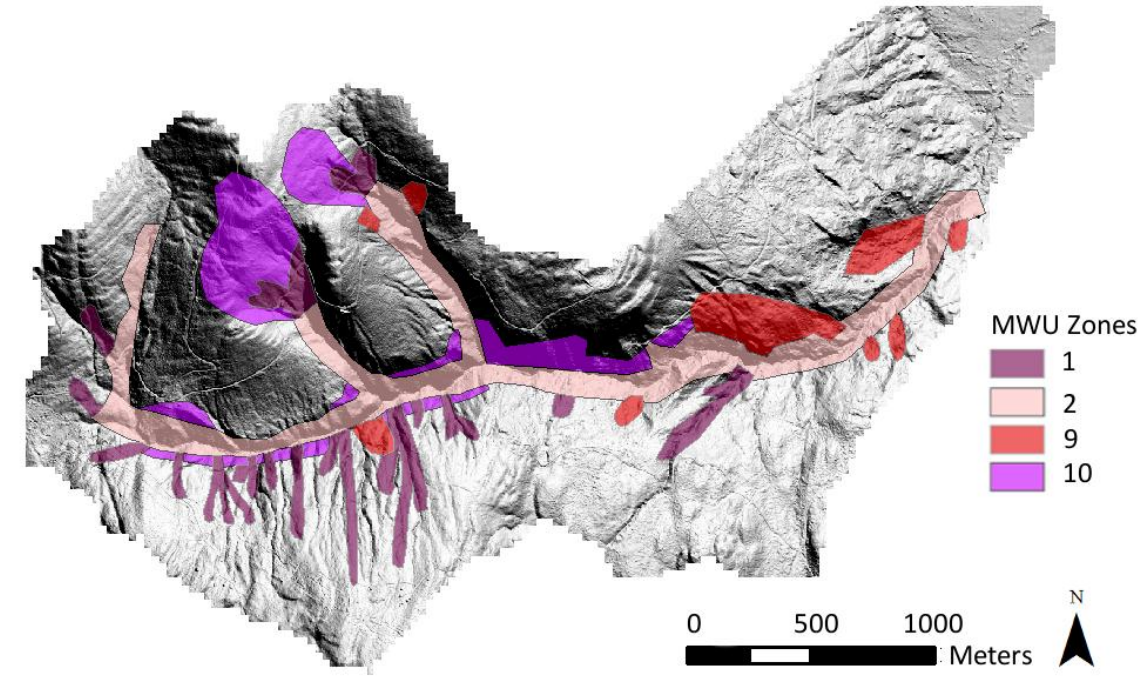

Figure 8. Mass Wasting Units (MWUs) in the Jones Creek watershed (Crown Pacific Limited Partnership, 1999).

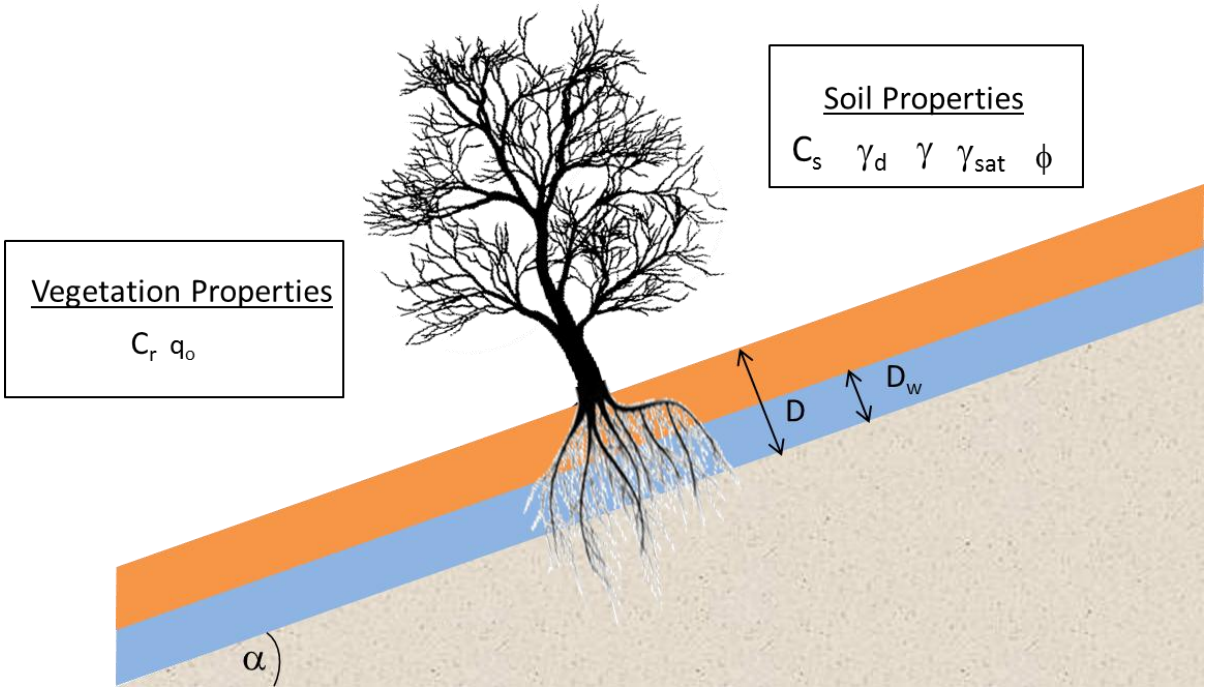

α = slope of ground surface (^{o})
D = total soil thickness (m)
D_w = saturated soil thickness (m)
C_r = root cohesion (kPa)
q_0 = vegetation surcharge (kPa)
C_s = soil cohesion (kPa)

ϕ = angle of internal friction (^{o})
γ_d = dry soil unit weight (kg/m^3)
γ= moist soil unit weight (kg/m^3)
γ_{sat} = saturated unit weight (kg/m^3)

Figure 9. Conceptual setup for infinite slope failure, where a thin mantle of soil overlies a less permeable soil unit or bedrock. Infinite slope assumes the soil-rock interface and water table to be approximately planar and parallel (Hammond et al., 1992).

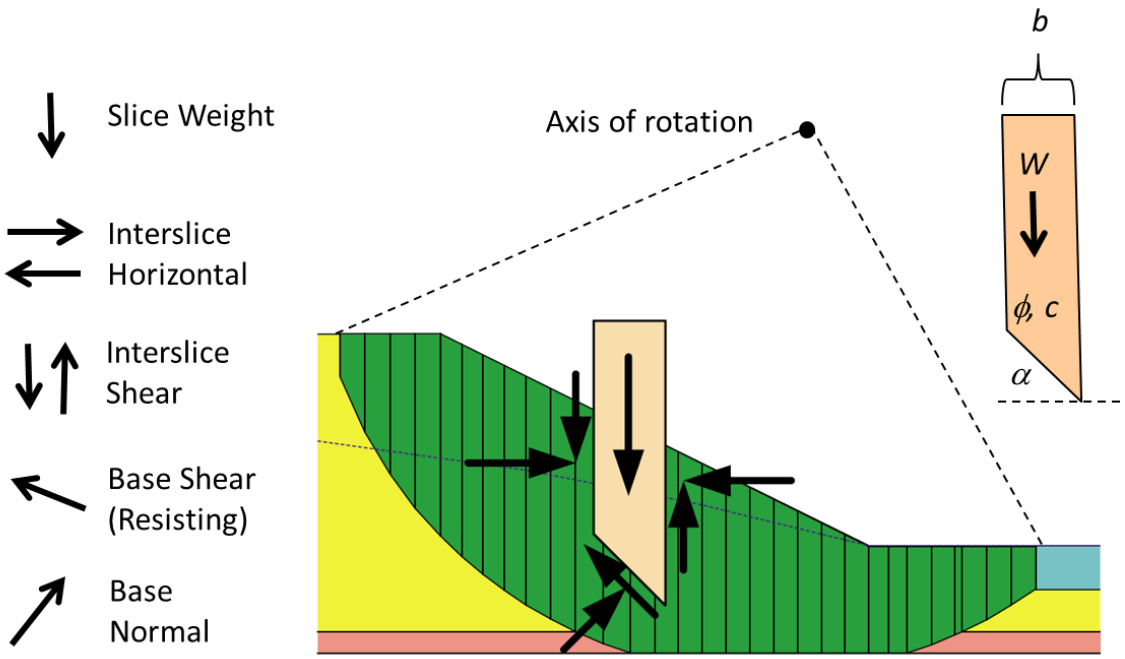

Figure 10. Conceptual setup for a method of slices analysis. Weight, interslice horizontal, horizontal, interslice shear, base normal, and base resisting force vectors act on each slice. The parameters that influence the calculated factor of safety include soil weight (*W*), friction angle (ϕ), cohesion (*c*), slice width (*b*), and slope angle (α). The factor of safety is calculated either by summing the forces acting at the base of each slice, or summing the moments acting around an axis of rotation at the base of each slice. The Bishop's Simplified Method, used in this study, ignores the effects of interslice shear forces. Modified from Krahn (2003).

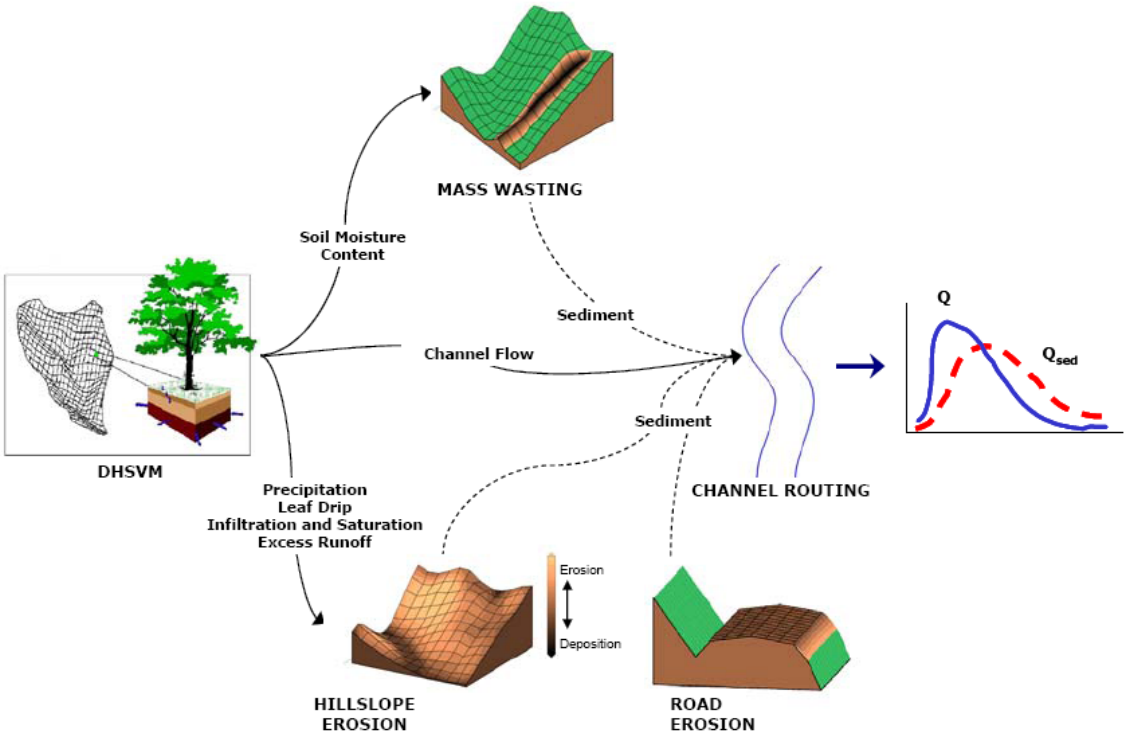

Figure 11. Conceptual setup for the DHSVM sediment module (Doten et al., 2006). Mass wasting is the only sediment module algorithm considered in this study.

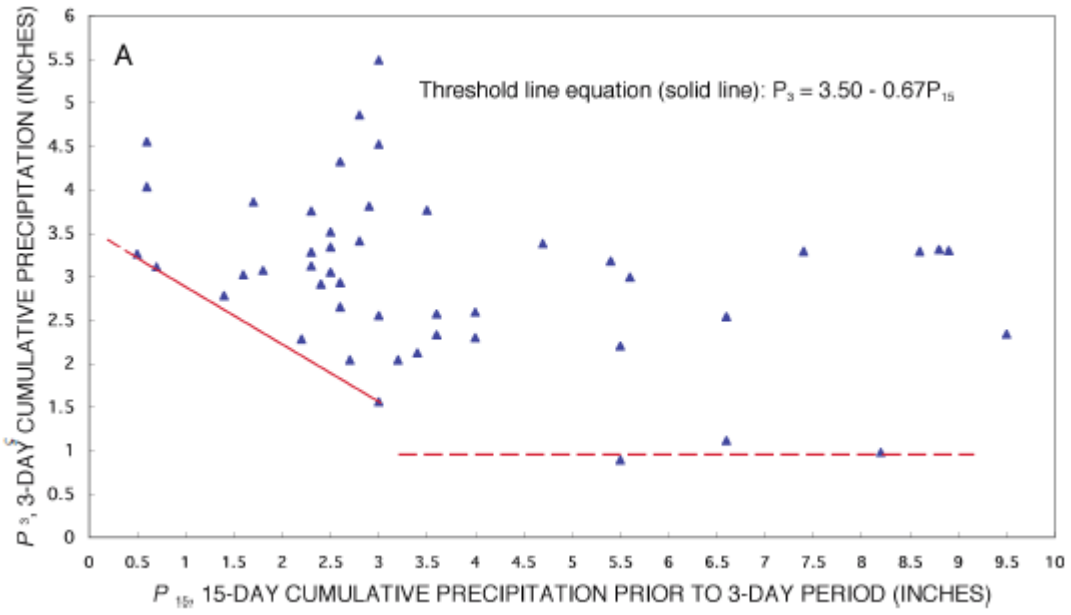

Figure 12. The Chleborad (2000) cumulative precipitation threshold for the prediction of landslides in the Seattle, WA area. Historical storms that triggered landslides are plotted according to the cumulative precipitation during the three days prior to failure (P_3), and cumulative precipitation during the fifteen days prior to the three day antecedent precipitation (P_{15}). A precipitation threshold for the initiation of landslides is interpreted and characterized with a linear function relating P_3 and P_{15}.

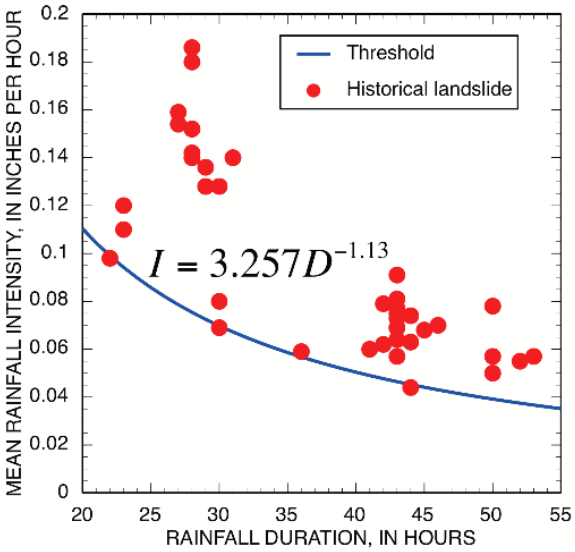

Figure 13. The Godt (2004) intensity-duration precipitation threshold for the prediction of landslides in the Seattle, WA area. Historical storms that triggered landslides are plotted according to storm duration (D) and average intensity (I). A precipitation threshold for the initiation of landslides is interpreted and characterized with an exponential function relating storm duration and intensity.

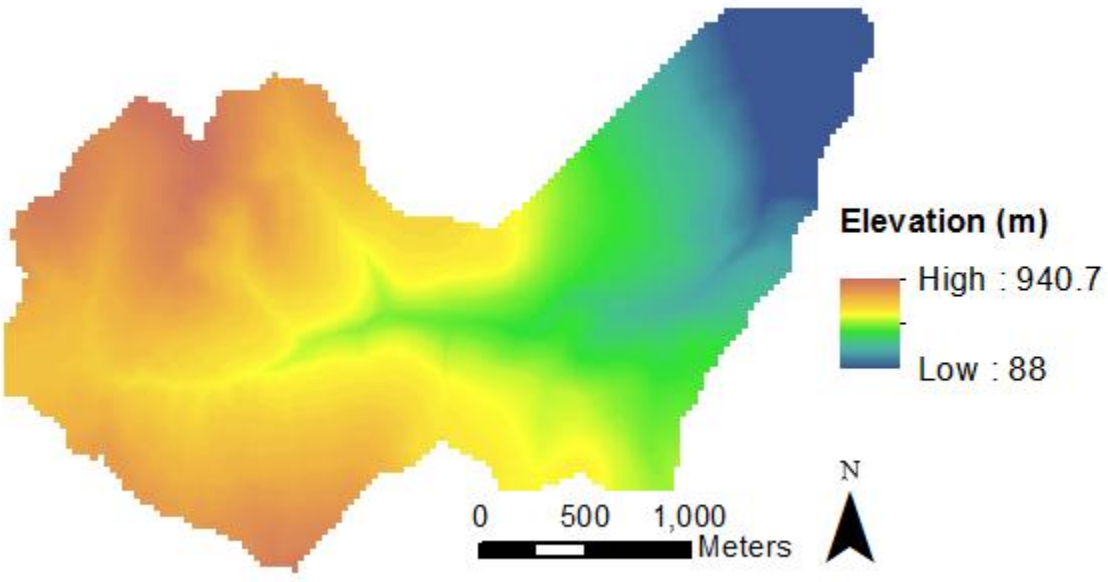

Figure 14. Elevation in the Jones Creek watershed (Puget Sound LiDAR Consortium, 2006).

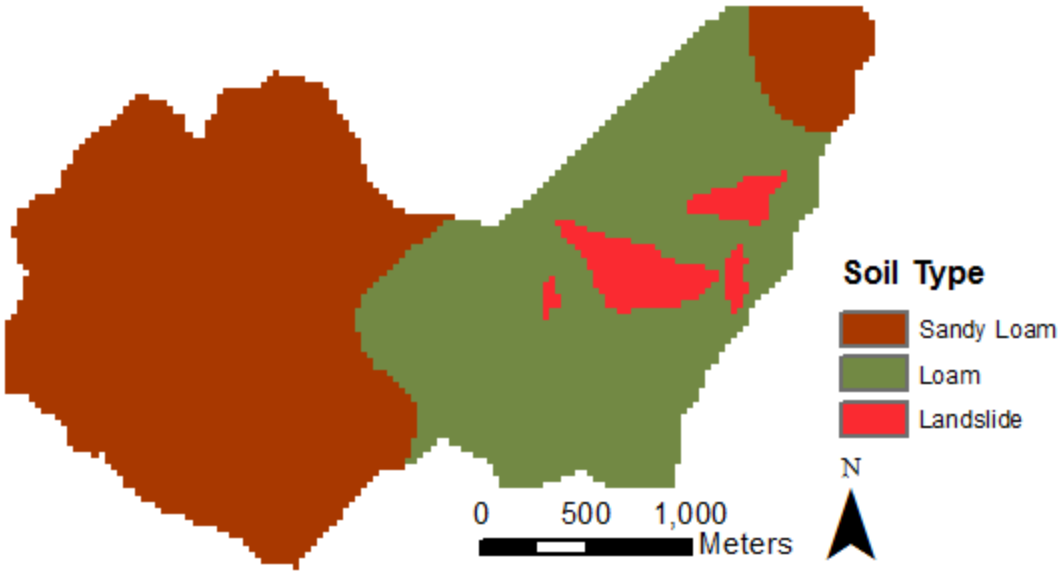

Figure 15. Soils in the Jones Creek watershed (NRCS). Deep seated landslides, which are likely to have different hydrologic and mechanical properties than the surrounding soils, are not recognized in the NRCS soil data and have been assigned a unique DHSVM soil class.

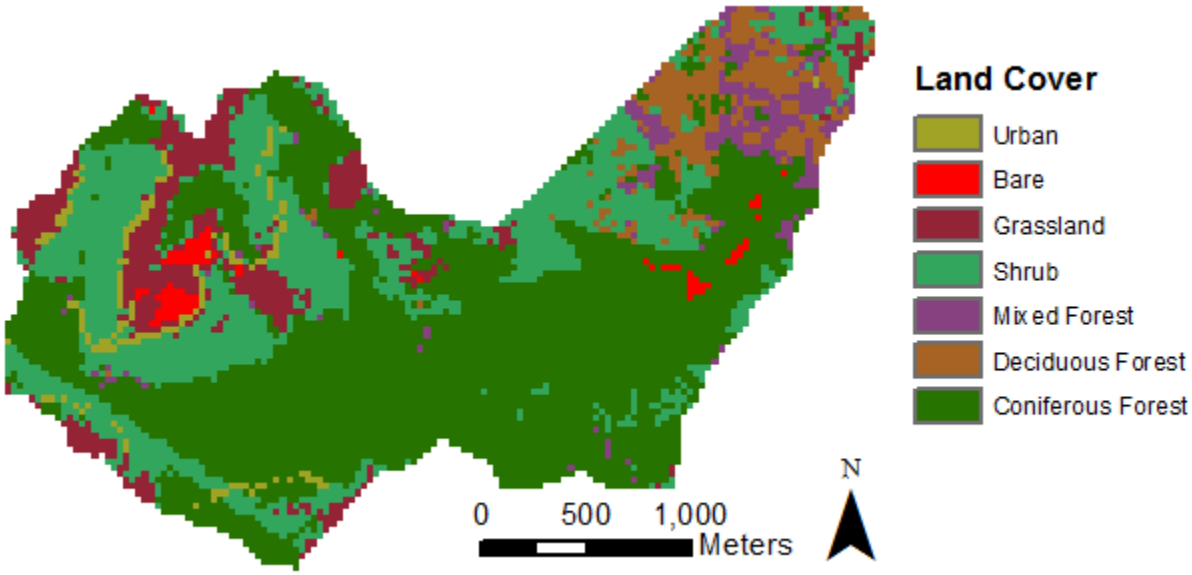

Figure 16. Land cover in the Jones Creek watershed (NOAA, 2006). The unvegetated regions of the deep seated landslides are not recognized in the NOAA data and have been reclassified as bare.

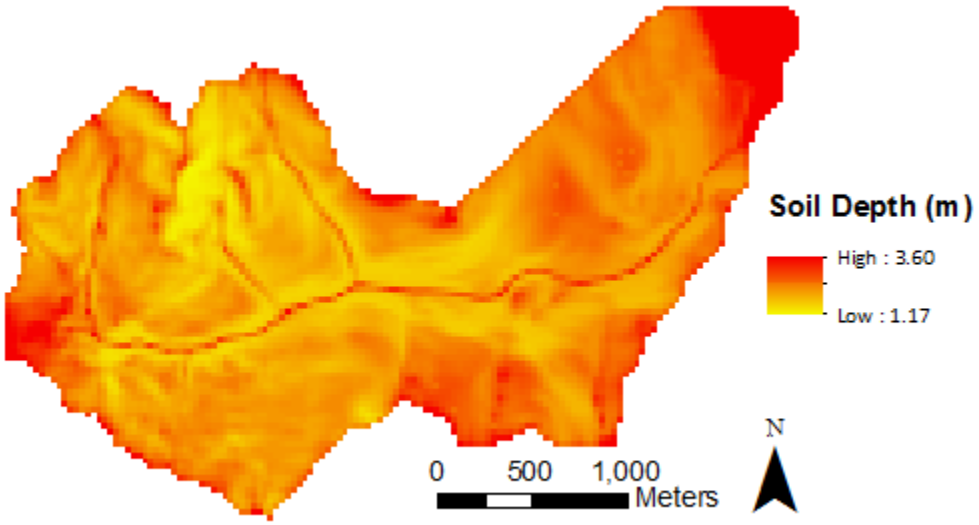

Figure 17. Soil depth in meters for the Jones Creek watershed. DHSVM soil depths are generated with an arc macro language script, based on slope.

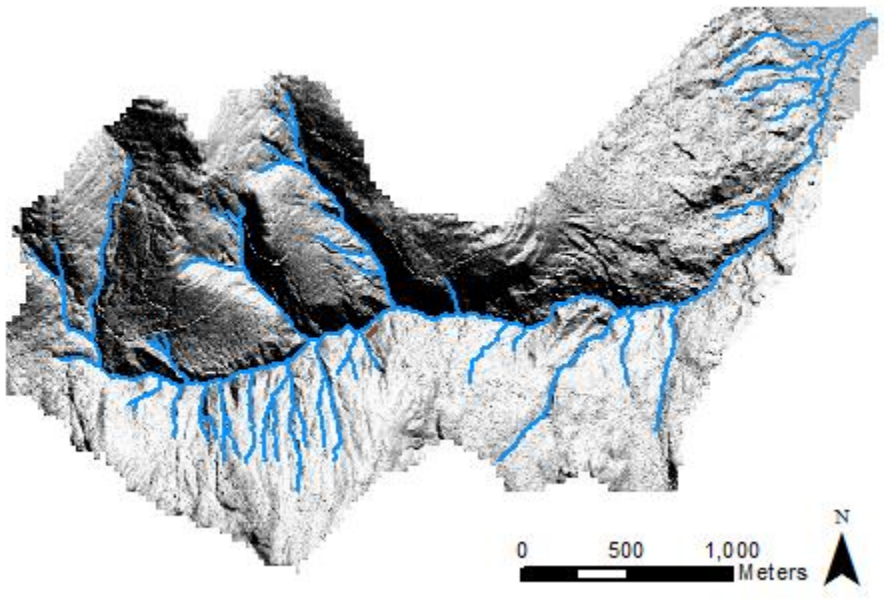

Figure 18. Jones Creek stream network. DHSVM stream networks are generated with an arc macro language script based on slope and topography.

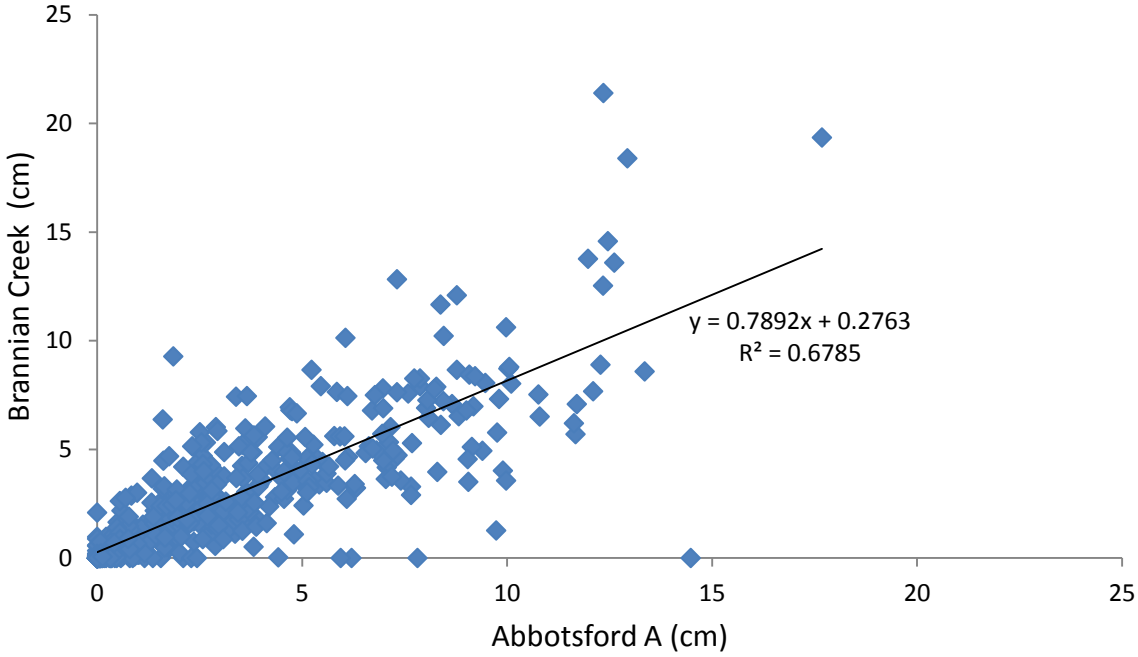

Figure 19. Ten year comparison of weekly precipitation at Abbotsford A and Brannian Creek. A simple linear regression model indicates that Abbotsford A records slightly more precipitation.

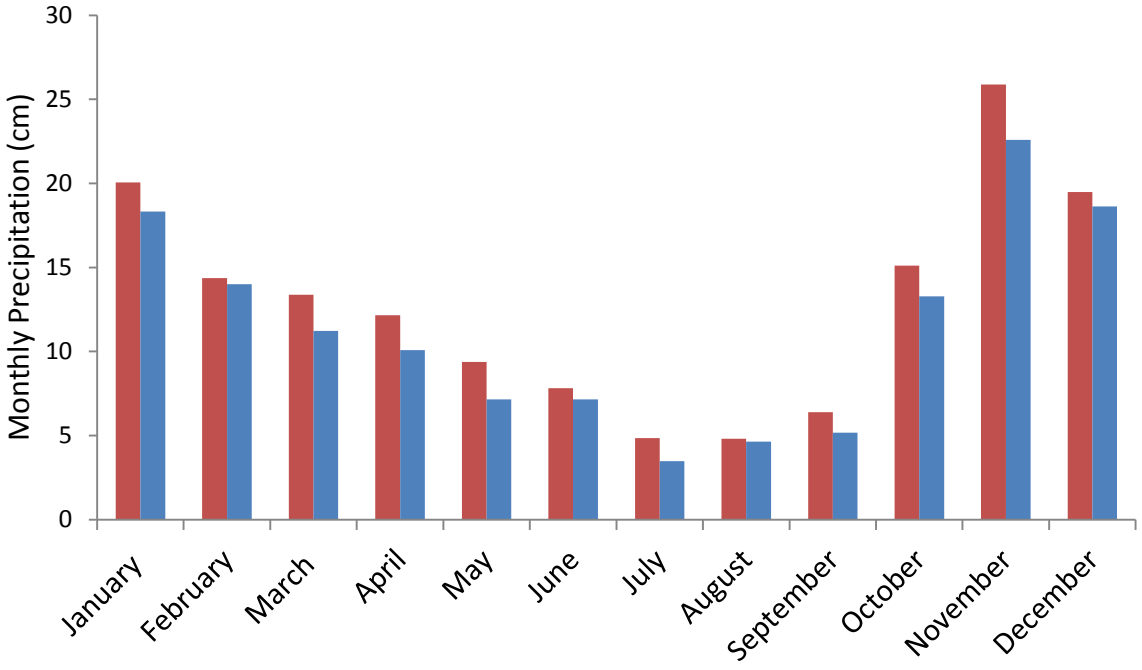

Figure 20. Mean monthly precipitation at the Abbotsford A (red) and Brannian Creek (blue) weather stations, from 1990 through 1999. During the wet months from November through March, mean monthly precipitation at Abbotsford A ranges from 0.36 to 3.3 centimeters greater than Brannian Creek, with the greatest difference in November.

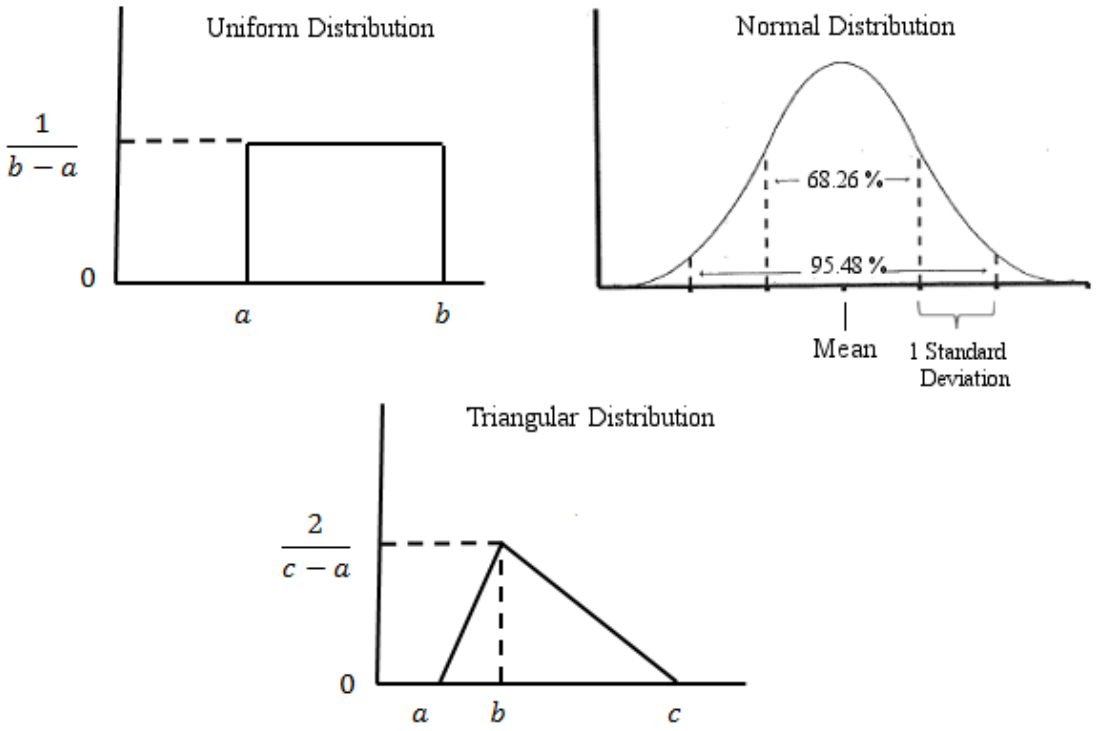

Figure 21. Statistical Distributions used by DHSVM to define soil shear strength parameters. Uniform distributions are defined by a minimum (a) and maximum (b). Normal distributions are defined by a mean and a standard distribution. Triangular distributions are defined by a minimum (a), mode (b), and maximum (c). Modified from Hammond et al. (1992).

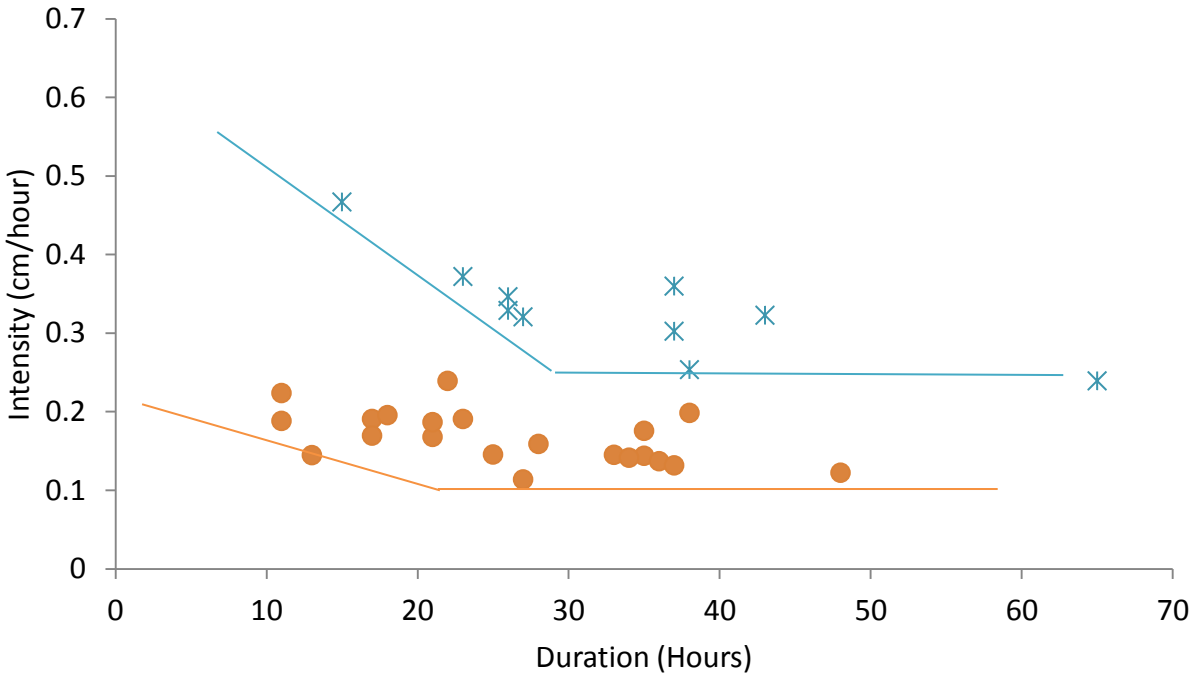

Figure 22. Example of the probability threshold construction process for the Straight slide. Modeled storms are plotted according to storm duration and average intensity, and coded according to failure probability. Minimum probability thresholds are interpreted at ten percent intervals. For simplicity, only storms with probabilities ranging from 10 to 20 percent (orange) and greater than 70 percent (blue) are shown here.

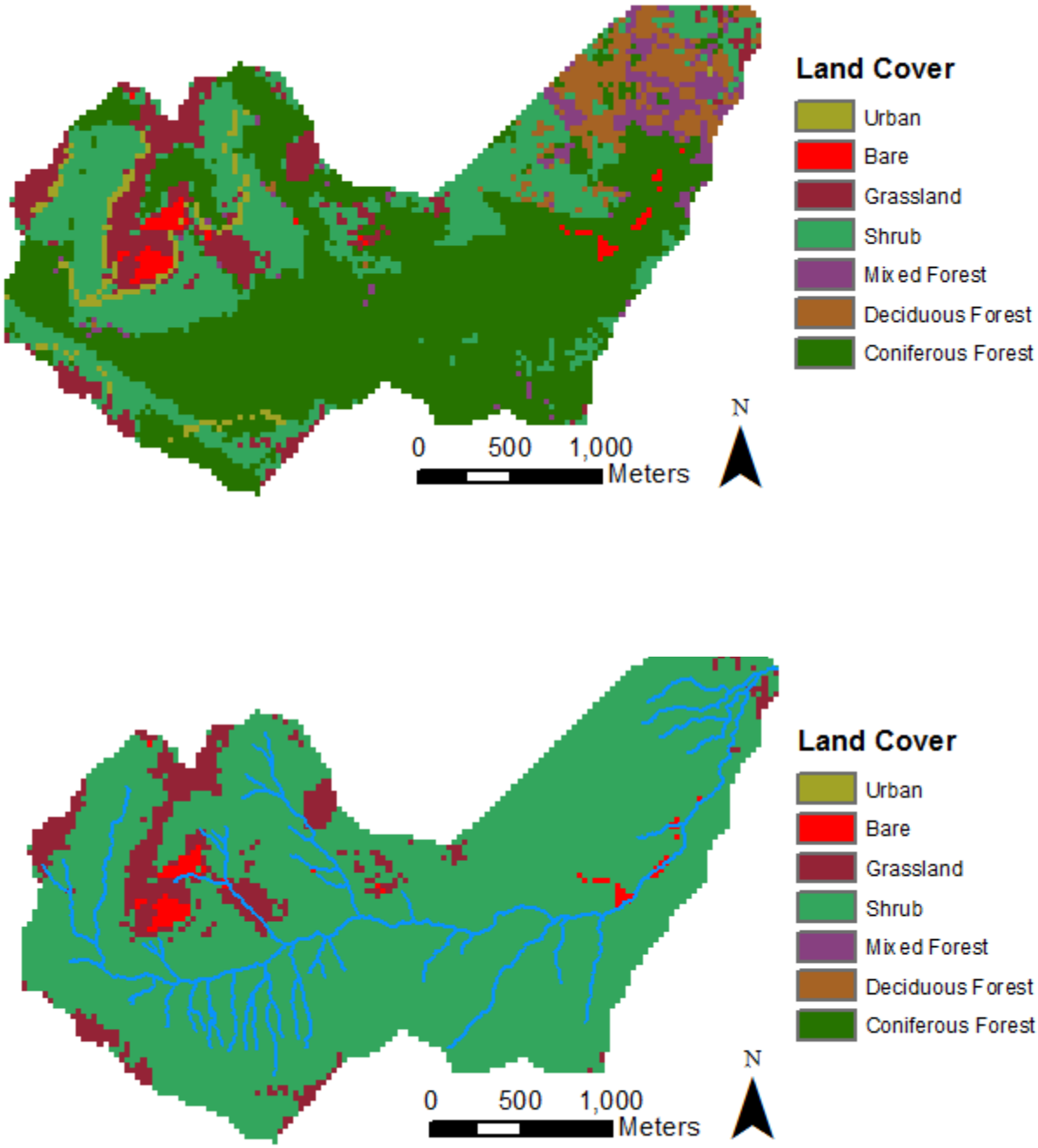

Figure 23. Pre-harvest (top) and post-harvest (bottom) simulated land cover. Mixed forest, deciduous forest, and coniferous forest classes are replaced with the shrub class for post-harvest land cover.

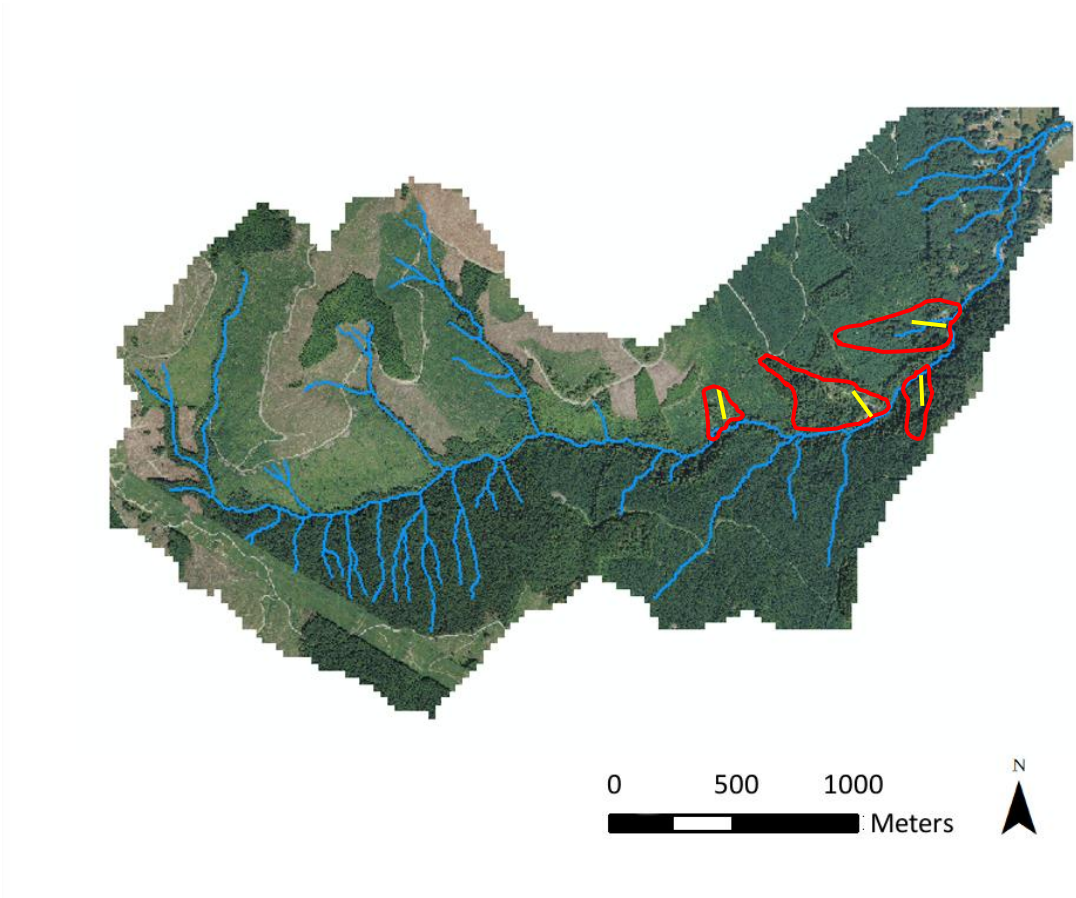

Figure 24. Profile transects used for rotational analysis of the deep-seated landslide toes (Figures 53-57). Landslides are outlined in red. Profile locations are shown in yellow.

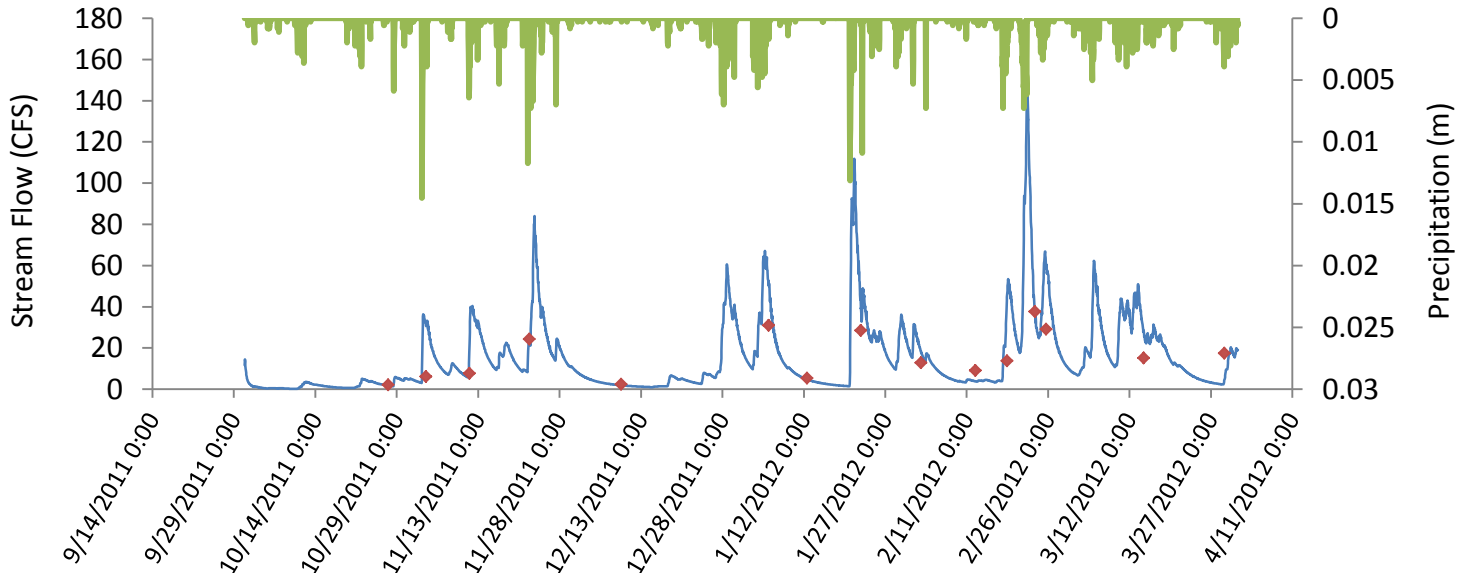

Figure 25. Calibrated simulated stream flow (blue line) and observed stream flow (red dots) at Jones Creek for the 2011-2012 winter season. Precipitation is shown in green.

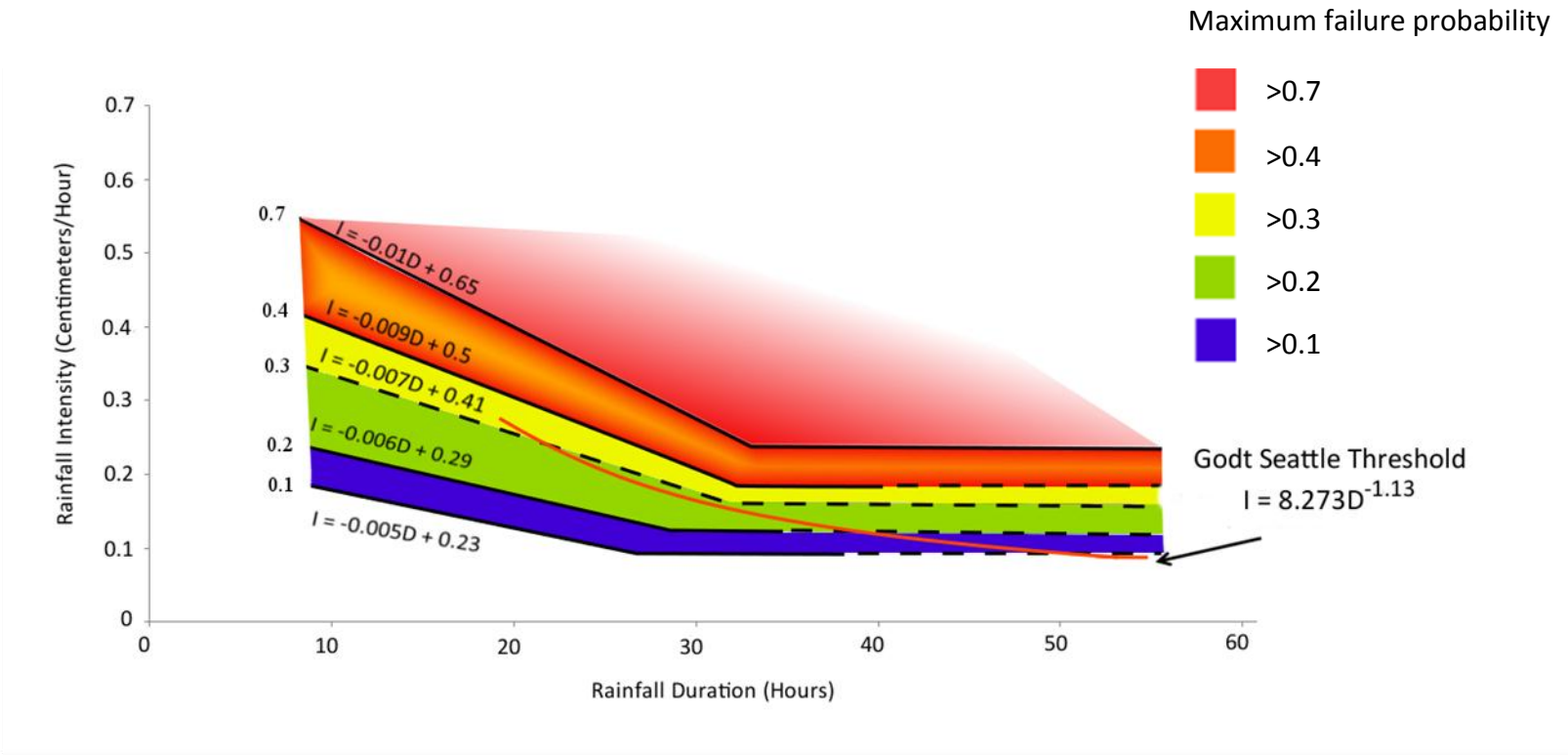

Figure 26. Precipitation intensity-duration probability thresholds for shallow slope failures on the toe the Straight landslide in the Jones Creek watershed. Modeled storms are plotted according to storm duration (D) and average intensity (I), and coded according to failure probability. Minimum probability thresholds are interpreted at 10 percent intervals and characterized with linear functions relating D and I. Thresholds are dashed where approximate. The Godt (2004) intensity-duration threshold, which has an exceedance probability of 0.42, is shown for comparison.

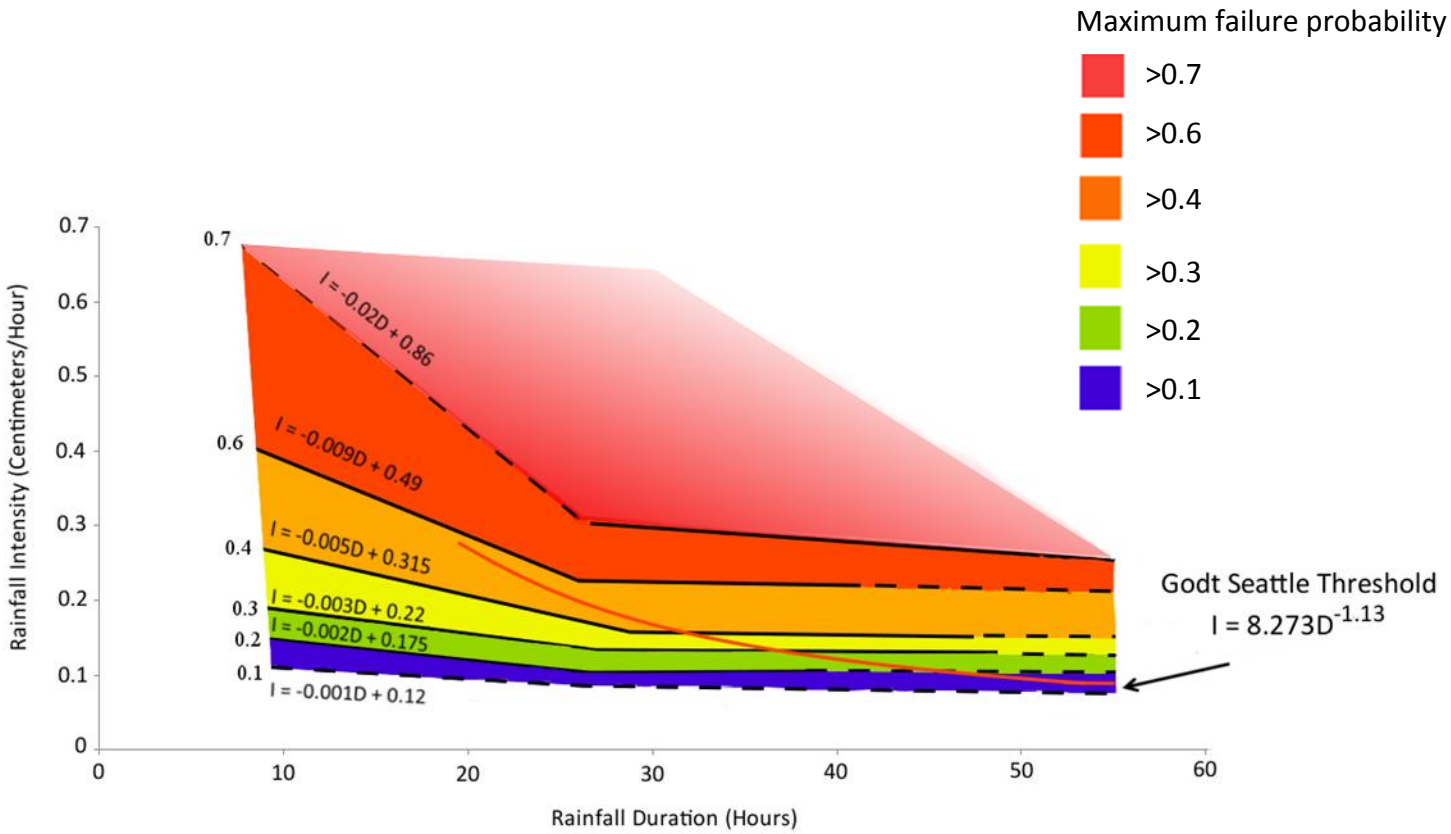

Figure 27. Precipitation intensity-duration probability thresholds for shallow slope failures on the toe the South landslide in the Jones Creek watershed. Modeled storms are plotted according to storm duration (D) and average intensity (I), and coded according to failure probability. Minimum probability thresholds are interpreted at 10 percent intervals and characterized with linear functions relating D and I . Thresholds are dashed where approximate. The Godt (2004) intensity-duration threshold, which has an exceedance probability of 0.42, is shown for comparison.

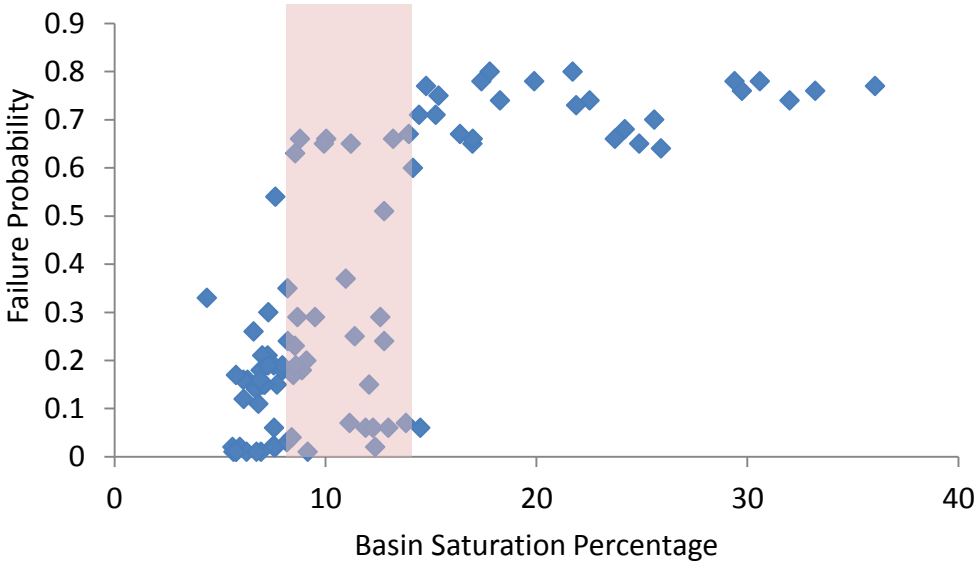

Figure 28. Failure probability at the toe of the Straight Landslide as a function of basin saturation. Across the shaded zone, small changes in saturation have a significant effect on failure probability.

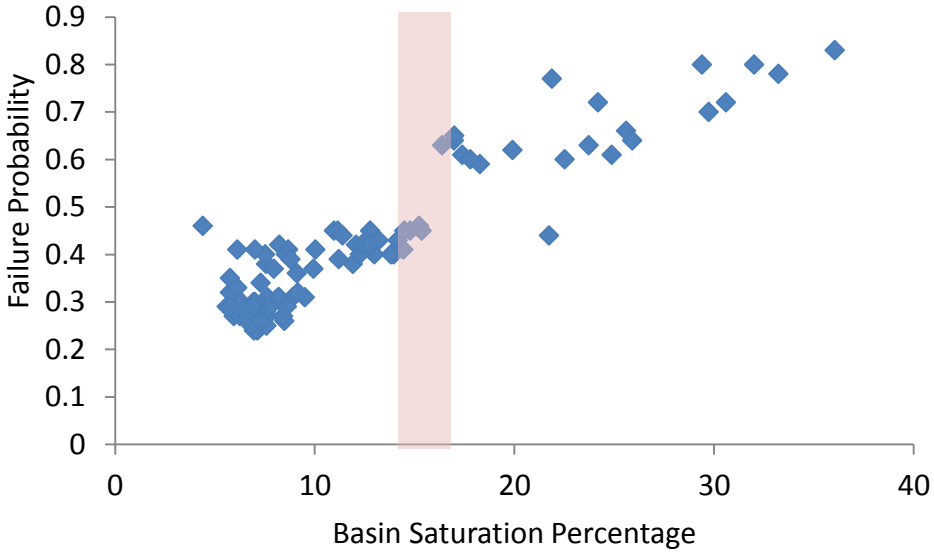

Figure 29. Failure probability at the toe of the South Landslide as a function of basin saturation. Across the shaded zone, small changes in saturation have a significant effect on failure probability.

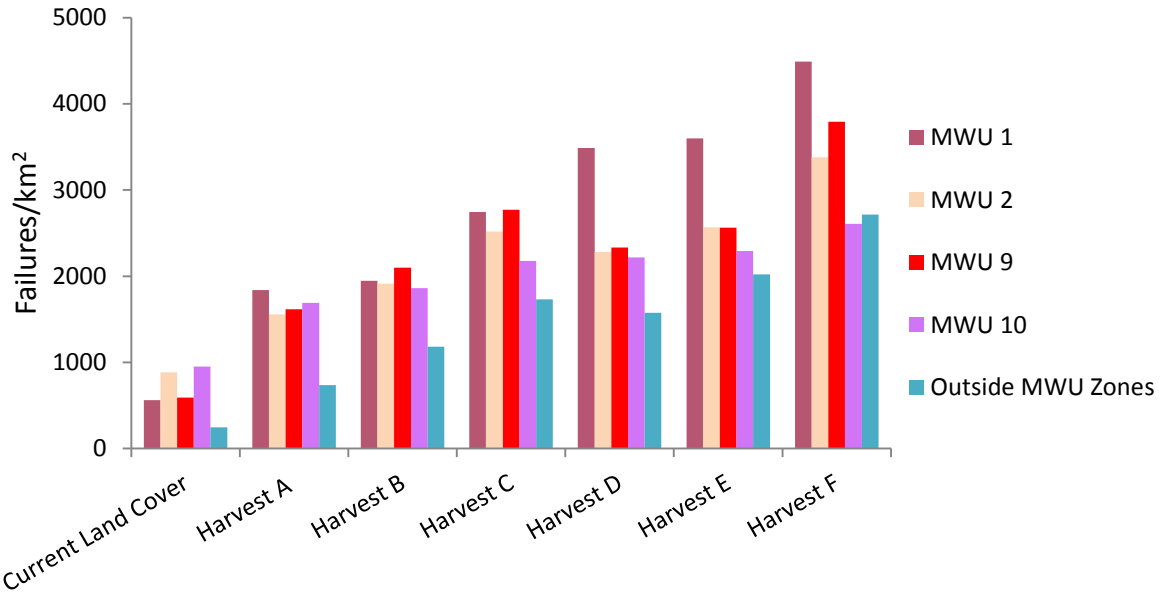

Figure 30. Failures per square kilometer by MWU zone for the timber harvest simulations.

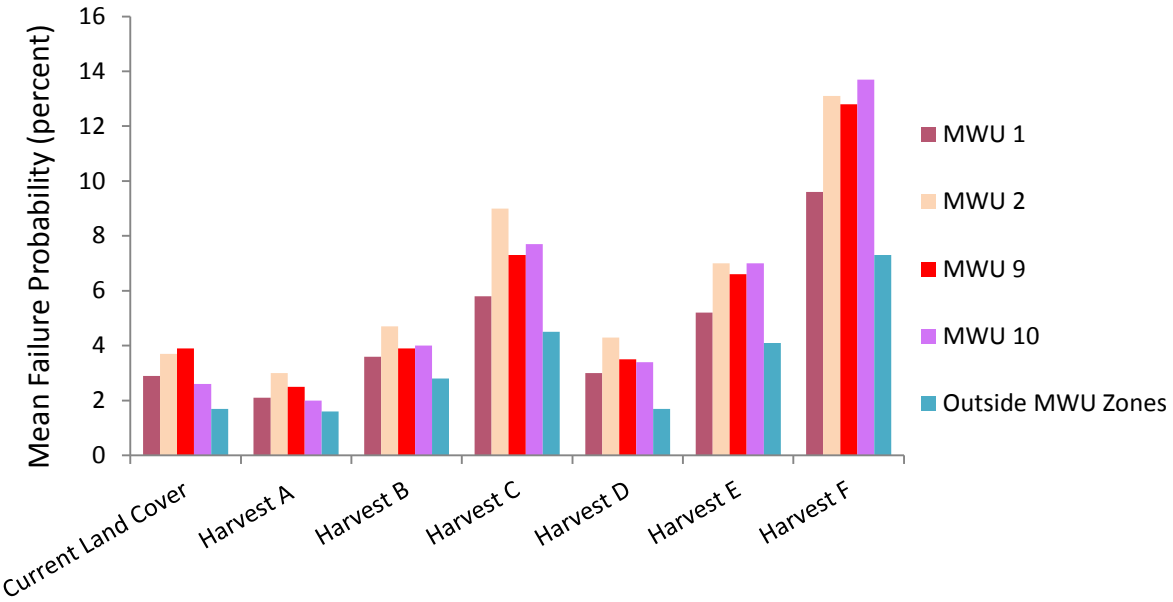

Figure 31. Mean failure probability for unstable cells by MWU zone for timber harvest scenarios.

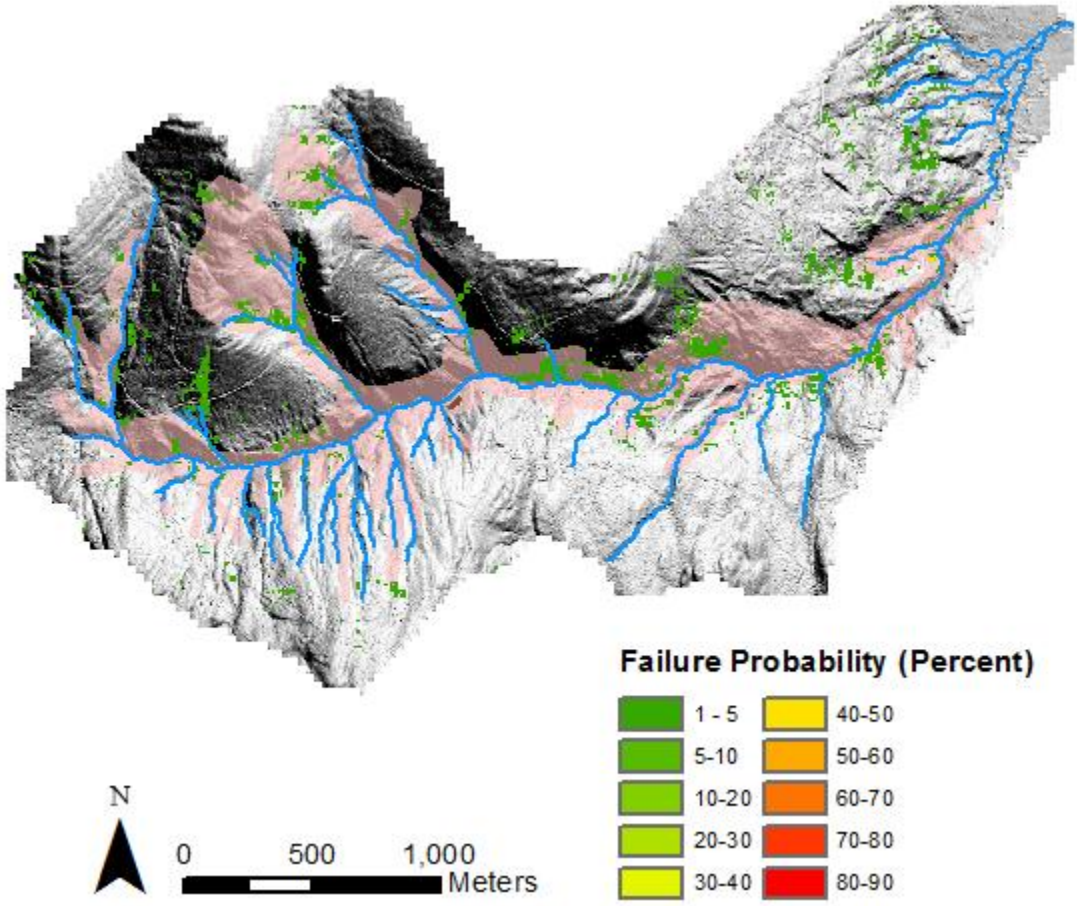

Figure 32. Simulated failure probability for the January, 2009 storm under currently land cover conditions. MWU zones are all shown in pink for simplicity.

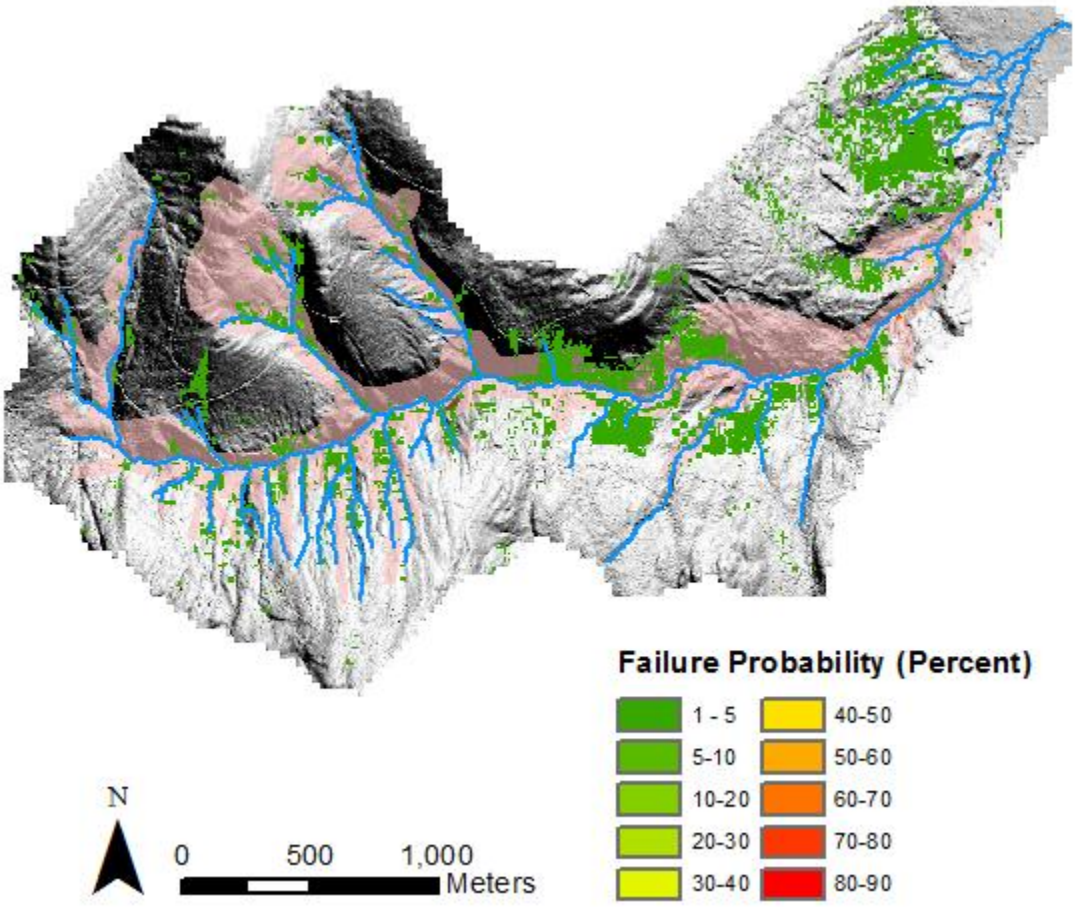

Figure 33. Simulated failure probability for the January, 2009 storm under the timber harvest A modeling scenario. Soil cohesion is the same as summarized in Table 2. Root cohesion is set to the DHSVM default for shrubs. MWU zones are all shown in pink for simplicity.

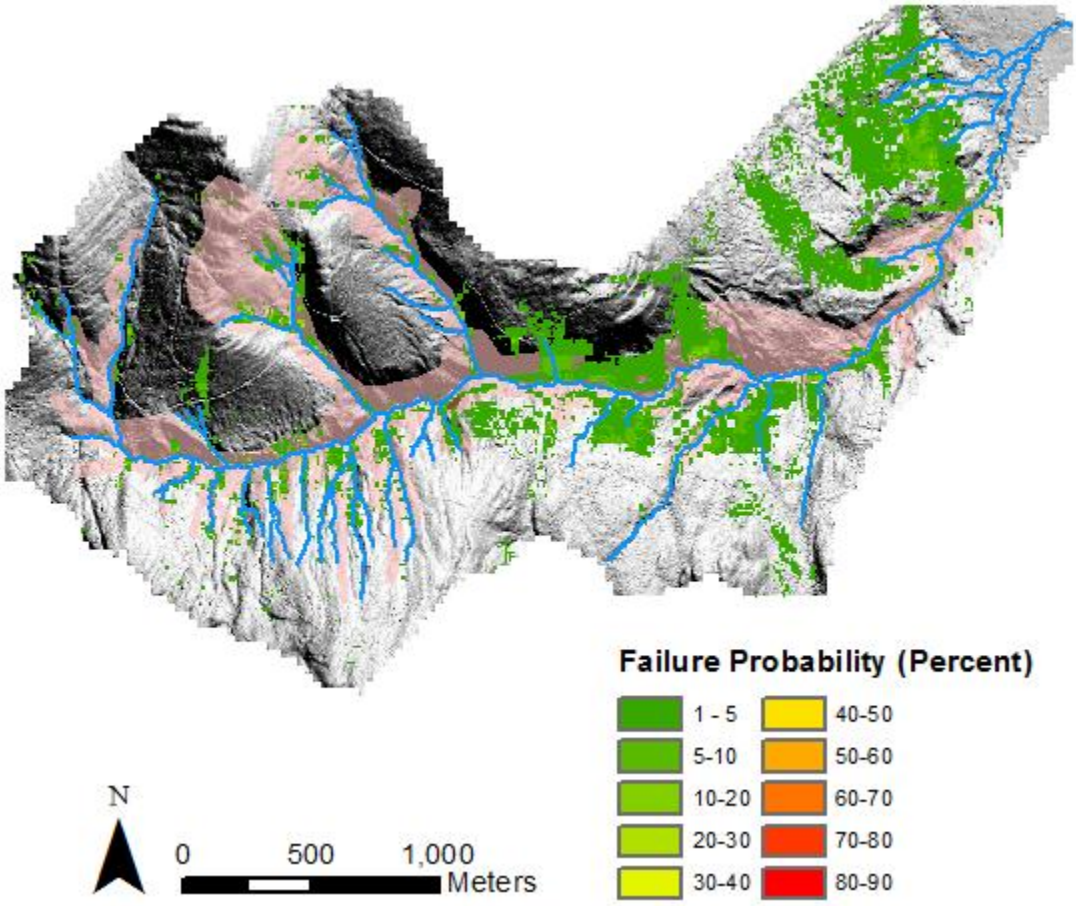

Figure 34. Simulated failure probability for the January, 2009 storm under the timber harvest B modeling scenario. Soil cohesion is reduced by approximately 25 percent compared to the study parameters summarized in Table 2. MWU zones are all shown in pink for simplicity.

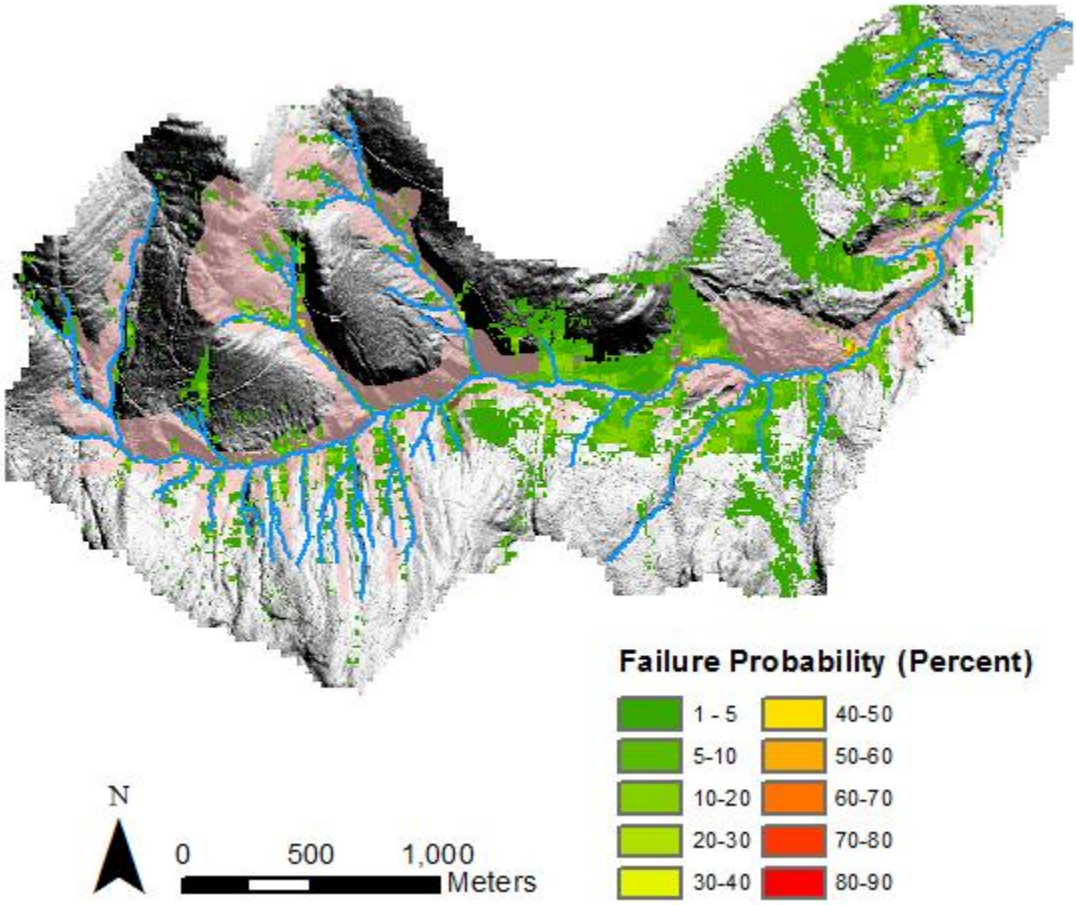

Figure 35. Simulated failure probability for the January, 2009 storm under the timber harvest C modeling scenario. Soil cohesion is reduced by approximately 50 percent compared to the study parameters summarized in Table 2. MWU zones are all shown in pink for simplicity.

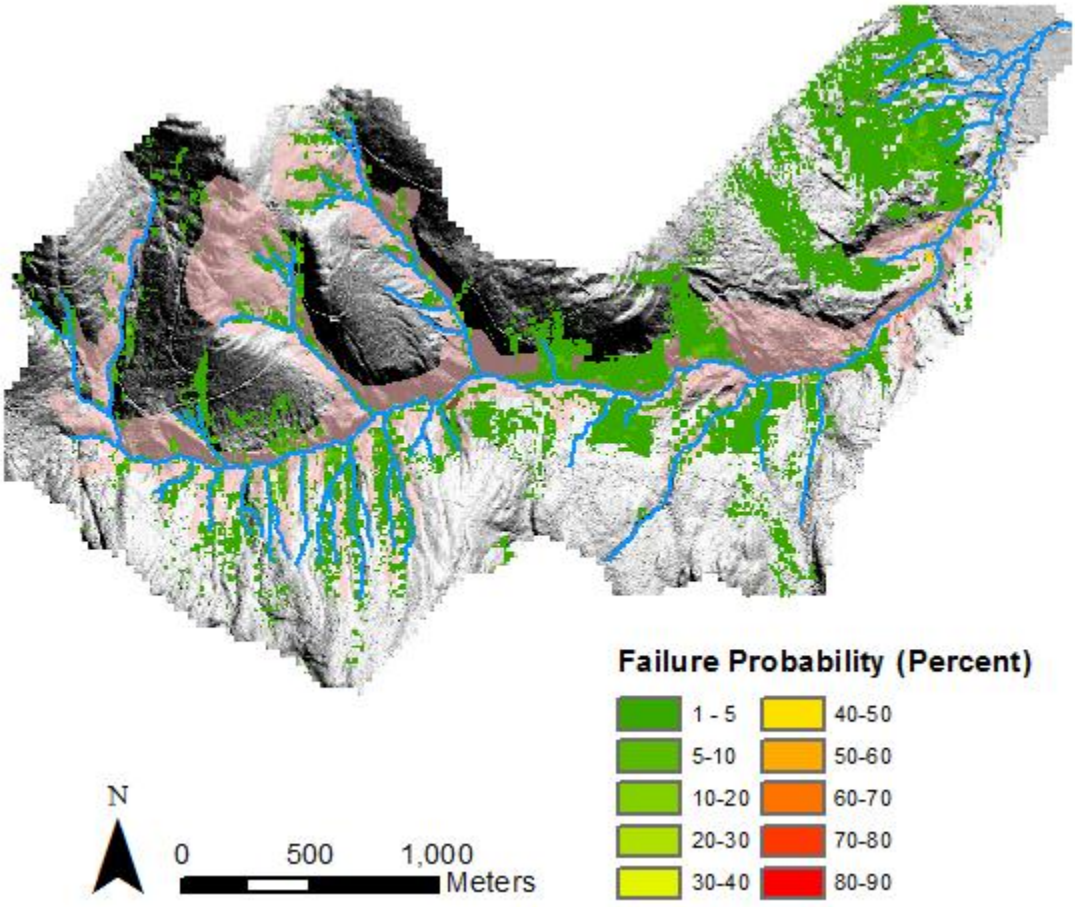

Figure 36. Simulated failure probability for the January, 2009 storm under the timber harvest D modeling scenario. Root cohesion is reduced by approximately 50 percent compared to the DHSVM default for shrubs. MWU zones are all shown in pink for simplicity.

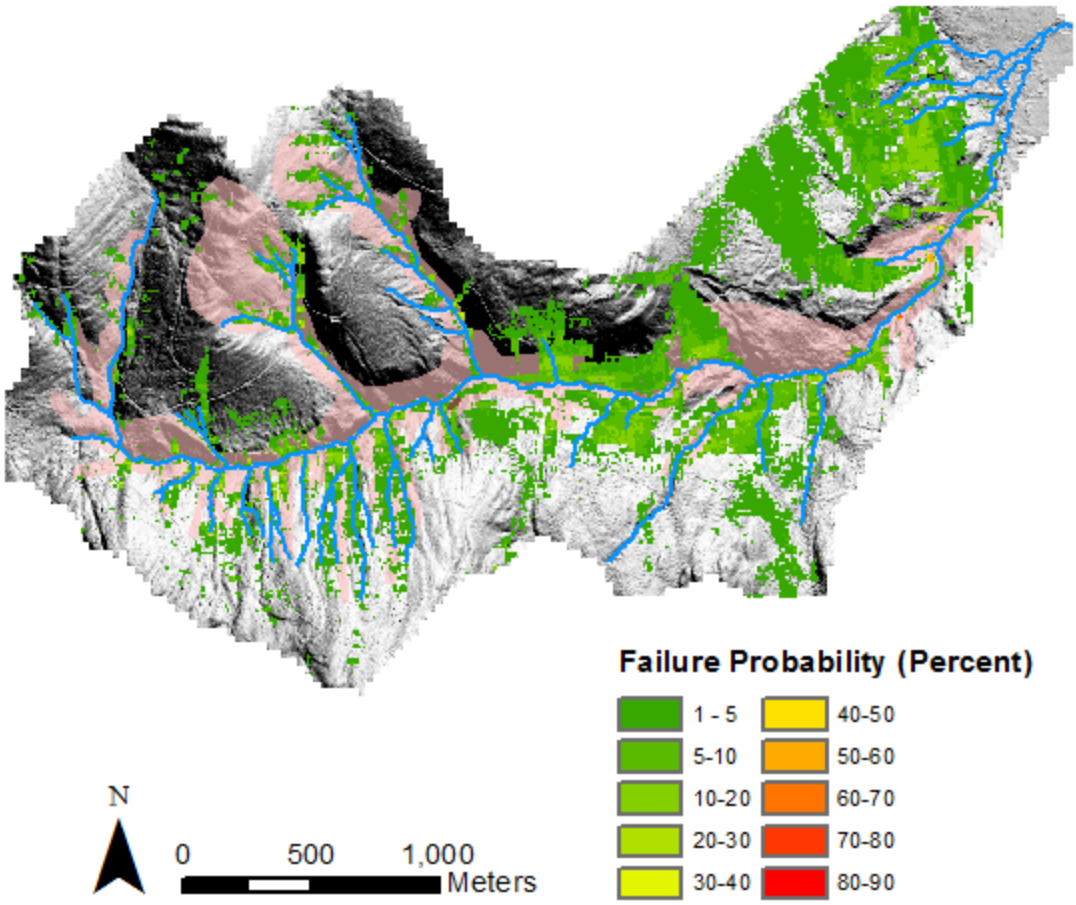

Figure 37. Simulated failure probability for the January, 2009 storm under the timber harvest E modeling scenario. Soil cohesion is reduced by approximately 25 percent compared to the parameters summarized in Table 2. Root cohesion is reduced by approximately 50 percent compared to the DHSVM default for shrubs. MWU zones are all shown in pink for simplicity.

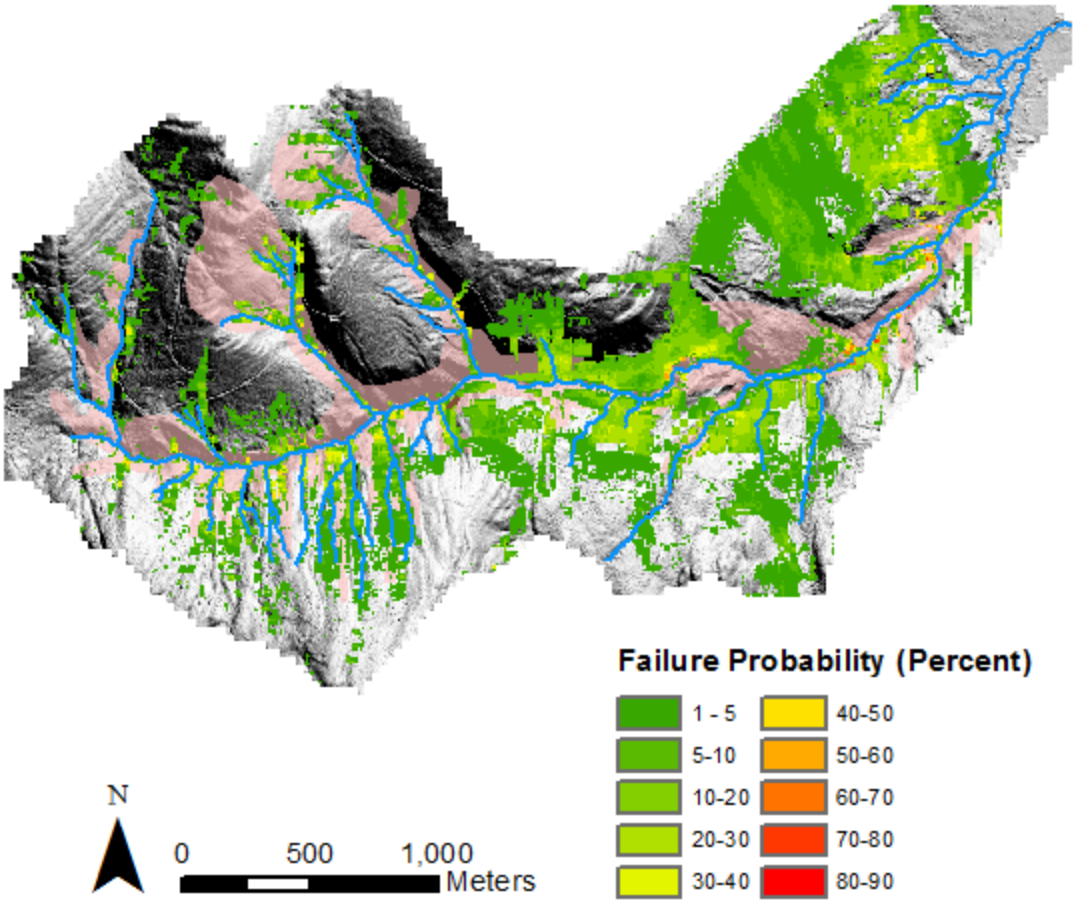

Figure 38. Simulated failure probability for the January, 2009 storm under the timber harvest F modeling scenario. Soil cohesion is reduced by approximately 50 percent compared to the parameters summarized in Table 2. Root cohesion is reduced by approximately 50 percent compared to the DHSVM default for shrubs. MWU zones are all shown in pink for simplicity.

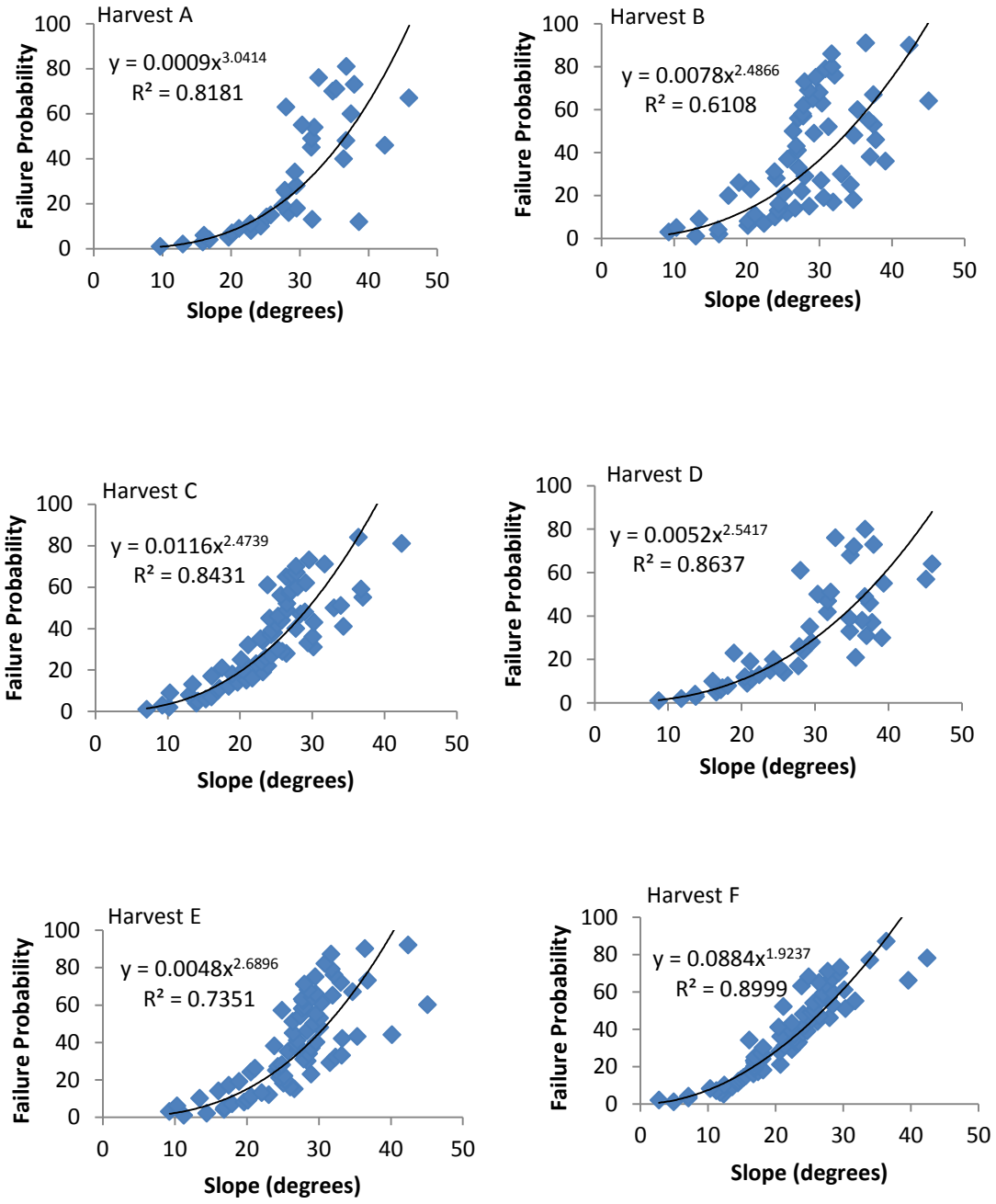

Figure 39. Exponential regression models describing the relationship between the minimum slope angle (x-axis) required to trigger failure probability (y-axis) for timber harvest scenarios. As soil and root cohesion is reduced, slopes angles are associated with progressively higher failure probabilities. The regression equations are applied to a high-resolution slope grid to derive failure susceptibility maps for each harvest scenario.

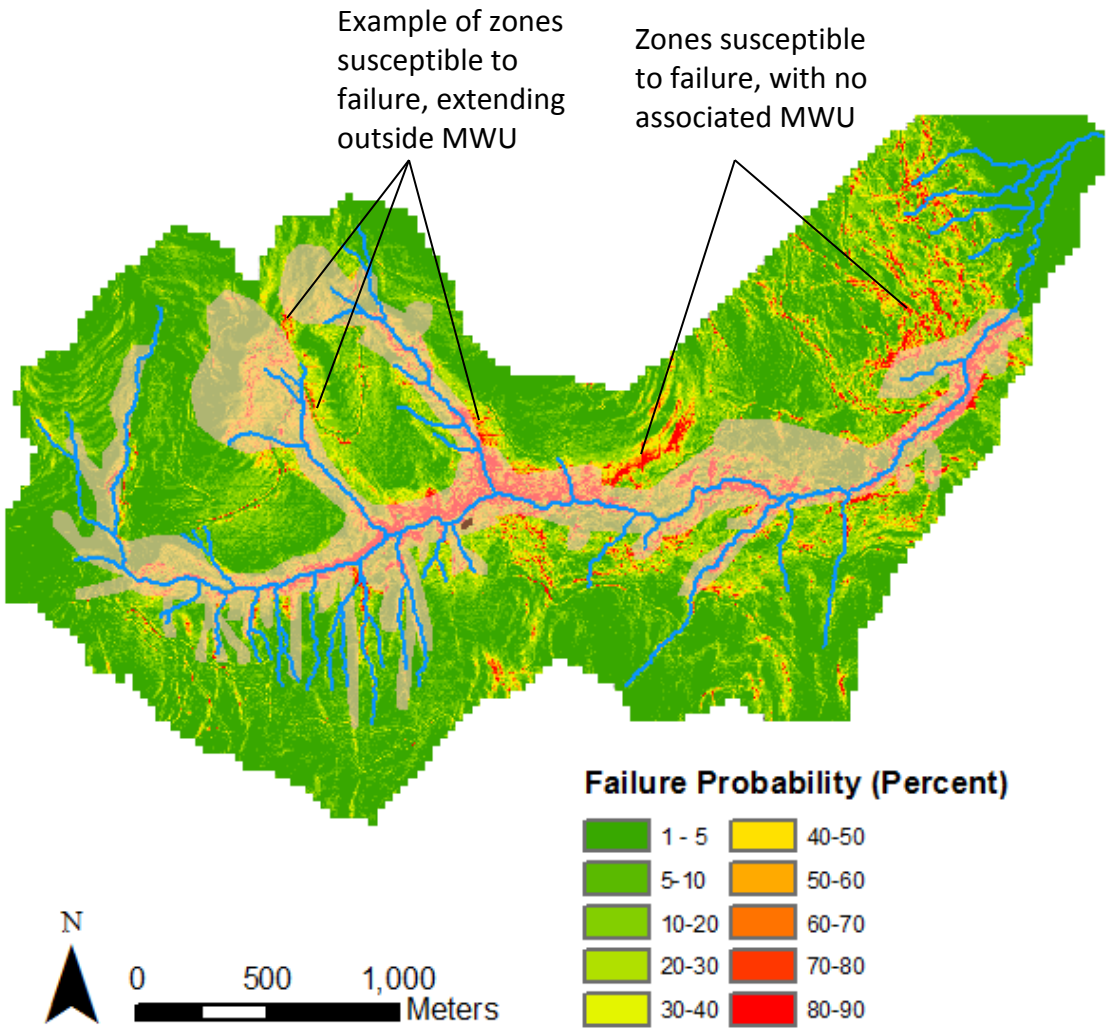

Figure 40. Interpreted failure susceptibility map from the timber harvest A scenario regression. MWU zones are shown in pink for simplicity. In the lower watershed, there are two zones that are particularly susceptible to failure with no associated MWU. In the upper basin, unstable zones with failure probability exceeding 50 percent extend outside of MWU boundaries in some places.

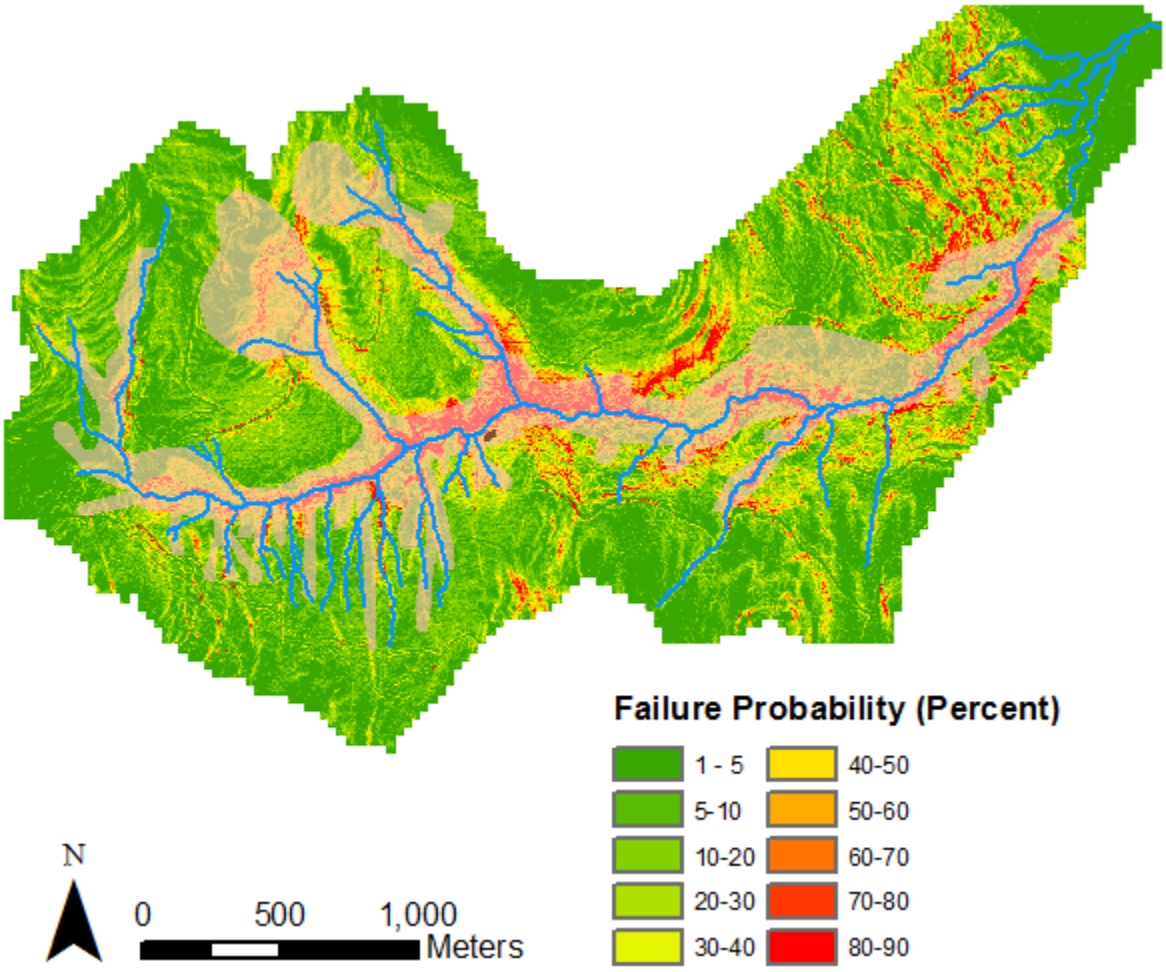

Figure 41. Interpreted failure susceptibility map from the timber harvest B scenario regression. MWU zones are shown in pink for simplicity.

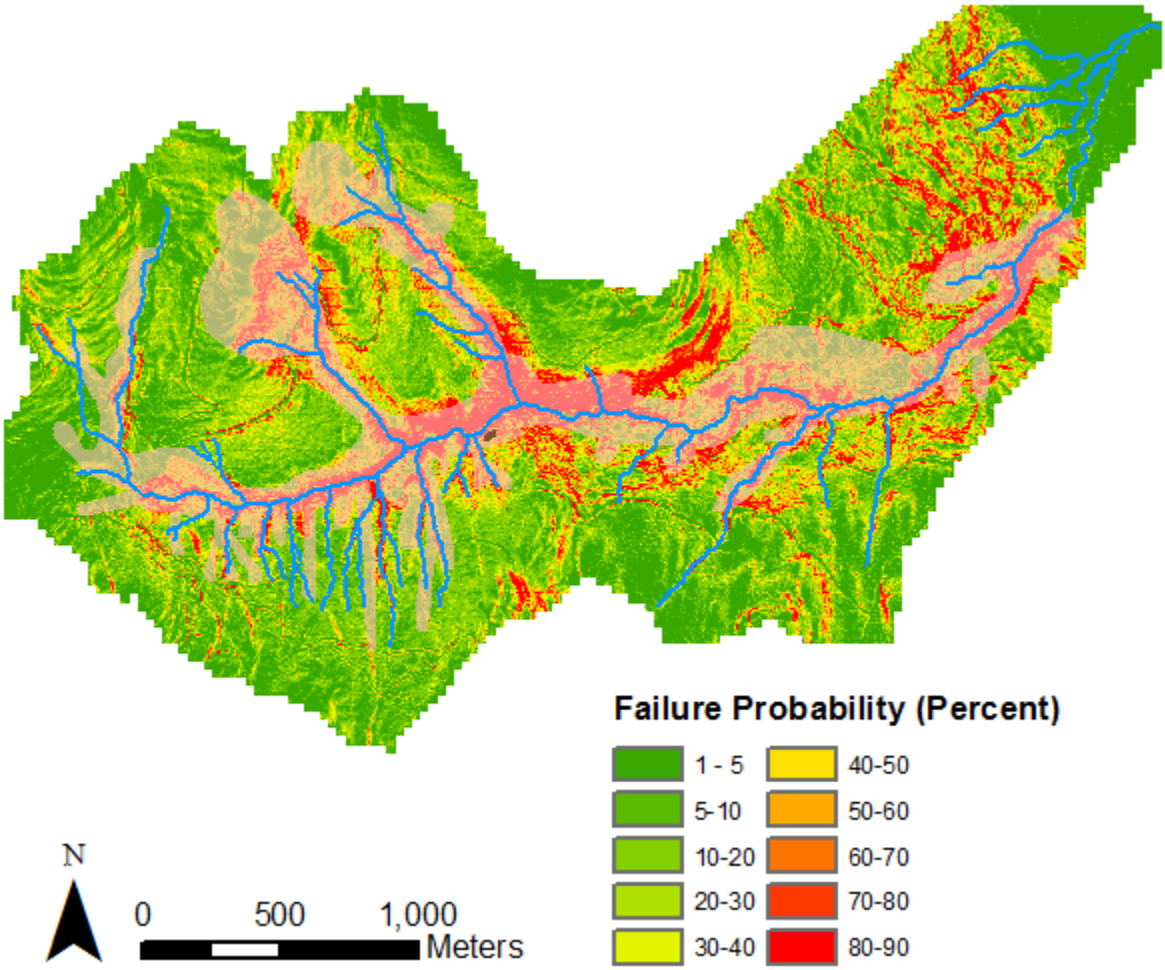

Figure 42. Interpreted failure susceptibility map from the timber harvest C scenario regression. MWU zones are shown in pink for simplicity.

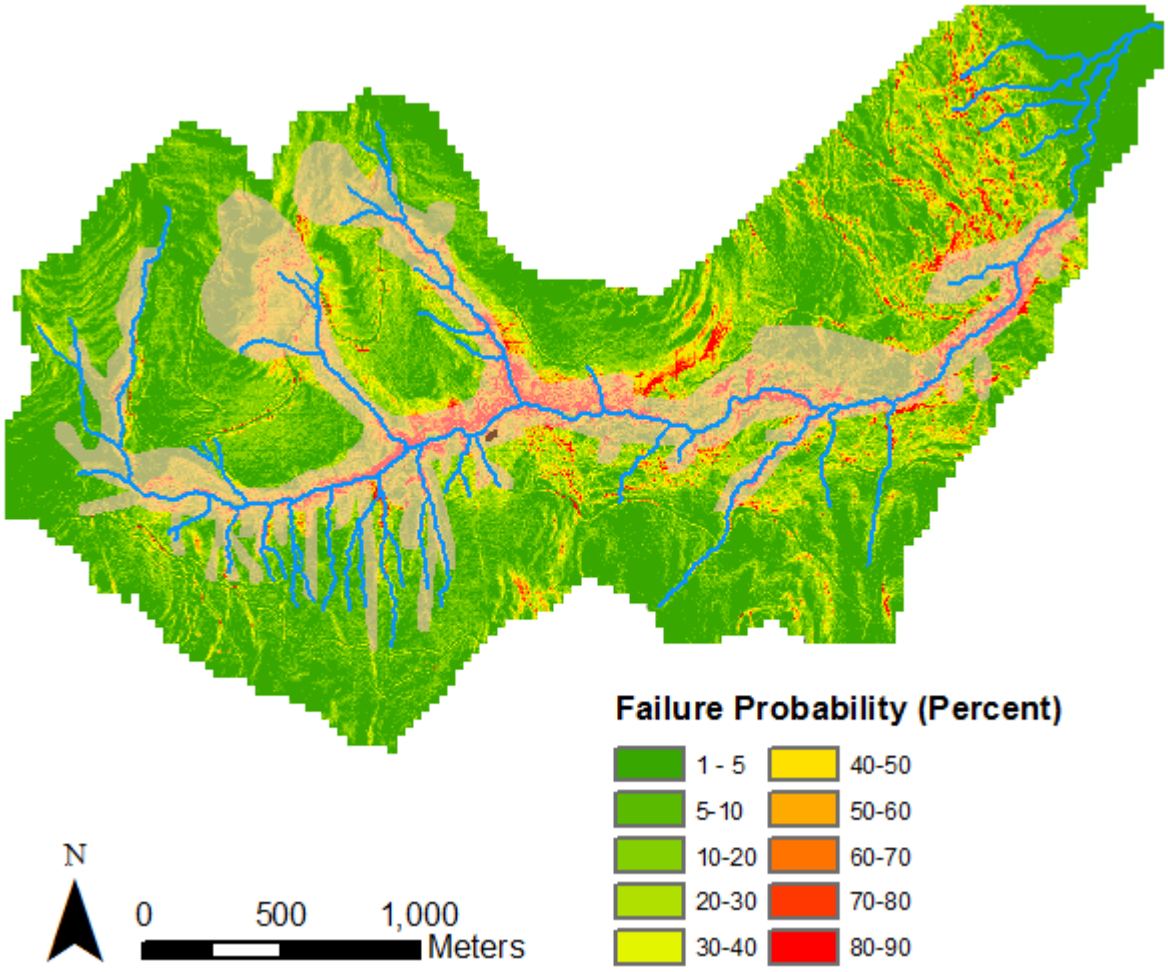

Figure 43. Interpreted failure susceptibility map from the timber harvest D scenario regression. MWU zones are shown in pink for simplicity.

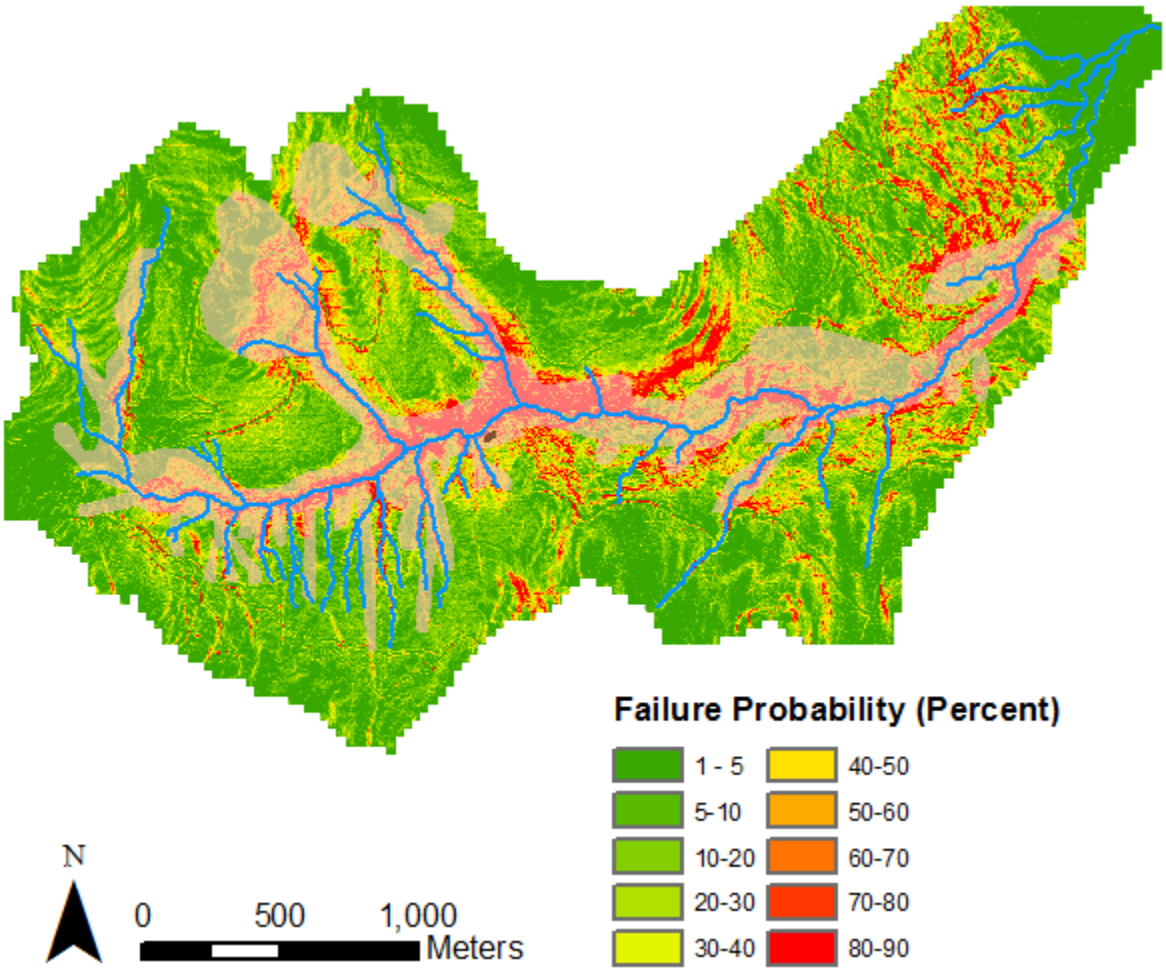

Figure 44. Interpreted failure susceptibility map from the timber harvest E scenario regression. MWU zones are shown in pink for simplicity.

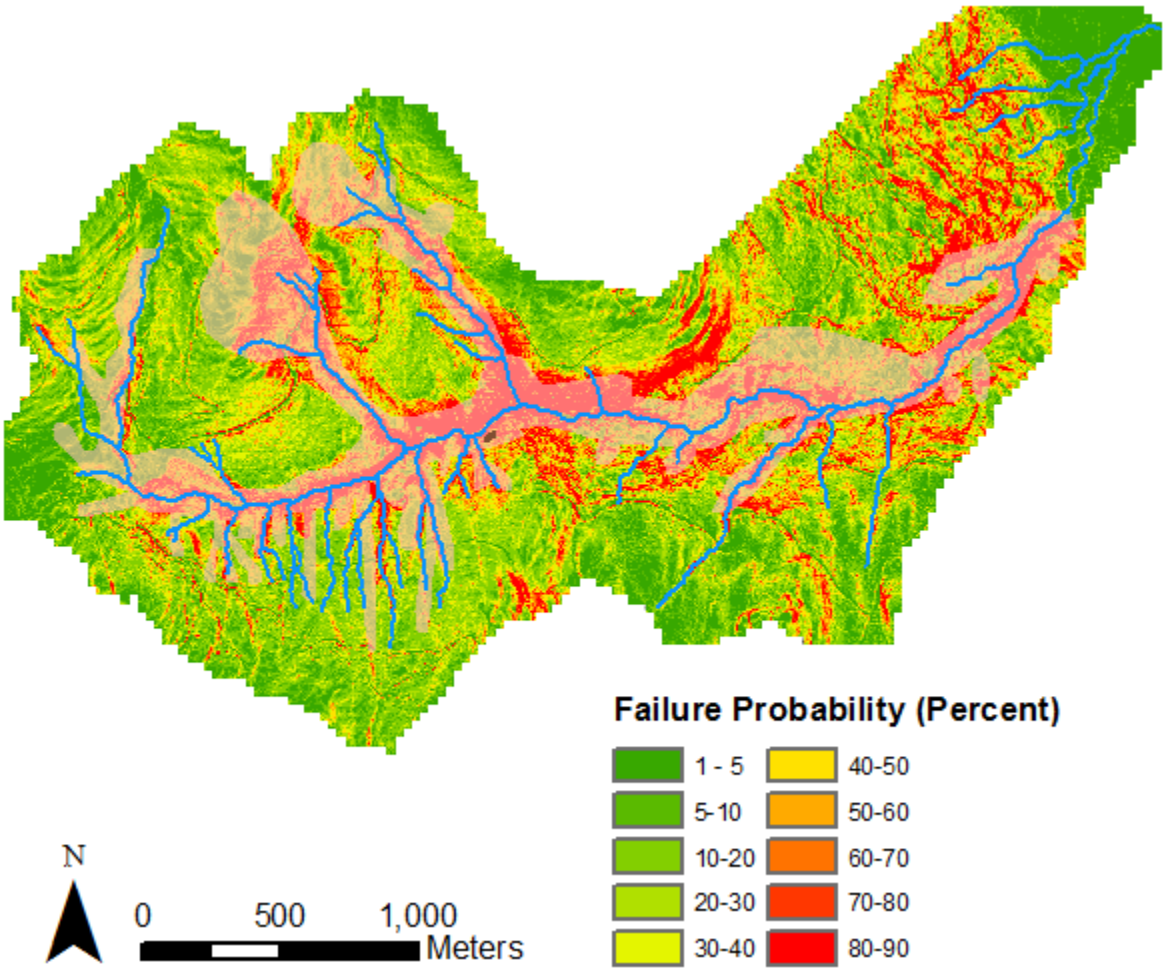

Figure 45. Interpreted failure susceptibility map from the timber harvest F scenario regression. MWU zones are shown pink for simplicity.

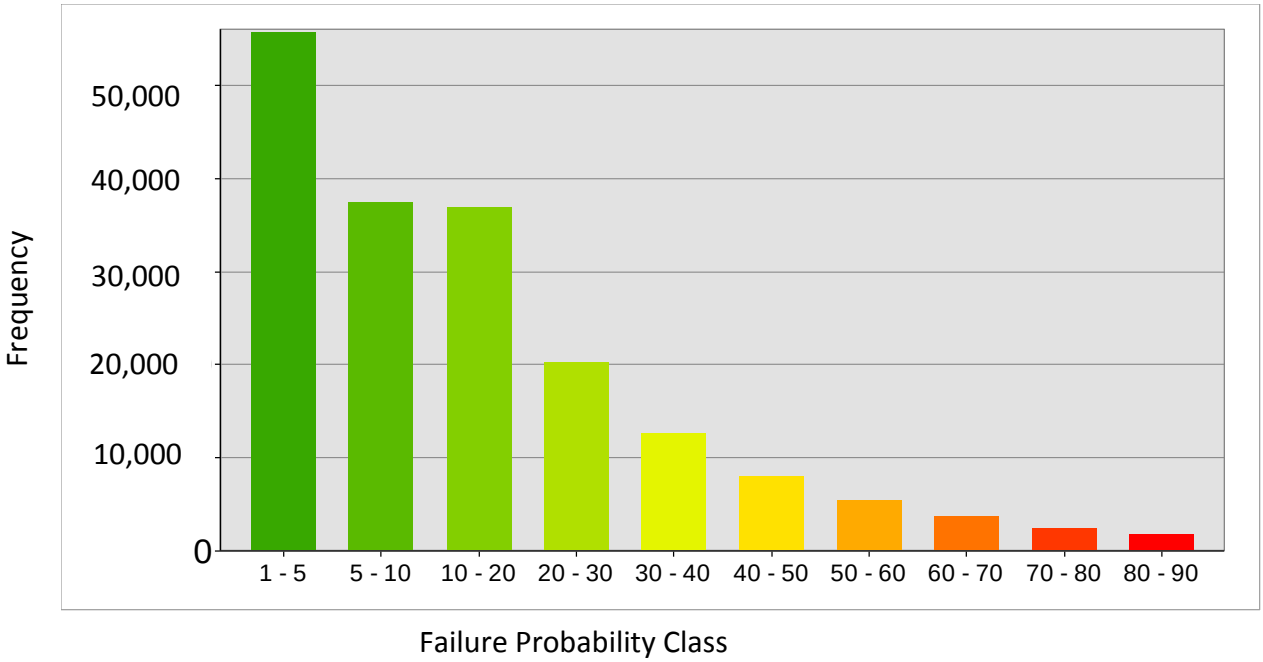

Figure 46. Unstable cell frequency by failure probability class for the timber harvest A scenario.

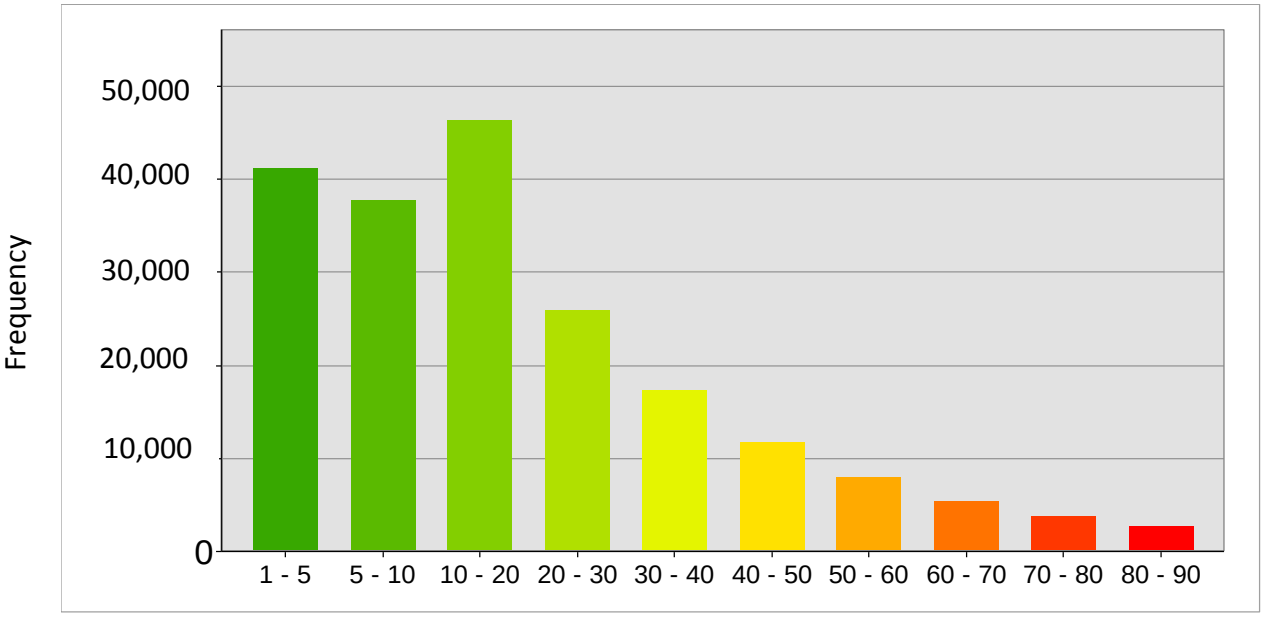

Figure 47. Unstable cell frequency by failure probability class for the timber harvest B scenario.

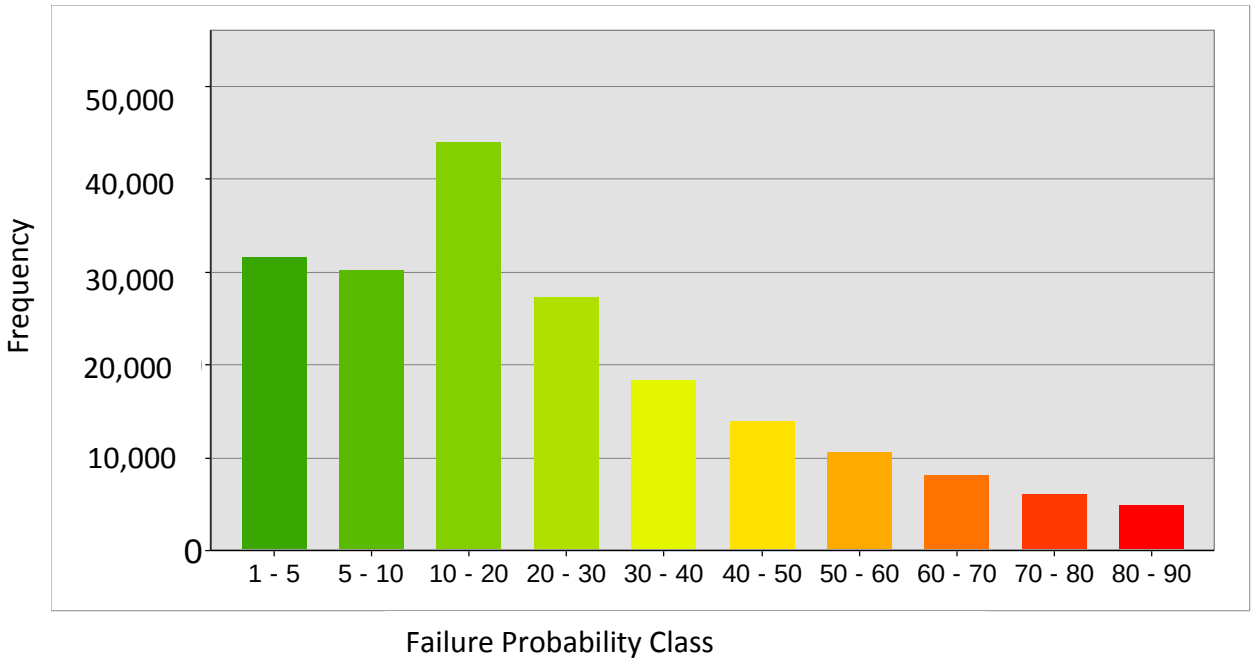

Figure 48. Unstable cell frequency by failure probability class for the timber harvest C scenario.

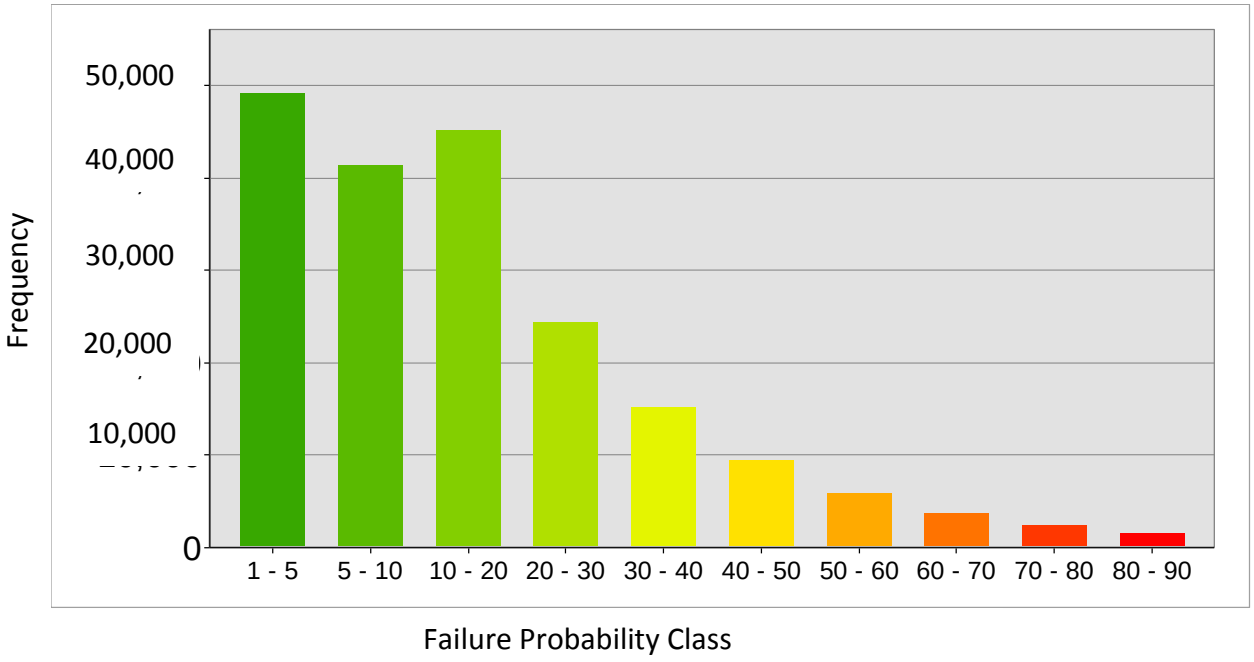

Figure 49. Unstable cell frequency by failure probability class for the timber harvest D scenario.

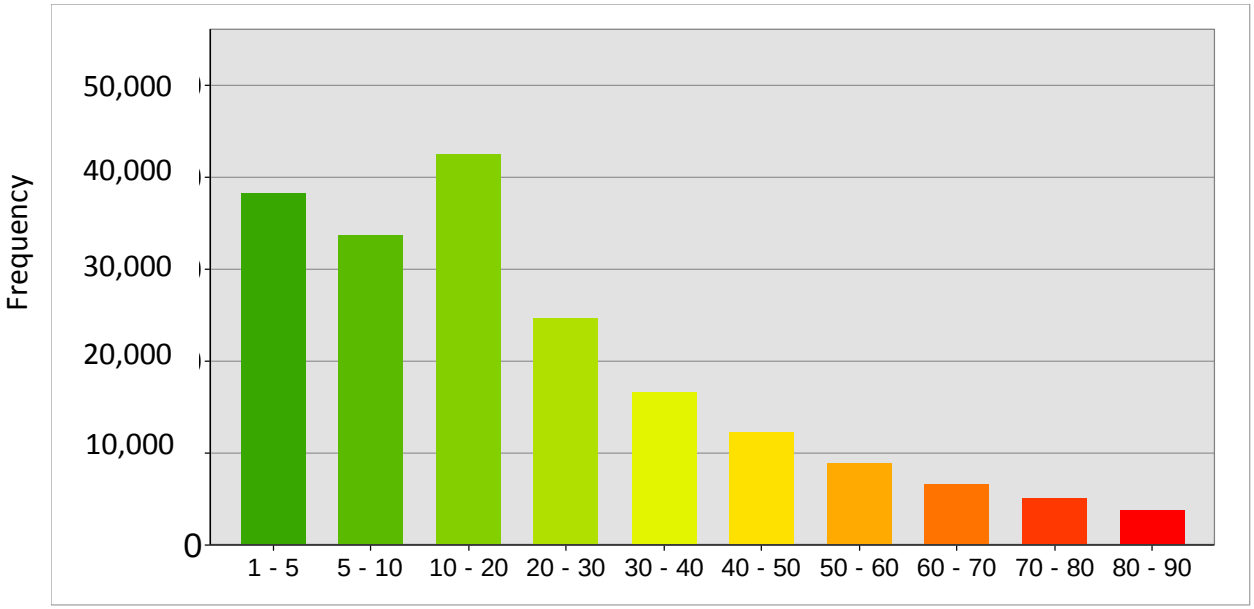

Figure 50. Unstable cell frequency by failure probability class for the timber harvest E scenario.

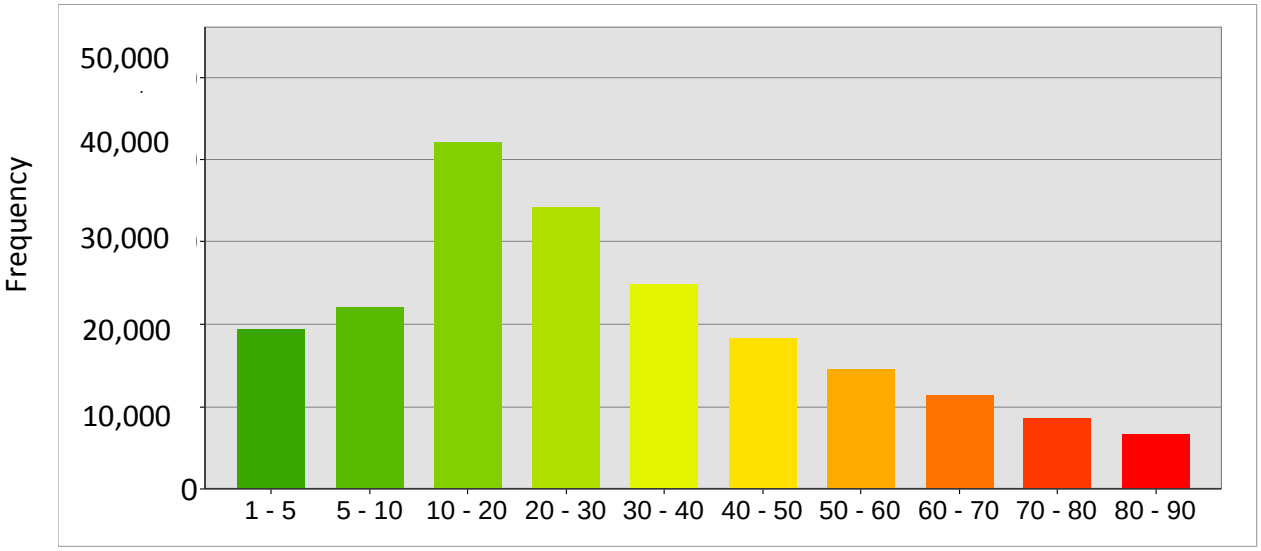

Figure 51. Unstable cell frequency by failure probability class for the timber harvest F scenario.

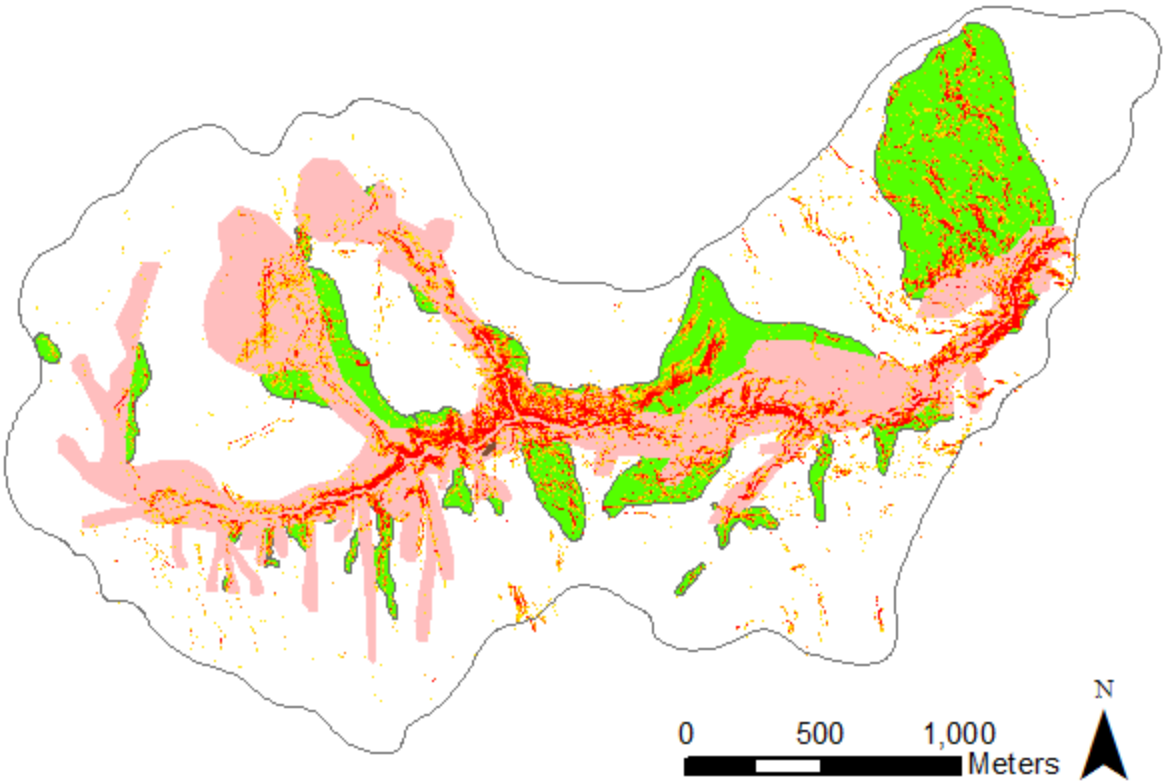

Figure 52. Expanded logging restriction recommendations based on the timber harvest scenario A. Unstable cells from timber harvest scenario A with failure probability at least 40 percent are shown in yellow and red. MWUs are shown in pink. Additional logging restricted areas recommended in this study are shown in green.

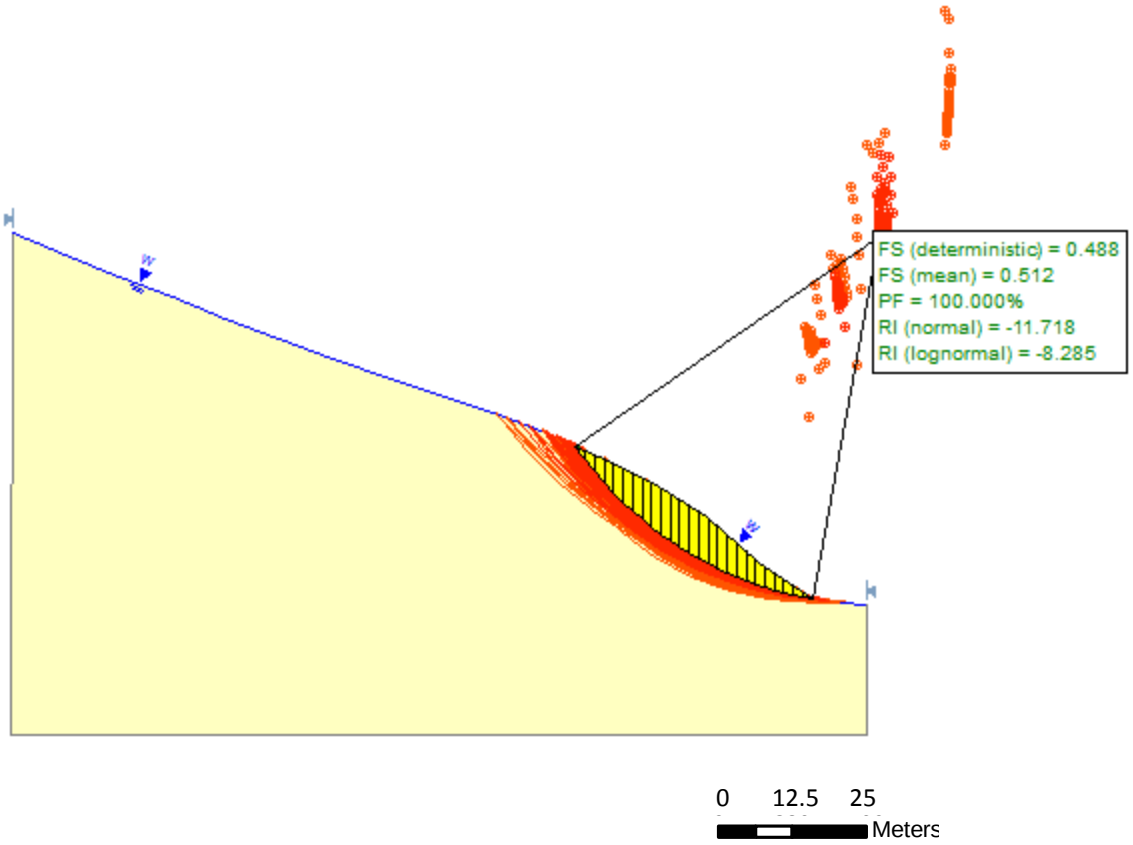

Figure 53. Bishop's Simplified method of slices analysis for the Cutblock slide, with a uniform, saturated soil profile. The factor of safety for the mostly likely failure surface is 0.5. Slices are shown for the most likely failure surface, shown in black. Other surfaces, and associated rotation axes, are shown in red. For simplicity, only the 500 most likely failure surfaces are shown.

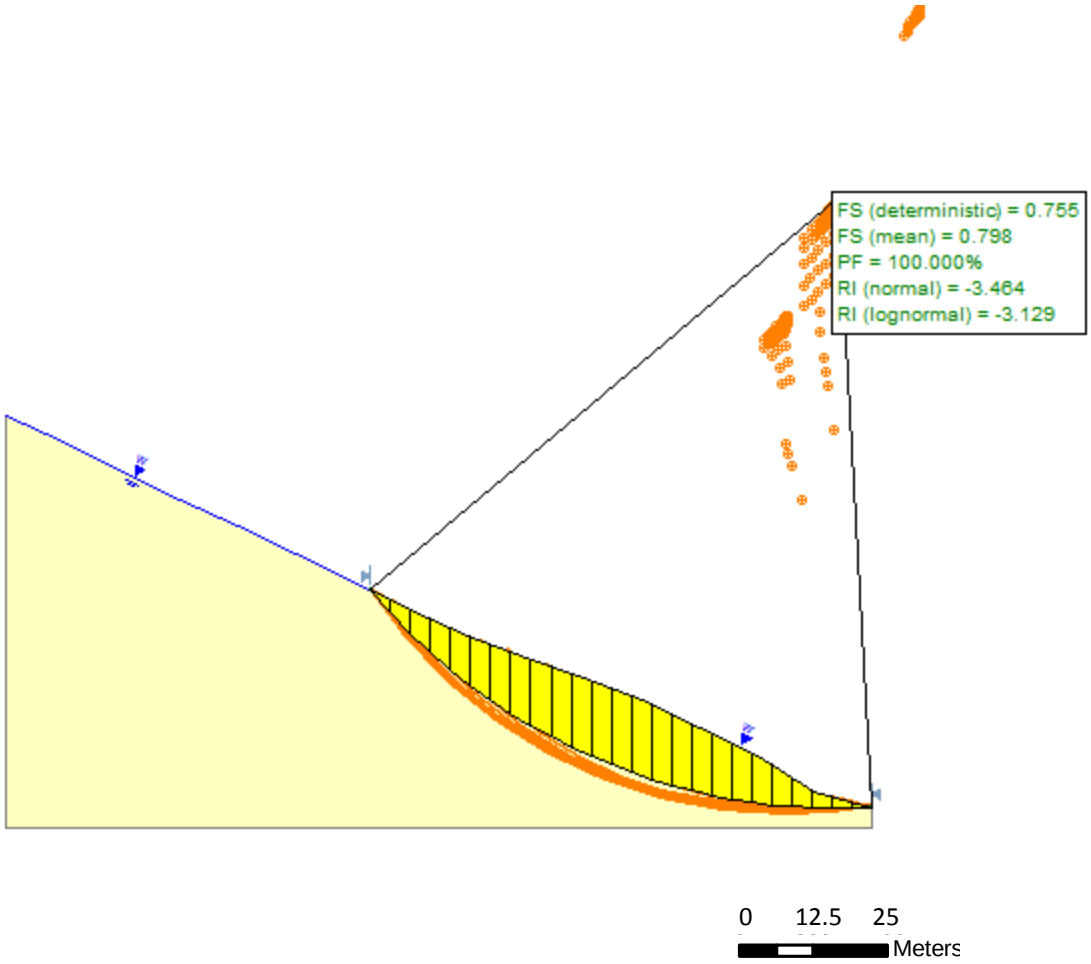

Figure 54. Bishop's Simplified method of slices analysis for the Darrington slide, with a uniform, saturated soil profile. The factor of safety for the mostly likely failure surface is 0.79. Slices are shown for the most likely failure surface, shown in black. Other surfaces, and associated rotation axes, are shown in orange. For simplicity, only the 500 most likely failure surfaces are shown.

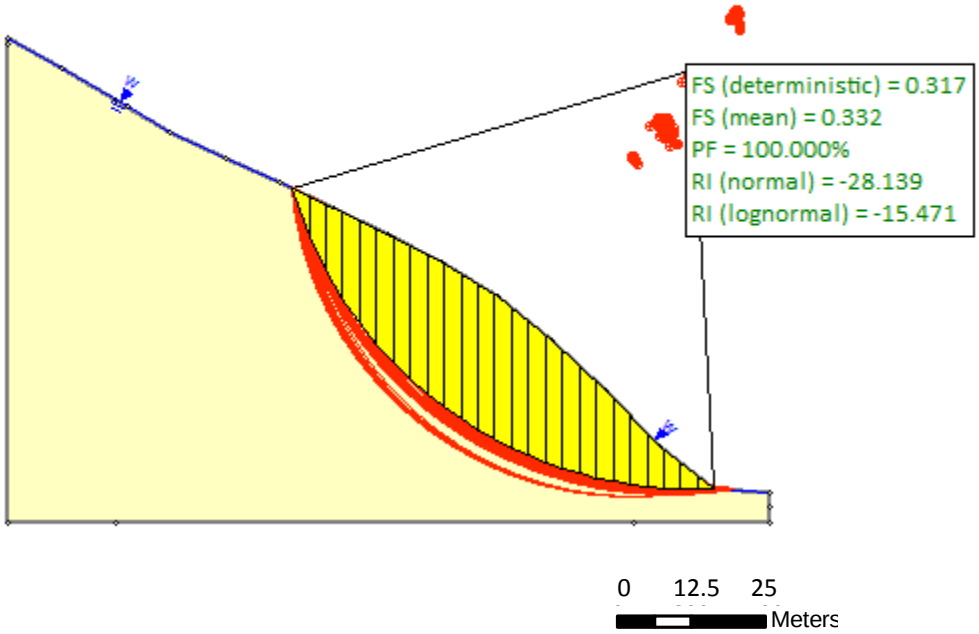

Figure 55. Bishop's Simplified method of slices analysis for the Straight slide, with a uniform, saturated soil profile. The factor of safety for the mostly likely failure surface is 0.33. Slices are shown for the most likely failure surface, shown in black. Other surfaces, and associated rotation axes, are shown in red. For simplicity, only the 500 most likely failure surfaces are shown.

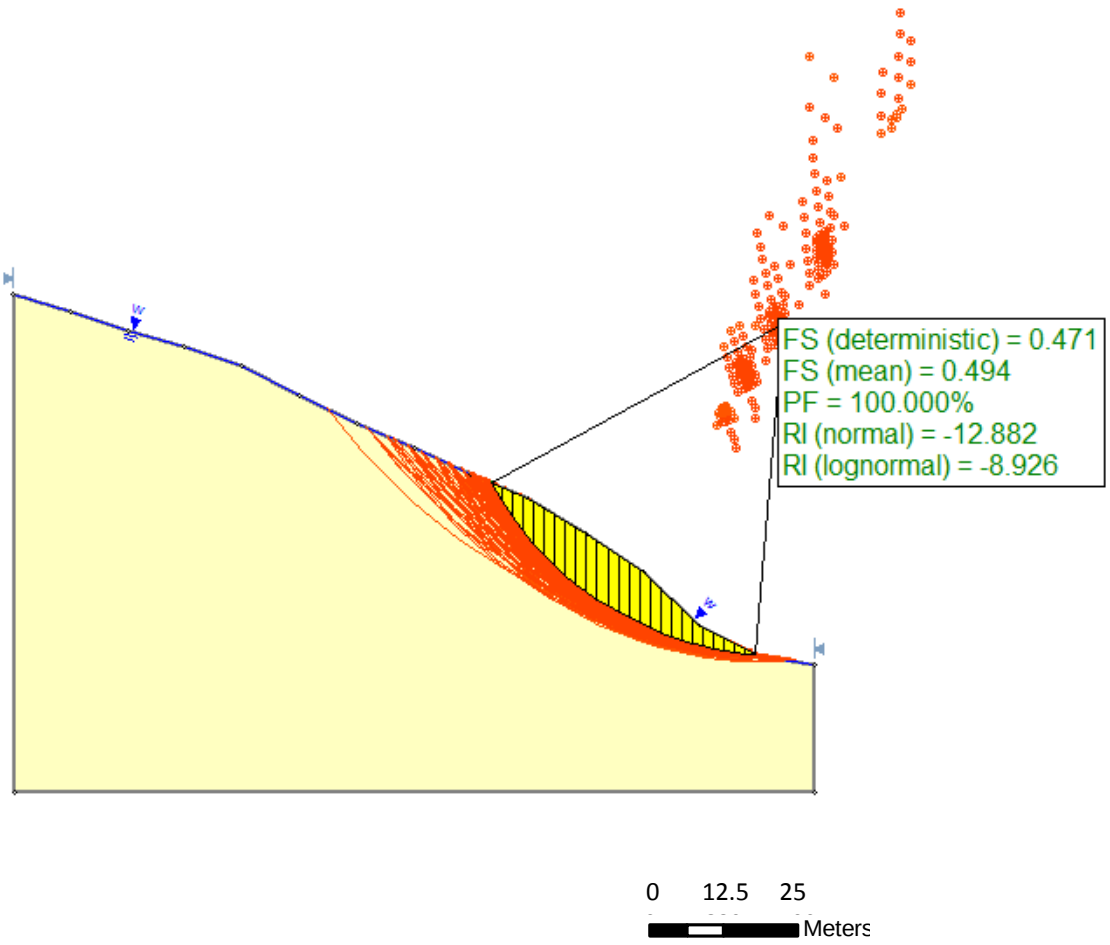

Figure 56. Bishop's Simplified method of slices analysis for the South slide, with a uniform, saturated soil profile. The factor of safety for the mostly likely failure surface is 0.49. Slices are shown for the most likely failure surface, shown in black. Other surfaces, and associated rotation axes, are shown in red. For simplicity, only the 500 most likely failure surfaces are shown.

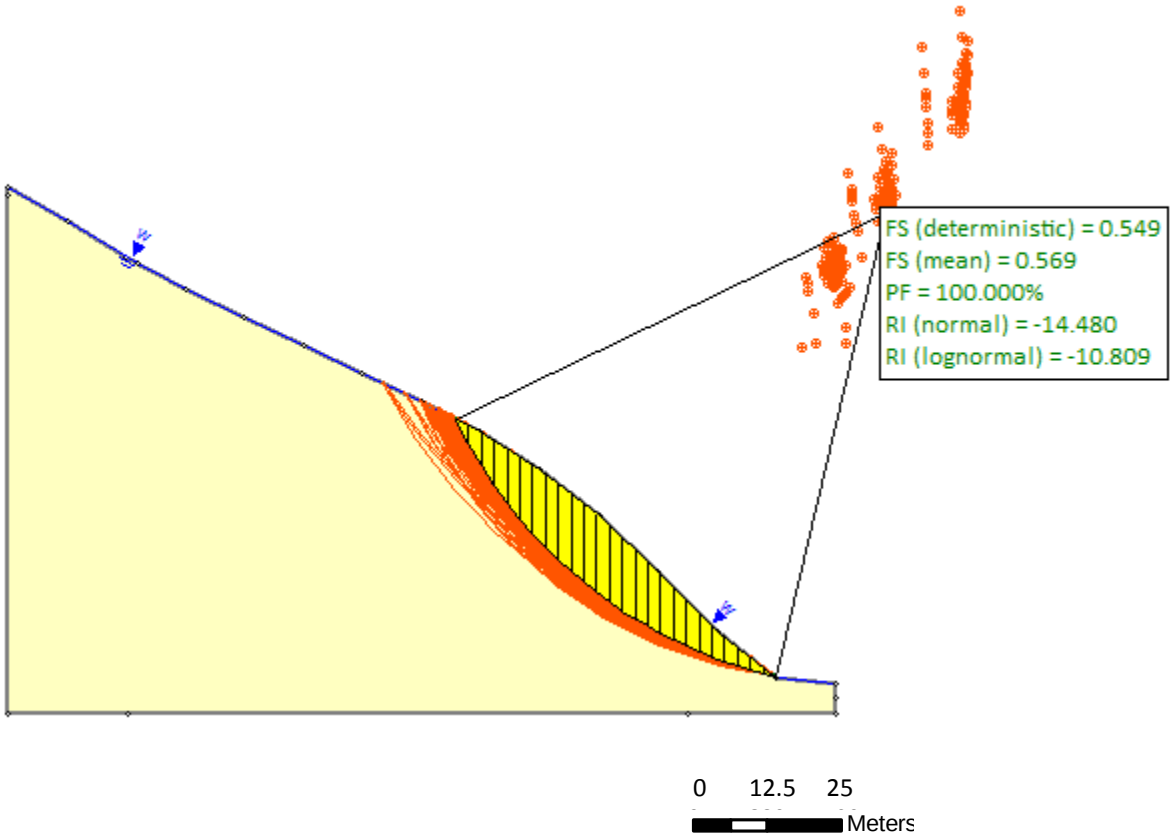

Figure 57. Bishop's Simplified method of slices analysis for the Straight Slide, with unrealistically high soil shear strength. Safety factors are well below one, even with increased shear strength. Slices are shown for the surface with the lowest predicted factor of safety, shown in black. Other surfaces, and rotation axes, are shown in orange. For simplicity, only the 500 surfaces with the lowest calculated safety factors are shown.